A THEORETICAL MODEL FOR ORIENTATION EFFECTS IN ELECTRON TRANSFER REACTIONS

Thesis by

Robert J. Cave

In Partial Fulfillment of the Requirements

for the Degree of

Doctor of Philosophy

California Institute of Technology

Pasadena, California

1986

(Submitted July 29, 1985)

"Accept salvation . . ."

—Paul of Tarsus, ca. 60 *A.D.*

Acknowledgments

I want to express my appreciation to Professor R. A. Marcus for the freedom he has given me to explore a variety of topics while at Caltech. I have appreciated his patience, good humor, and intense curiosity. He has impressed upon me the need for theory to be in dialogue with experiment, and I am truly grateful for this. He also taught me to use the dictionary.

I am grateful to Professor W. A. Goddard III for the opportunity I have had to interact with him, and for the thoughtful, intelligent advice he has given. Professors A. Kuppermann and M. J. Weaver have each been exciting communicators of the beauty of their respective areas. I am privileged to have benefited from interactions with them both.

Paul Siders has been a marvelous friend, as well as co-worker. He has helped me develop confidence in my abilities, and his wit and outlook are special joys to me. The work in Chapters 2 through 4 was done in collaboration with him.

I have enjoyed my interactions with various people at Caltech, including (in no particular order), Steven Lederman, Tom Gibson, Dave Wardlaw, Greg Voth, Stephen Klippenstein, Francis Celii, Dave Beratan, Paul Hipes, Dave Baxter, and Vasil Babamov. Chapter 6 describes work done in association with Stephen Klippenstein, without whom it might never have been completed. My thanks to Art Voter, a good friend, to Barry Olafson for good times on and off the "diamond," and to Dan Schofield for frequent visits and faithful friendship. Also, thanks to fellow Torrancian Bill Wood, for many mind-bending discussions.

I would also like to express deep thanks to my parents, June and Joseph Reedy, and Robert and Lois Cave for their constant love, concern, and support in each part of my life. Thanks to Art and Beth Muller for their complete acceptence of me into their family, which has been one of the joys of my time here. Thanks also to Bernadette Miller, one of the true wonders of Caltech, for her help when I needed it, and her continued friendship.

Finally, I would thank my wife, Susan Cave, for her part in all of this. I am grateful for her patience, encouragement, and interest in me. Most of all, I am grateful to her for the richness she has brought, not only to my graduate experience, but to all aspects of my life.

Abstract

In this thesis, the development and application of a model for the examination of orientation effects in electron transfer reactions are considered. The model is designed to describe broad features of the electronic interactions between large molecules, where the transferred electron is delocalized in both reactant and product.

The model employs spherical or oblate-spheroidal potentials of constant depth for the donor and acceptor sites. The Schrödinger equation is solved for the exact eigenfunctions of such a potential, and the electron transfer matrix element, T_{BA}, is calculated using these wavefunctions. T_{BA} is the principal distance and orientation dependent quantity in current theories of nonadiabatic electron transfer. By comparison of results obtained using spherical and spheroidal wells, it was determined that both orbital shape and well shape (i.e., molecular shape) effects are important in determining the magnitude and orientation dependence of T_{BA}.

The model was used to examine orientation dependence in electron transfer reactions between porphyrins and porphyrin derivatives. T_{BA} was examined for a variety of mutual orientations, including: 1) face-to-face transfers, where it was found that T_{BA} for forward transfer from photoexcited reactants was considerably larger than that for back transfer to yield ground state products, 2) edge-to-edge orientations, and 3) models of possible initial donor-acceptor pairs in a bacterial photosynthetic electron transfer system (*Rhodopseudomonas viridis*). It was observed that T_{BA} was a sensitive function of orbital shape and orienta-

tion.

In order to simplify the model, a semiclassical approximation was examined for the donor and acceptor wavefunctions, for both the spherical- and spheroidal-well states. The accuracy of the approximation supports the interpretations of the results obtained from the exact calculations. It also substantially reduced the calculational time involved.

Table of Contents

Chapter 1

Review of Classical and Quantum Electron Transfer Theories

I. Introduction

Electron transfer reactions have been frequently termed "the simplest chemical reactions." In conventional "outer sphere" electron transfer reactions no bonds are made or broken upon transfer and these reactions are thus inherently simpler than atom transfer reactions. The present chapter outlines the classical and quantum theories of electron transfer. They are complementary in approach and, in general, present similar pictures of the electron transfer problem. It will be shown that the principal distance and orientation dependent quantity in both the classical and quantum rate expressions is the quantity T_{BA}, the electron transfer matrix element. This thesis is concerned with the development and testing of a model for the calculation of orientation effects on T_{BA}. After examining the classical and quantum theories, previous attempts at the calculation of T_{BA} will be reviewed briefly. Finally, in the Appendix to this chapter, a rederivation of the nonadiabatic electron transfer rate expression will be presented which does not assume exact single site eigenfunctions for initial and final electronic states. This provides a link between T_{BA} calculated in one-electron theories (which frequently utilize single-site eigenfunctions) and the quantity calculated in many-electron theories.

IIA. Classical Theory

Homogeneous electron transfer may be loosely viewed as occurring in three steps: 1) approach of the two species to some reaction distance R, 2) electron exchange, and 3) separation to yield products. The initial (final) electronic state is assumed to be principally localized on the donor (acceptor) molecule.

Motions of the constituent atoms of the reacting species, as well as motions of the medium, will in general affect the energy of the reactant and product electronic states. These medium effects occur via electrostatic interactions of the electronic charges with the charges and dipoles of the medium. Since the electron is charged it will polarize the medium and the equilibrium position for this polarization will change depending on whether the electron is localized on the donor or acceptor. Similarly, the electron will frequently play a role in bonding in the molecule and thus upon electron transfer the equilibrium bond lengths of the donor and/or acceptor may readjust.

These effects can be summarized pictorially using a potential energy diagram (Fig. 1) as introduced by Marcus in the consideration of the electron transfer problem.[1] The curve R denotes a cut through the potential energy function of the reactants in the many-dimensional configuration space of the system. R shows the dependence of the total electronic energy of the system on the nuclear coordinates and is appropriate to the case of the electron localized on the donor. In like manner, the curve denoted P is the total electronic energy of the system when the electron is localized on the acceptor. The two curves have different minima, corresponding to the different equilibrium configurations of the nuclei before and after electron transfer. The abscissa, denoted the "reaction coordinate" describes a concerted motion of the nuclei which leads from reactants to products. This motion can involve the translational, vibrational, and rotational motion of the solvent, the vibrational motion of the reactants or products, or some combination of these motions, as is generally the case. The rate of electron transfer is the rate of transitions from curve R to curve P.

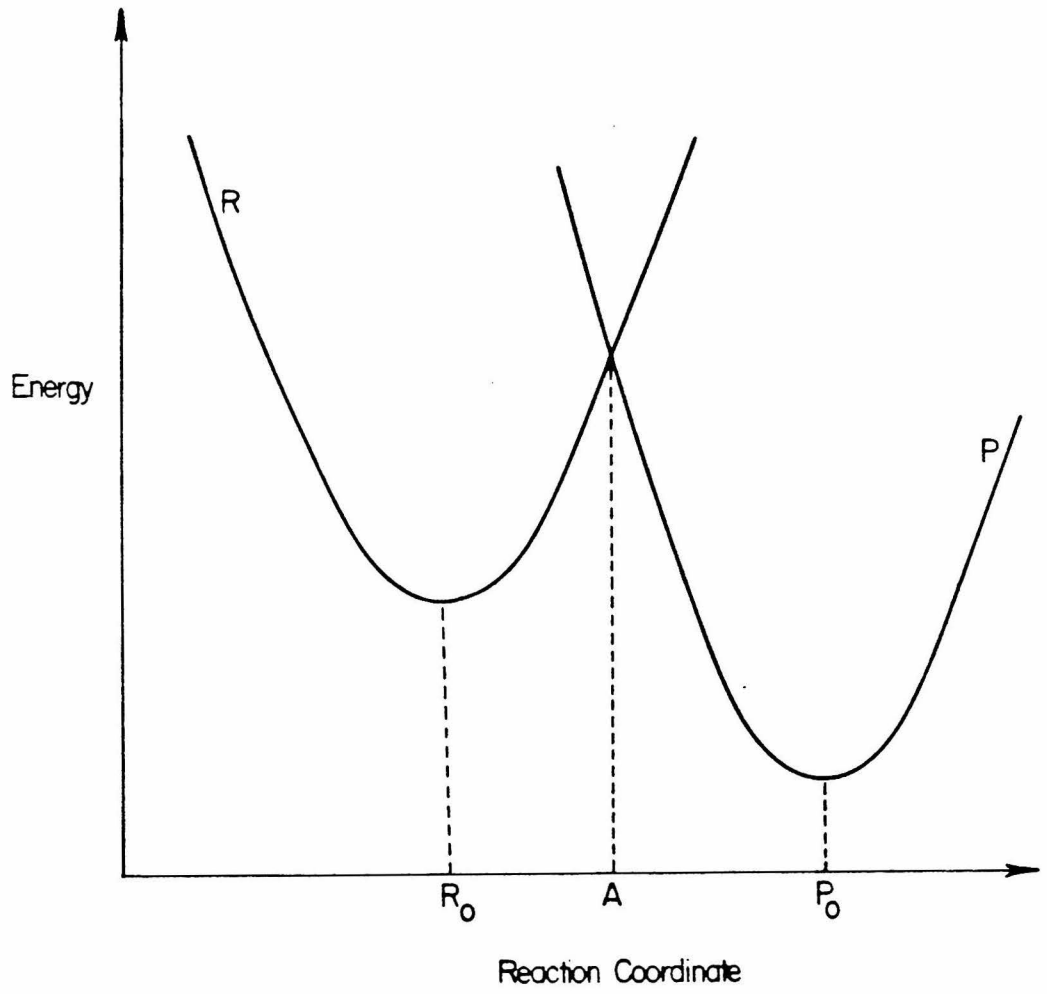

Fig. 1. Nuclear potential energy surfaces for reactants and products of an electron transfer reaction. R (P) is the nuclear potential energy surface when the transferable electron is localized on the donor (acceptor) molecule. R_0 and P_0 are the equilibrium nuclear configurations for the reactant and products, respectively. A is the transition state.

It is convenient to divide the nuclear part of the system into "inner sphere" and "outer sphere" parts.[1,2] The inner sphere part is loosely defined as any species chemically bound to either the donor or acceptor. For transition metal complexes this comprises the central metal atom and the ligands in the first coordination sphere. For molecules such as quinones or porphyrins, all the atoms in the molecule are considered to make up the inner sphere part of the system. The outer sphere part is then made up of all non-covalently attached solvent and counterion molecules. These definitions are tentative as the possibility of specific solvent interactions [3] indicates that the inner sphere portion of the system may be considerably larger than the above simple definition.

The modern theory of electron transfer began with a suggestion of Libby's in 1952.[4] He speculated that electron transfer would occur with the nuclear configuration frozen, i.e., via a Franck-Condon transition. The first quantitative application of this suggestion was made by Marcus.[5] Marcus calculated the rate of electron transfer using transition state theory, the transition state being a nuclear configuration where a Franck-Condon transition may occur while still conserving energy (cf. point *A* in Fig. 1). It should be noted that the transition state is not a point but an $N-1$ dimensional hypersurface for atomic and molecular motion, N being the number of nuclear degrees of freedom in the system. In the Marcus theory of electron transfer[1,5] nuclear motion is executed classically on the nuclear potential energy surfaces. A model was assumed for the nuclear potential energy surface as a function of nuclear coordinate and the free energy of activation ($\Delta G^{\ddagger}$) was calculated, thus yielding the rate.

Those considerations pertinent to the outer sphere portion of the

problem will be discussed here briefly. While the formalism governing the inner sphere portion is somewhat different than that for the outer sphere portion there is still a strong conceptual analogy between the two. Therefore, the result for the inner sphere part will merely be stated below.

The equilibrium value of the nuclear potential energy for reactants occurs at the point R_0 of Fig. 1. In order to react the system must pass through the region A which possesses a nonequilibrium distribution of the solvent molecules. The free energy of such a nonequilibrium distribution is required to obtain the rate of reaction.

Frequently, solvent molecules will have some permanent dipole moment. In the presence of an electric field there will also be some induced dipole moment as the molecular charges respond to the field.[5,6] The motions of these two types of dipoles in response to an external field occur on different time scales. Realignment of the permanent dipole requires motion of the molecule as a whole and is intrinsically slower than the change in the induced dipole. The change in the induced dipole is principally due to electronic motions which can be considered to respond instantaneously to the motion of the transferring electron.

The Marcus model for the solvent[5,6] employs a dielectric continuum with two polarizations, P_{ir} and P_{op}. The former is the slowly responding solvent polarization, the latter the rapidly responding polarization. Expressions were derived[5] for the free energy of any nonequilibrium distribution of the solvent (calculated via a reversible two-state changing process). The actual free energy of activation was obtained by requiring a dielectric polarization with equal free energies for reactant and product charge distributions and by then minimizing the energy of this configuration, subject to the constraint that the free energy difference

between reactants and products be a constant. The expression for the rate of electron transfer obtained is

$$k_{bi} = \kappa_{el} \rho Z_{bi} \exp(-w_r / k_B T) \exp(-\Delta G^* / k_B T) \quad . \tag{1}$$

κ_{el} is a transmission coefficient which is discussed below. Z_{bi} is the bimolecular collision frequency, ρ is a quantity generally close to one and ΔG^* is the free energy of activation. The expression obtained for ΔG^* is[1]

$$\Delta G^* = \frac{\lambda_o}{4}\left[1 + \frac{\Delta G^0}{\lambda_o}\right]^2 \quad . \tag{2}$$

In the dielectric continuum approximation for the solvent the expression for λ_o, "termed the outer sphere reorganization energy," is[1,5]

$$\lambda_o = (\Delta e)^2 \left[\frac{1}{2a_1} + \frac{1}{2a_2} - \frac{1}{R}\right]\left[\frac{1}{D_{op}} - \frac{1}{D_s}\right] \quad . \tag{3}$$

D_{op} and D_s are the optical and static dielectric constants, respectively, a_1 and a_2 the radii of the assumed spherical reacting species, and R is the distance between the centers of the reactants.

Two general features of the electron transfer rate expression can be deduced from Eqs. (2) and (3). First, for fixed λ_o, k_{bi} should go through a maximum as ΔG^o decreases. This has been termed "inverted behavior."[1] Recent experimental studies have apparently observed such behavior in a well-defined series of intramolecular electron transfers.[7] Second, as the dielectric constant of the medium increases the rate will decrease for regions of ΔG^o not in the inverted region.

The contribution of inner sphere reorganization effects to the rate can also be included in the rate expression. Under the assumption of harmonic inner sphere modes an identical expression for ΔG^* to that in Eq. (2) is obtained[1] with λ_o replaced by λ where

$$\lambda = \lambda_i + \lambda_o \quad . \tag{4}$$

λ_o is as defined in Eq. (3), λ_i is defined in Eq. (5) within the harmonic approximation using reduced force constants for the inner sphere modes.[5]

$$\lambda_i = \tfrac{1}{2}\sum_{j,k} f_{jk}\Delta q_j \Delta q_k \quad . \tag{5}$$

The Δq_i are normal coordinate displacements, the f_{ij} are the reduced force constants. λ_i is clearly related to the energy required to stretch or compress the inner sphere modes in the approach to the transition state.

On the basis of the above relations an expression was obtained relating the rate of a given cross reaction (rate constant k_{12}, equilibrium constant K_{12})

$$A^+ + B \rightarrow A + B^+ \tag{6}$$

to the rates of the so-called "self exchange" reactions (rate constants k_{11} and k_{22}, respectively)

$$A^+ + A \rightarrow A + A^+ \tag{7}$$

$$B + B^+ \rightarrow B^+ + B \quad . \tag{8}$$

The expression has the form[1]

$$k_{12} = (k_{11}k_{22}K_{12}f)^{\frac{1}{2}} \tag{9}$$

where

$$\ln f = \frac{(\ln K_{12})^2}{4\ln(k_{11}k_{22}/Z_{bi}^2)} \quad . \tag{10}$$

f is frequently close to unity. Certain plausible additivity assumptions regarding λ_o and κ_{12} were made in obtaining Eq. (9). Eq. (9) has been the

subject of extensive testing and its successes have served to establish the validity of the classical theory.[2]

Another important contribution of the Marcus theory is the relation given in Eq. (11) between the electrochemical rate of electron transfer at zero activation overpotential and the homogeneous self-exchange rate constant.[1]

$$(k_{bi} / Z_{bi})^{1/2} = k_{el} / Z_{el} \tag{11}$$

The equality in Eq. (11) applies when the distance from the center of the reacting ion to the electrode is equal to the molecular radius.

The transmission coefficient, κ_{el}, included in Eq. (1) is intended to account for the possibility that electron transfer might not occur on each passage of the nuclear subsystem through the transition state. The κ_{el} in Eq. (1) is a thermal average of the transmission coefficients (calculated, say, using a Landau-Zener[8] expression) over all nuclear velocities.[1] The transmission coefficient is related to the splitting of the pair of diabatic nuclear potential energy surfaces at the point A. This splitting is a function of the interaction between the *electronic* states of the donor and acceptor molecules. The interaction between donor and acceptor states is nonzero because the localized states are not eigenstates of the full electronic Hamiltonian, only of the single-site Hamiltonians of the donor (or acceptor) plus solvent system.

A distinction is generally made between different regimes for the size of κ_{el}. When κ_{el} is close to unity, electron transfer occurs on each passage of the nuclear subsystem through the transition state. This behavior is termed "adiabatic" in that electron motion (i. e., the transfer of the electron) accompanies the motion of the nuclear subsystem. In

the classical theory the reaction is assumed to be "weakly adiabatic," implying that electron transfer occurs upon each passage through the transition state, but the electronic interaction is weak enough so as not to affect the estimate of ΔG^*. When κ_{el} is small electron transfer occurs infrequently upon passage through the transition state region. This is termed "nonadiabatic" behavior.

Using a Landau-Zener expression to calculate κ Brunschwig et. al.[9] obtained an expression for the unimolecular electron transfer rate constant at fixed R when the reaction is nonadiabatic, given by

$$k_{el}(R) = \frac{2|T_{BA}|^2}{h}\left[\frac{\pi^3}{(E_{out} + E_{in})k_B T}\right]^{1/2} \exp(-\Delta G^*/k_B T) \quad . \qquad (12)$$

T_{BA} is made up of total Hamiltonian matrix elements involving the initial and final electronic states (see Appendix A). E_{in} and E_{out} are related to the inner sphere and outer sphere reorganization energies.[10]

There are two main distance dependent parts of Eq. (12), λ_o and T_{BA}. The distance dependence of λ_o can be seen from Eq. (3); as the separation distance between the reactants increases, λ increases, thus decreasing k in the non-inverted region. T_{BA}, being the interaction of two electronic states localized at different sites, decreases basically as the overlap of the wavefunctions. For electron transfer between large molecules λ_o is expected to be small; thus, changes in λ_o will not significantly affect the rate. Furthermore, at large distances λ_o asymptotes to a constant value, whereas T_{BA} continuously decreases. In general, T_{BA} is expected to be principally responsible for the distance dependence of k_{el}.

The orientation dependence of Eq. (12) is also principally due to T_{BA}. λ_o will doubtless change to some extent as the orientation of a highly

asymmetric donor-acceptor pair is varied. This change should be much smaller than the change in interaction of the electronic states. Therefore, it is expected that T_{BA} is also chiefly responsible for the orientation dependence of the rate.

It should be stressed that only in the nonadiabatic region is the rate sensitive to changes in T_{BA}. When the electron transfer is adiabatic the electronic interaction is already strong enough to insure electron transfer upon reaching the transition state, thus, increasing T_{BA} does not increase k. However, any electron transfer can be made nonadiabatic by increasing the separation distance between the reactants. Therefore, the considerations here are pertinent to the effects of T_{BA} on reaction rate for all reactions at large enough distances.

The quantum theory of electron transfer is summarized next. It will be seen that T_{BA} is again the principal orientation and distance dependent quantity in the rate expression.

IIB. Quantum Theory

The quantum theory of electron transfer was introduced by Levich and Dogonadze[11] and was later elaborated by a number of authors.[2,12-15] The rate expression is obtained using first-order time dependent perturbation theory.[16] A derivation of the rate constant for fixed particle separation and orientation is presented in Appendix A of this chapter. The concepts involved and the assumptions made in deriving the rate constant are summarized here.

The electron transfer is viewed as the decay of an initially prepared state having the transferable electron initially localized on a donor molecule. The decay occurs into a manifold of states characterized by

the electron being localized on the acceptor molecule. A single electronic state is considered on either site. In general, some motions of the nuclear system will be strongly coupled to the electronic motion and the equilibrium positions and force constants of these modes may be different before and after electron transfer. As in the classical theory, the extent of these changes in the nuclear part of the system determines the rate of electron transfer. Assuming for simplicity that only a single nuclear mode is coupled to the electronic motion, the rate constant for electron transfer becomes[2]

$$k_{B\leftarrow A} = \frac{2\pi}{\hbar}|T_{BA}|^2 \sum_{i,j} \exp(-E_{iA}/kT)\,|\langle \chi_{jB}|\chi_{iA}\rangle|^2 \delta(E_{iA} - E_{jB}) \quad . \quad (13)$$

The pair of sums in Eq. (13) is over all vibrational levels of the electronic states with the electron localized on the donor (i) and acceptor (j). The electron transfer matrix element, T_{BA}, is, again, composed of matrix elements of the total electronic Hamiltonian between the initial and final electronic states (see Appendix A).

The main assumptions employed in obtaining Eq. (13) are:[2, 11-15]

1. The depletion of state ψ_A due to reaction is a minor perturbation on the population of ψ_A. This conditon arises because perturbation theory is used to obtain the rate expression. It implies that T_{BA} is small.[15]

2. The Condon approximation has been made.[2,15] This allows removal of T_{BA} from the integral over nuclear coordinates. T_{BA} is, in general, dependent upon nuclear geometry through the wavefunctions' nuclear coordinate dependence. The assumption has been tested qualitatively for the Fe^{3+}/Fe^{2+} electron exchange and was shown to be valid for that system.[17]

3. The interaction time between the systems is short relative to the electron transfer rate. This yields the delta function in Eq. (13) which is responsible for energy conservation. For longer times the energy width of the initially prepared state must be considered.[18]

Within this set of assumptions the quantum theory has been extensively used to discuss condensed phase electron transfer.[2,11-14,19] It should be noted that assumption 1 above limits the quantitative application of the theory to nonadiabatic transfers. Therefore, T_{BA} will play a role in determining the orientation and distance dependence of Eq. (13) wherever Eq. (13) is applicable.

Eq. (13) can be straightforwardly extended to include cases where the transferring electron has an effect on several nuclear modes by addition of the appropriate summations and Franck-Condon factors. All modes which are not affected by electron transfer do not affect the rate of transfer and are not considered explicitly. It is of interest to examine the method used to obtain the Hamiltonian for the nuclear portion of the problem for comparison with the classical theory.

The inner sphere modes are assumed to be the individual bond bending and stretching coordinates of the donor and acceptor molecules. It is common to assume these coordinates are harmonic; thus, normal modes can be defined and the vibrational wavefunctions can be represented as harmonic oscillators.[5,12,15] The expressions for the overlap integrals between displaced harmonic oscillators are well known and the contributions of such modes to the rate are readily obtained.[20,21]

For the outer sphere portion of the system a dielectric continuum description of the medium is used, as in the classical theory.[2,11]

Assuming a linear response of the dielectric to an external electric field, the potential energy and kinetic energy of the polarization can be obtained. This yields a harmonic oscillator Hamiltonian for the polarization field.[2] Note: this description does not depend for its validity on the motions of the individual solvent molecules' being harmonic, only on a linear relation between the polarization and an external field.[22]

Dielectric dispersion can be taken into account by representing the polarization in frequency and wave vector space and then assuming that each (k, ω) component responds linearly to the corresponding component of an external electric field.[2] A set of uncoupled harmonic oscillators is then obtained at given frequencies as a representation of the dielectric response of the solvent. In practice, only a few modes are included in a rate calculation.[20,21]

The interaction of the medium with the transferring electron and the permanent ionic charges is dealt with in a similar fashion.[2] A linear coupling between the components of the polarization and the position of the charge is assumed. This produces a shift in the equilibrium positions of the solvent modes (relative to when there is no charge present) and a decrease in total energy (arising due to solvation).[2]

Once the Hamiltonian for the nuclear modes has been obtained a rate can be calculated. Assuming a single solvent mode and taking the high temperature limit of Eq. (13) one obtains

$$k = \frac{2|T_{BA}|^2}{h}\left(\frac{\pi^3}{\lambda_o k_B T}\right)^{1/2} \exp -\frac{\lambda_o}{4k_B T}\left(1 + \frac{\Delta E_0}{\lambda_o}\right)^2 . \qquad (14)$$

Eq. (14) corresponds closely to Eq. (12), the only difference being the presence of ΔE_0 in the exponential rather than ΔG_0. This difference occurs due to the use of energy surfaces rather than free energy surfaces

for nuclear motion in the quantum theory. The difference can be important when entropy effects are significant for the reaction, in which case the classical theory will generally be more useful.

It is apparent from Eq. (14) that the quantum theory also predicts inverted behavior. This is not confined to the high-temperature limit of Eq. (13),[20,21] nor is it confined to the use of harmonic oscillator nuclear functions.

One aspect of electron transfer which has been illuminated by the quantum theory is the low temperature behavior. In the classical expression the rate goes to zero as T goes to zero. Quantum mechanically there exists the possibility of nuclear tunneling which is temperature independent from a given vibrational level; thus, the rate approaches a constant as T goes to zero. At any temperature other than $T = 0$ it may be that some modes behave classically while others behave quantum mechanically, depending on the vibrational frequencies of interest. Quantum modes require explicit calculation of the terms in the Franck-Condon sum (Eq. (13)) and only a few modes generally contribute ($h\nu > kT$). Classical modes ($h\nu < kT$) can be treated via a limiting process, thus removing the Franck-Condon sums over these coordinates.

Due to the similarity between the treatments of the nuclear modes in the classical and quantum theories it is apparent that the comments regarding distance and orientation dependence made for the classical theory will apply here also. As before, the inner sphere modes are neither orientation nor distance dependent. The outer sphere distance and orientation dependence are expected to be weak for large molecules or long distance transfer. Thus T_{BA} is the quantity which dictates the distance and orientation dependence of the rate.

The expression for k in Eq. (13) has been explicitly evaluated in a number of model studies in an effort to compare quantum and classical effects on the rate.[20,21,23] These calculations used a model functional form for T_{BA}. Several other theoretical attempts have been made to estimate the dependence of T_{BA} on distance and orientation. These studies are summarized next.

III. Prior Examinations of H_{BA}

The simplest estimates of the dependence of T_{BA} on distance utilize one-dimensional wavefunctions appropriate to delta function[24] or square well potentials.[24,25] The form obtained for T_{BA} is

$$T_{BA}(R) = A\exp(-\alpha R) \quad , \tag{15}$$

where A is a constant which depends on the energies of the states involved and $\alpha = (-2mE/\hbar^2)^{1/2}$. Several experimental studies have examined electron transfer between donors and acceptors trapped in glasses.[26-28] An exponential decay of T_{BA} with distance was inferred from these studies. However, the energy dependence of T_{BA} was not nearly as strong as that predicted by the simple square well model. Furthermore, such a model precludes the consideration of any orientation effects on T_{BA}.

Orientation effects have been considered in other theoretical studies of electron transfer in glasses. The donors and acceptors are assumed fixed but distributed randomly, thus producing a distribution of orientations. The orientation effects can be considered relative to what would be obtained for the same random distribution when T_{BA} is orientation independent.

Qualitative effects of orientation on T_{BA} have been considered by Brocklehurst.[29] He used atomic-like functions to model molecular wavefunctions and derived approximate expressions for S (the orbital overlap, which was assumed proportional to T_{BA}) as a function of orientation of the two centers. He also considered the effects of different radial functions on S.

Doktorov et al.[30] considered various empirical forms for T_{BA} as a function of distance and orientation and examined the effects of these on the orientation-averaged, distance-dependent tunneling rate for transfer in glassy matrices. They found no qualitative effects of orientation on the rate other than a lowering of $k(R)$ relative to that which would be found if T_{BA} were orientation independent. Rice and Pilling[31] have also considered the effects of orientation on $k(R)$ in glassy matrices and arrived at similar conclusions.

This is not an unexpected result. When the orientations of a large number of donor and acceptor pairs are distributed randomly, in general one would expect some averaged value between the possible extremes for T_{BA}. Thus, while the rate will be lowered relative to an analogous orientation independent system, the distance dependence would still be predominantly exponential. Orientation dependence will more likely be important in systems where the donor and acceptor are held in fixed positions relative to one another.

The above studies calculate T_{BA} based on a direct interaction between donor and acceptor. A somewhat different approach to the calculation of the distance dependence of T_{BA} has been suggested by a number of authors[32-35] and is based on a superexchange mechanism similar to that proposed for magnetic interactions in crystals.[36] In this

mechanism the donor and acceptor states build in small components of charge transfer character with the surrounding medium (counterions, bridging and nonbridging ligands, or solvent). While such effects are usually small they can nevertheless decrease the rate of decay of T_{BA}. Studies of such effects on intramolecular electron transfer aided by saturated bridging ligands[34,35] have shown that this mechanism can dominate the so-called "direct interaction" for long distance transfers.

The studies mentioned above examined the qualitative effects of a variety of factors on the magnitude and behavior of T_{BA}. The ideal of any theoretical examination of T_{BA} would be to make a quantitative comparison with experiment. This is frequently not possible due to the simplicity of the models required to treat the electron transfer problem. The results which most nearly approach this ideal are those of Beratan and Hopfield.[34] They calculated the decrease in T_{BA} as a function of increasing donor-acceptor separation for sites connected by rigid bridging group. An extended Hückel formalism was used to obtain the one electron wavefunctions of the system. Systems of this size preclude the use of *ab initio* techniques at present. However, applications of *ab initio* techniques have been made in studies of the Fe^{3+}/Fe^{2+} self-exchange reaction by Newton and coworkers[17,37,38] to obtain quantitative estimates of the electron transfer matrix element.

All d electrons were considered explicitly in these studies. Localized states were obtained with the nominal electronic occupations $Fe^{2+} - Fe^{3+}$ and $Fe^{3+} - Fe^{2+}$. These calculations allow for readjustment of the electronic distribution on each center in response to the presence or absence of the extra electron. Thus, static many-body effects are included in the calculation of T_{BA}. Also, the coupling between the two

configurations is calculated from first principles, based on the true electronic Hamiltonian for the system. First solvent-sphere effects were also included. Initially, due to the size of the system, a point charge representation for the assumed H_2O ligands was used. In later calculations three intervening waters on each center were explicitly included in an *ab initio* sense. The two treatments for the ligands yielded similar results.

A number of interesting results were obtained from these studies.[17] First, the reaction was predicted to be weakly adiabatic when the solvent spheres of the two reactants partially interpenetrated. Second, the electronic matrix element was found to be orientation dependent.[17] Third, for some ligands charge transfer effects had a consideable effect on T_{BA}.[38] Fourth, the Franck-Condon approximation appeared to be qualitatively valid for this system.[18] Fifth, the main contribution to the electron transfer rate came from a small region of interparticle separation distances about the distance of closest approach. Sixth, at least for one orientation, the electronic coupling matrix element went through zero at finite R.

Such studies are valuable and are presumably only the beginning of cooperative ventures between bound state theory and electron transfer theory. Clearly, approximations needed which will make larger systems tractable. However, this does not imply that simple, model calculations will be made obsolete when such calculations are feasible. On the contrary, model calculations will still be valuable in interpreting the results obtained from more exact methods, in particular, in elucidating the importance of many-body and solvation effects.

IV. Present Work

The purpose of the work presented in this thesis was to develop and test an approximate model for orientation effects on electron transfer rates between large, asymmetric molecules. In Chapters 2 and 3 the model is introduced and the qualitative features of the model are discussed. The model uses three-dimensional square-well potentials (spherical and oblate-spheroidal). Exact eigenfunctions at each site are obtained and the electron transfer matrix is calculated using these eigenfunctions. It will be shown that both the orbital shape and the well shape play important roles in determining the behavior of T_{BA}. In Chapter 4 the model is applied to the study of orientation effects in electron transfer between porphyrins. In Chapter 5 a semiclassical approximation is tested for the eigenfunctions of spherical wells. The accuracy of the approximation is demonstrated and several methods for speeding the calculation of T_{BA} are presented. Finally, in Chapter 6, an approximate method for obtaining the spheroidal well states is presented using semiclassical approximations for the spheroidal basis functions. The method is reasonably accurate and significantly faster than that using the exact method.

The work in Chapters 2 through 4 was done in collaboration with Paul Siders. The work in Chapter 6 was done in collaboration with Stephen J. Klippenstein.

Appendix A: Golden Rule Rate Derivation

In this appendix the Golden Rule rate constant for electron transfer between two centers at fixed separation and orientation is obtained. It follows closely the derivation presented in Refs. 15 and 22; the major difference is that the present derivation does not assume exact single-site eigenfunctions to represent the initial and final states. This allows a direct association of the matrix element T_{BA} in the nonadiabatic electron transfer rate expression with the quantity obtained using *ab initio* methods. Following the derivation, the relationship between this general T_{BA} and that obtained from one-electron models using exact single-site wavefunctions is discussed.

The Hamiltonian for the system of donor, acceptor, and surrounding medium may be written as

$$\begin{aligned} H_{TOT} &= H^{el} + T^{nuc} + V^{nuc-nuc} + T^{solv} + V^{solv-solv} + V^{solv-nuc} \\ &= H^{el} + T^{N} + V^{N}, \end{aligned} \tag{A1a}$$

where

$$\begin{aligned} T^{N} &\equiv T^{nuc} + T^{solv} \\ V^{N} &\equiv V^{nuc-nuc} + V^{solv-solv} + V^{solv-nuc} \end{aligned} \tag{A1b}$$

H^{el} is the total electronic Hamiltonian for the system, T^{nuc} and T^{solv}, the kinetic energies for the donor and acceptor molecules and the solvent, respectively, and all V's are potential energy terms for the various interactions between the nuclear parts of the problem.

H^{el} can, in principle, include all the electronic degrees of freedom in the system. In practice, most of the electronic portion of the system must be treated using some form of pseudopotential. It will be assumed that H^{el} explicitly includes all electrons bound to the donor and

acceptor. The solvent is then treated in some approximate manner. H^{el} has the form

$$H^{el} = T^{el} + V^{el-nuc} + V^{el-solv} + V^{el-el} \quad . \tag{A2}$$

T^{el} is the kinetic energy operator for all the electrons and the V's are the various potential interactions experienced by the electrons. Since the solvent is treated using a pseudopotential, $V^{el-solv}$ includes average interactions with both the nuclear and the electronic parts of the solvent.

It is conventional to write[15,22]

$$H^{el} = H_A^{el} + V_B^{el} = H_B^{el} + V_A^{el} \quad , \tag{A3}$$

implying a convenient separation of the electronic potential. For the many electron case no such separation is possible[38] and the present discussion will be restricted to consideration of H^{el}.

The electron transfer problem can be viewed as decay of an initially prepared state having an extra electron localized on the donor. We seek the solution of the time dependent Schroedinger equation

$$H^{TOT}\Psi = i\hbar\frac{\partial\Psi}{\partial t} \quad . \tag{A4}$$

$\Psi \equiv \Psi(\mathbf{q},\mathbf{Q},t)$ where $\mathbf{q}$ and $\mathbf{Q}$ denote electronic and nuclear coordinates, respectively. Eq. (A4) is a second-order partial differential equation. To remove the dependence on $\mathbf{q}$, Ψ is expanded as

$$\Psi = \sum_i c_i(\mathbf{Q},t)\psi_i(\mathbf{q};\mathbf{Q}) \quad . \tag{A5}$$

The ψ_i are Born-Oppenheimer type electronic wavefunctions. To simplify the calculation it is generally assumed that the electronic basis set can be truncated at two functions chosen to correspond to the total electronic wavefunctions of the system for an extra electron localized either

on the donor or acceptor. This choice achieves a good description of the initial and final states with as small a basis as possible. The most accurate many-electron wavefunctions available presently can be obtained using *ab initio* molecular structure techniques. These many-electron functions are not in general eigenfunctions of any part of H^{el} but are assumed to well represent the electron distribution of the donor and acceptor and to mimic the dependence of the true wavefunction on **Q**. It will be assumed in what follows that the ψ_i are suitably chosen wavefunctions for the initial and final states, dependent on the form of H^{el}. Ψ then becomes

$$\Psi = c_A\psi_A + c_B\psi_B \quad . \tag{A6}$$

The explicit coordinate dependencies have been omitted for brevity. The superscript A corresponds to the electron localized on the donor, B to the electron localized on the acceptor. Substituting into Eq. (A4) one obtains

$$(H^{el} + T^N + V^N)\sum_i c_i\psi_i = i\hbar\sum_i \frac{\partial c_i}{\partial t}\psi_i \quad . \tag{A7}$$

The l.h.s. of Eq. (A7) may be rewritten as[22]

$$\text{l.h.s.} = \sum_i \left[c_i H^{el}\psi_i + \psi_i T^N c_i + V^N\psi_i c_i + L_i c_i\right] \quad , \tag{A8}$$

where

$$L_i \equiv [T^N,\psi_i] \quad . \tag{A9}$$

To eliminate the dependence on electronic coordinates, one left multiplies by ψ_j^*, where $j = A, B$, and integrates over all electronic coordinates to yield

$$\sum_i \left[c_i \langle \psi_j | H^{el} | \psi_i \rangle + S_{ji} T^N c_i + S_{ji} V_N c_i + \langle \psi_j | L_i \rangle c_i \right] = \quad \text{(A10)}$$

$$i\hbar \sum_i \frac{\partial c_i}{\partial t} S_{ji} \quad .$$

The inverse electronic overlap matrix is defined by the relation

$$\delta_{kl} = \sum_i S^{-1}_{ki} S_{il} \quad . \quad \text{(A11)}$$

Premultiplying Eq. (A10) by S^{-1}_{kj} and summing over j one obtains

$$T^N c_k + V^N c_k - i\hbar \frac{\partial c_k}{\partial t} = -\sum_j \sum_i \left[S^{-1}_{kj} H^{el}_{ji} c_i + S^{-1}_{kj} \langle \psi_j | L_i \rangle c_i \right] \quad . \quad \text{(A12)}$$

The terms H^{el}_{ji} and $\langle \psi_j | L_i \rangle$ act to couple different electronic states. The latter term is akin to a Born-Oppenheimer breakdown term and when diabatic electronic states are used as basis states it can be assumed to be small[39] for moderate distance electron transfers[40]. It will be neglected here relative to H^{el}_{ji}. There being only two electronic states, Eq. (A12) becomes

$$T^N c_B + V^N c_B - i\hbar \frac{\partial c_B}{\partial t} + S^{-1}_{BB} H^{el}_{BB} c_B + S^{-1}_{BA} H^{el}_{AB} c_B = \quad \text{(A13)}$$
$$-(S^{-1}_{BA} H^{el}_{AA} + S^{-1}_{BB} H^{el}_{BA}) c_A$$

and a similar equation with B and A reversed.

If the right-hand side of Eq. (A13) is small, a zeroth order solution for c_B can be taken as the solution to the l.h.s of Eq. (A13). To obtain this it is realized that

$$S^{-1}_{BA} H^{el}_{AA} + S^{-1}_{BB} H^{el}_{BA} = \frac{1}{1 - |S_{AB}|^2} (H^{el}_{BB} - S_{BA} H^{el}_{AB}) \quad . \quad \text{(A14)}$$

The first term in parentheses on the r.h.s. of Eq. (A14) dominates, as the second is of order S^2. Thus, the quantity in Eq. (A14) is seen to be essen-

tially the electronic energy of the system when the extra electron is localized on the acceptor. Therefore, neglecting the time derivative term, the l.h.s. of Eq. (A13) is seen to be a vibrational Hamiltonian for the nuclear motion of the entire system when the electron is localized on the acceptor. c_B can then be written as

$$c_B(\mathbf{Q},t) = \sum_r c_{rB}^0(t)\chi_r^B(\mathbf{Q})\exp\frac{-iE_{rB}t}{\hbar} , \tag{A15}$$

where χ_r^B satisfies the equation

$$(T^N + V^N + S_{BB}^{-1}H_{BB}^{el} + S_{BA}^{-1}H_{AB}^{el})\chi_r^B = E_{rB}\chi_r^B . \tag{A16}$$

An analogous definition can be used for c_A. These two definitions are then substituted into Eq. (A13) and after premultiplication by χ_s^{B*} and integration over $\mathbf{Q}$ one obtains

$$\frac{\partial c_{sB}^0}{\partial t} = \frac{-i}{\hbar}\sum_t c_{tA}^0 <s\,|\,S_{BA}^{-1}H_{AA}^{el} + S_{BB}^{-1}H_{BA}^{el}\,|\,t>\exp\left[\frac{-i(E_{tA} - E_{sB})t}{\hbar}\right] . \tag{A17}$$

Assuming that only one vibrational state of A is populated and that $c_{tA}^0(t) = \delta_{it}$, that is, c_{iA} does not change with time, Eq. (A17) can be integrated and becomes

$$c_{sB}^0 = \frac{<s\,|\,S_{BA}^{-1}H_{AA}^{el} + S_{BB}^{-1}H_{BA}^{el}\,|\,i>}{(E_{iA} - E_{sB})}\left[1 - \exp\left[\frac{-i(E_{iA} - E_{sB})t}{\hbar}\right]\right] . \tag{A18}$$

The total probability density in state $|sB>$ as a function of time is

$$|c_{sB}^0|^2 = \frac{4\,|<s\,|\,S_{BA}^{-1}H_{AA}^{el} + S_{BB}^{-1}H_{BA}^{el}\,|\,i>|^2}{(E_{iA} - E_{sB})}\sin^2\left[\frac{(E_{iA} - E_{sB})t}{2\hbar}\right] . \tag{A19}$$

Using standard arguments[16] the rate of electron transfer from a single state $|iA>$ to the manifold of states of electronic state B is

$$k = \frac{2\pi}{\hbar}\sum_s |<s\,|\,S_{BA}^{-1}H_{AA}^{el} + S_{BB}^{-1}H_{BA}^{el}\,|\,i>|^2\delta(E_{iA} - E_{sB}) . \tag{A20}$$

If the electronic matrix elements of H^{el} are weakly nuclear dependent the matrix elements may be removed from the integral over nuclear coordinates to obtain

$$k = \frac{2\pi}{\hbar} |S_{BA}^{-1} H_{AA}^{el} + S_{BB}^{-1} H_{BA}^{el}|^2 \sum_s |<s|i>|^2 \delta(E_{iA} - E_{sB}) \quad . \tag{A21}$$

Finally, averaging over the thermally populated levels of electronic state A the thermal rate of electron transfer is

$$k = \frac{2\pi}{\hbar} \frac{|S_{BA}^{-1} H_{AA}^{el} + S_{BB}^{-1} H_{BA}^{el}|^2}{Q_A} \sum_{s,i} \exp\left[\frac{-E_{iA}}{kT}\right] |<s|i>|^2 \delta(E_{iA} - E_{sB}) \tag{A22}$$

Eq. (A22) is the nonadiabatic rate expression originally obtained by Levich and Dogonadze.[11]

The electronic prefactor to the Franck-Condon sum may be written as

$$S_{BA}^{-1} H_{AA}^{el} + S_{BB}^{-1} H_{BA}^{el} = \frac{(H_{BA}^{el} - S_{AB} H_{AA})}{1 - |S_{AB}|^2} \quad . \tag{A23}$$

The l.h.s. of Eq. (A23) is the quantity calculated by Newton[17,37,38] using *ab initio* wavefunctions. When only the transferable electron is considered explicitly a considerable simplification can be made in evaluating Eq. (A23).

In the one-electron case H^{TOT} can be written as in Eq. (A3) and suitable eigenfunctions at sites A and B can be defined. Using these functions H_{BA} becomes

$$<B|T^{el} + V_A + V_B|A> = E_A S_{BA} + <B|V_B|A> \tag{A24}$$

since $(T^{el} + V_A)|A> = E_A|A>$. Similarly,

$$<A|T^{el} + V_A + V_B|A> = E_A + <A|V_B|A> \quad . \tag{A25}$$

Therefore, Eq. (A23) simplifies to

$$\frac{(H_{BA}^{el} - S_{AB}H_{AA})}{1 - |S_{AB}|^2} = \frac{<B|V_B|A> - S_{AB}<A|V_B|A>}{1 - |S_{AB}|^2} . \qquad \text{(A26)}$$

Due to the assumed local nature of V_B and the exponential decay of the electronic states it is generally true that $<B|V_B|A> \gg S_{AB}<A|V_B|A>$; thus $T_{BA} \approx H_{BA}$. This is not true in the many-electron case since H_{BA}^{el} and $S_{AB}H_{AA}^{el}$ are both are of the order of $E_A S_{BA}$.

References

1. R. A. Marcus, J. Chem. Phys. **43,** 679 (1965).

2. J. Ulstrup, *Charge Transfer Proceses in Condensed Media: Lecture notes in Chemistry, No. 10* (Springer, New York, 1979).

3. J. C. Curtis, B.P. Sullivan, and T. J. Meyer, Inorg. Chem. **22,** 224 (1983).

4. W. F. Libby, J. Phys. Chem. **56,** 863 (1952).

5. R. A. Marcus, J. Chem. Phys. **24,** 966 (1956).

6. R. A. Marcus, J. Chem. Phys. **24,** 979 (1956).

7. J. R. Miller and G. L. Closs, unpublished results.

8. Cf. M. S. Child, *Molecular Collision Theory* (Academic, New York, 1974).

9. B. S. Brunschwig, J. Logan, M. D. Newton, and N. Sutin, J. Am. Chem. Soc. **102,** 5798 (1980).

10. N. Sutin, Adv. Inorg. Chem. **30,** 441 (1983).

11. V. G. Levich and R. R. Dogonadze, Collect. Czech. Chem. Commun. **26,** 193 (1961); Translator, O. Boshko, Univ. of Ottowa, Ontario, Canada.

12. V. G. Levich and R. R. Dogonadze, Dokl. Akad. Nauk. SSSR, **133,** 591 (1960).

13. R. R. Dogonadze and A. M. Kuznetsov, Sov. Electrochem. **3,** 1189 (1967).

14. R. R. Dogonadze, A. M. Kuznetsov, and M. A. Vorotyntsev, Zeit. Phys. Chem. Neue Folg. **100,** 1 (1976).

15. N. R. Kestner, J. Logan, and J. Jortner, J. Phys. Chem. **78,** 2148 (1974).

16. L. I. Schiff, *Quantum Mechanics*, 3rd ed. (McGraw Hill, New York, 1968).

17. J. Logan and M. D. Newton, J. Chem. Phys. **78,** 4086 (1983).

18. C. Cohen-Tannoudji, B. Diu, and F. Laloe, *Quantum Mechanics*, Vol. 2 (Wiley, New York, 1977).

19. J. Jortner, J. Am. Chem. Soc. **102,** 6676 (1980).

20. P. Siders and R. A. Marcus, J. Am. Chem. Soc. **103,** 741 (1981).

21. P. Siders and R. A. Marcus, J. Am. Chem. Soc. **103,** 748 (1981).

22. P. D. Siders, Ph. D. thesis, California Institute of Technology, Pasadena, California, 1983, Chap. 5, Appendix A. Available from University Microfilms, Ann Arbor, MI, No. 83-22, 674.

23. E. Buhks, M. Bixon, J. Jortner, and G. Navon, Inorg. Chem. **18,** 2014 (1979).

24. M. Redi and J. J Hopfield, J. Chem. Phys. **72,** 6651 (1980).

25. J. R. Bardeen, Phys. Rev. Lett. **6,** 57 (1961).

26. J. V. Beitz and J. R. Miller, J. Chem. Phys. **71,** 4579 (1979).

27. I. V. Alexandrov, R. F. Khairutdinov, and K. I. Zamaraev, Chem. Phys. **32,** 123 (1978).

28. S. Strauch, G. McLendon, M. McGuire, and T. Guarr, J. Phys. Chem. **87,** 3579 (1983).

29. B. Brocklehurst, J. Phys. Chem. **83,** 536 (1979).

30. A. B. Doktorov, R. F. Khairutdinov, and K. I. Zamaraev, Chem. Phys. **61,** 351 (1981).

31. S. A. Rice and M. J. Pilling, Prog. React. Kinet. **9,** 93 (1978).

32. H. M. McConnell, J. Chem. Phys. **35,** 508 (1961).

33. J. Halpern and L. E. Orgel, Discuss. Faraday Soc. **29,** 32 (1960).

34. D. N. Beratan and J. J. Hopfield, J. Am. Chem. Soc. **106.** 1584 (1984).

35. S. Larsson, J. Phys. Chem. **88,** 1321 (1984), and references cited therein.

36. P. W. Anderson, Phys. Rev. **115,** 2 (1959).

37. M. D. Newton, Int. J. Quantum Chem.: Quantum Chem. Symp. **14,** 363 (1980).

38. M. D. Newton, in *Mechanistic Aspects of Inorganic Reactions*, ACS Symp. Ser. No. 198, D. B. Rorabacher and J. F. Endicott, eds. (ACS, Washington, D. C., 1982), p.255.

39. M. D. Newton and N. Sutin, Ann. Rev. Phys. Chem. **35,** 437 (1984).

40. D. N. Beratan and J. J. Hopfield, J. Chem. Phys. **81,** 5753 (1984).

Chapter 2

General Discussion of the Model for Orientation Effects Using Eigenstates of Spherical Wells

I. Introduction

The extent of coupling between a donor and acceptor in an electron-transfer reaction is a question of interest in many areas of chemistry. Biological electron transfers,[1] solution electron transfers,[2] electrochemical oxidation and reduction reactions,[3] and certain specialized surface techniques[4] all depend for their theoretical interpretations on an understanding of the coupling between donor and acceptor. The amount of coupling can vary drastically, even within a given system, depending on, for example, the geometric parameters, orbital energies of donor and acceptor, etc. A simple example will illustrate the range of such interactions.

Consider the system H-atom plus proton. At large distances a localized description is appropriate; i.e., the electron is bound for essentially all time to the proton with which it was originally associated. At relatively large, but finite distances, the electron is localized on a single center but there is a finite probability of finding it on the second proton. Finally, at relatively short distances (< 1Å) it becomes more reasonable to consider the electron as delocalized; i.e., a bond is formed. The physics governing the transition from localized to delocalized behavior can be examined qualitatively within a simple two-electronic-state approximation[5]. The basis set for the problem is taken to be a single H 1s orbital on each center (φ_l, φ_r). It is assumed that the initially prepared state is φ_l. The probability of electron transfer (i. e., the probability of observing the electron in φ_r) is[5]

$$P_{lr}(t) = \frac{1}{2}\left[(1 + S^2) - (1 - S^2)\cos[(E_+ - E_-)t/\hbar]\right] \qquad (1)$$

where

$$S = \langle \varphi_l | \varphi_r \rangle \tag{2}$$

and

$$E_{\pm} = \frac{H_{ll} \pm H_{lr}}{1 \pm S} \tag{3}$$

where

$$H_{ij} = \langle \varphi_i | -\frac{1}{2}\nabla^2 - \frac{1}{R_l} - \frac{1}{R_r} | \varphi_j \rangle. \tag{4}$$

It is seen that the frequency of oscillation of P_{12} is essentially $(E_+ - E_-)/2\hbar$ which is $(H_{lr} - H_{ll}S)/(1 - S^2)$. That is, the frequency of transfer is related to the size of the interaction matrix element. At large R it is obvious that $H_{lr}, S \ll 1$; thus $P_{12} \approx 0$ on any time scale of interest. At short R, H_{lr} increases, due to strong interaction of the electronic basis functions, and the oscillation in P_{12} becomes rapid, reducing the usefulness of a localized description.

It is desirable to be able to examine the behavior of this coupling for larger systems than H_2^+. Further, it is of interest to know how this coupling depends on the orientation of the donor and acceptor, and on the types of orbitals involved in the transfer. One approach to this would be through use of more advanced wavefunctions for describing larger systems, such as *ab initio* wavefunctions.[6-8] Presently however, the size of such calculations makes extensive use of them prohibitive, except for cases of high symmetry. For example, charge transfer states of a D_{4h} diporphyrin system have been examined but lower symmetry states have not been considered.[8]

Furthermore, while such calculations yield as accurate a value for $(H_{lr} - SH_{ll})/(1-S^2)$ as possible at present, there is a danger of "losing

the forest for the trees." That is to say, since so little is presently known about orientation effects on the rate of electron transfer, there is also a need for simple models in which to examine qualitative orientation effects. An understanding of these simple models may then allow interpretation of more complicated effects seen in detailed calculations. It is to this end that our work has been undertaken.

One level of simplification which has been adopted in prior considerations of electron transfer (except, of course, the few *ab initio* studies) is use of a one-electron model.[9] Here, only the transferable electron is explicitly considered. H_{tr} is then calculated using suitably chosen one-electron orbitals for basis functions and H includes the effective interaction of the transferable electron with the core electrons on both centers. Recent work on superexchange mechanisms has extended such one-electron models to metal-metal interaction through an intervening medium via an Extended Hückel formalism.[10,11]

Another assumption implicitly made for electron transfer between two isolated redox centers is that one need only consider transfer between a pair of localized electronic states. For low driving force transfers from ground state reactants this is certainly a plausible assumption, since the need to conserve energy restricts the states to which the electron can transfer. (Actually, this is not strictly true since for longer times the Golden-Rule rate constant does yield transfer to non-isoenergetic states, or equivalently, the initially prepared state is not an eigenstate of the system and therefore has a finite energy width.[12] Nevertheless, given the immensity of such systems, and the assumed large energy gaps between electronic states of the acceptor, use of single donor and acceptor states will not be a limiting factor on the accuracy of

such calculations.)

On a more detailed level, another class of assumptions is the use of model potentials. The need for this is obvious once the one-electron assumption is made. If the exact wavefunction were needed to construct an accurate enough effective potential, the utility of the one-electron approximation would be greatly diminished. Therefore, use is made of simple, model potentials, such as one-dimensional square well potentials,[9] hydrogen-like potentials,[13] or some effective Hamiltonian method.[10,11] While these potentials are crude relative to more sophisticated *ab initio* effective potentials, they are believed to contain the elements needed to qualitatively understand distance dependence within a one-electron framework.

Our studies used eigenfunctions of three-dimensional wells of either spherical or oblate-spheroidal shape. The model is introduced here using spherical wells, and the calculation of the electronic coupling between two such sites is detailed. Sample calculations are presented to illustrate well size, orbital shape, and orientation effects. These effects are also observed in the results using spheroidal wells of Chapters 3 and 4 and the spherical results aid in interpretation of the spheroidal results. The method of calculation of T_{BA} is completely analogous for the spherical and oblate-spheroidal potentials, the only difference being in the eigenfunctions. The procedure is quite straightforward, but can be obscured by the complexity of the spheroidal wavefunction when introduced via these calcuations.

II. Spherical-Well Single-Site Wavefunctions

Within the assumptions of the preceding section we choose single-site

potentials of the form

$$V = \begin{cases} -V_0 & r \le r_0 \\ 0 & r > r_0 \end{cases} . \tag{5}$$

These are spherical wells of constant depth. Solutions to the Schroedinger equation are easily obtained (e.g., see Schiff[14]). The method is outlined here.

The Schroedinger equation becomes (in atomic units)

$$(\nabla^2 + k_i^2)\psi_i(r,\theta,\varphi) = 0 \qquad r \le r_0 \tag{6a}$$

$$(\nabla^2 - k_o^2)\psi_o(r,\theta,\varphi) = 0 \qquad r \le r_0 \tag{6b}$$

with $k_i^2 = 2(E+V_0)$ and $k_o^2 = -2E$. In spherical polar coordinates ($0 \le r < \infty$, $0 \le \theta \le \pi$, $0 \le \varphi \le 2\pi$) Eq. (6a) becomes

$$\left[\frac{1}{r^2}\frac{\partial}{\partial r}r^2\frac{\partial}{\partial r} + \frac{1}{r^2\sin\theta}\frac{\partial}{\partial\theta}\sin\theta\frac{\partial}{\partial\theta} + \frac{1}{r^2\sin^2\theta}\frac{\partial^2}{\partial\varphi^2} + k_i^2\right]\psi_i(r,\theta,\varphi). \tag{7}$$

If $\psi(r,\theta,\varphi)$ is chosen to be of the form

$$\psi(r,\theta,\varphi) = R(r)\Theta(\theta)\Phi(\varphi) , \tag{8}$$

then Eq. (7) separates to yield three ordinary differential equations of the form

$$\left[\frac{\partial^2}{\partial\varphi^2} + m^2\right]\Phi(\varphi) = 0 \tag{9a}$$

$$\left[\frac{1}{\sin\theta}\frac{\partial}{\partial\theta}\sin\theta\frac{\partial}{\partial\theta} + l(l+1) - \frac{m^2}{\sin^2\theta}\right]\Theta(\theta) \tag{9b}$$

$$\left[\frac{1}{r^2}\frac{\partial}{\partial r}r^2\frac{\partial}{\partial r} + k_i^2 - \frac{l(l+1)}{r^2}\right]R(r) = 0. \tag{9c}$$

The solutions to these equations are each standard functions. One finds for $\Phi(\varphi)$

$$\Phi(\varphi) = C\cos m\varphi + D\sin m\varphi \; ; \tag{10}$$

i.e., any linear combination of $\cos m\varphi$ and $\sin m\varphi$ is a solution to Eq. (9a). The function $\Theta(\theta)$, which is a solution of Eq. (9b), is an Associated Legendre polynomial in $\cos\theta$. Eq. (9c) is the only one of the three separated equations which depends on E and V. Its solutions are spherical Bessel functions, either $j_l(k_i r)$ inside the well (where $k_i^2 > 0$) or $k_l(k_o r)$ outside the well. (Note te distinction between k_l, the lth modified spherical Bessel function and k_o the reduced energy appropriate to the region outside the well. In general, the $j_l(k_i r)$ can be thought of as oscillatory functions in r, whereas the $k_l(k_o r)$ are exponentially decaying functions in r. (For details on evaluation of the Associated Legendre polynomials and spherical Bessel functions, see Appendix A.)

Single-site eigenfunctions $\psi_l^m(r,\theta,\varphi;E) \equiv \psi_l^m$ valid over all space are obtained by requiring satisfaction of Eqs. (6a) and (6b) for a given value of E and having the wavefunction and its first derivative continuous across the boundary at $r = r_0$. (The continuity conditions lead to well-defined values of the probability and probability density current over all space.[14]) Since the differential equations satisfied by $P_l^m(\theta)$ and $\Phi(\varphi)$ do not depend on E or V continuity of the angular parts of the wavefunction can be obtained by requiring $l_{in} = l_{out}$, $m_{in} = m_{out}$. For the radial parts of the wavefunctions one obtains the conditions

$$Aj_l(k_i r_o) = Bk_l(k_o r_0) \tag{11a}$$

and

$$A\left[\frac{d}{dr} j_l(k_i r)\right]_{r=r_0} = B\left[\frac{d}{dr} k_l(k_o r)\right]_{r=r_0} . \tag{11b}$$

Or, rewriting in terms of a single condition one obtains

$$\left[\frac{d}{dr}\ln j_l(k_i r)\right]_{r=r_0} = \left[\frac{d}{dr}\ln k_l(k_o r)\right]_{r=r_0}. \tag{12}$$

For a given value of V, E is adjusted until Eq. (12) is satisfied, thus obtaining an eigenenergy of the potential for the chosen values of l and m. (For details on the search procedure used in calculating E, see Appendix B.) The wavefunctions can be normalized analytically using standard expressions for each part of the product wavefunction.[15,16]

The method was implemented by choosing l and m values to model some state of interest, choosing some value of E, and adjusting V_0 until the value of E was obtained as the eigenenergy for that V_0. The single-site wavefunction thus obtained was then used directly in the calculation of T_{BA}, outlined in the next section.

III. Calculation of T_{BA} Spherical-Well Functions

It will be assumed in what follows that two spherical wells have been chosen with one-electron states localized at each well obtained as in the preceding section. Electron transfer is considered as occurring from one of the states, labeled site A, to the state on the other well, labeled B. The formalism describing the rate of transfer between two such sites was given in Chapter 1. The primary orientation and distance dependent quantity in the rate expression is the electronic coupling matrix element T_{BA} given by

$$T_{BA} = \frac{H_{BA} - S_{AB}H_{AA}}{1 - S_{AB}^2} \tag{13}$$

where the various quantities have been defined in Chapter 1. In general,

for one-electron wavefunctions, it is expected that $H_{AA} < H_{BA}$ (for $H_{BA} \neq 0$) since ψ_A is exponentially decaying outside well A. Furthermore, for $S_{AB} \leq 0.3$, $1-S_{AB}^2 \approx 1$. As a first approximation to the orientation dependence of T_{BA}, H_{BA} will be considered. (It will be shown in Chapter 3 that for all states considered this is an excellent approximation for non-overlapping wells.)

The calculation of H_{BA} entails evaluation of

$$H_{BA} = -\int_{well\ B} d\tau (\psi_{i'}^{m'})^B V_B (\psi_i^m)^A. \tag{14}$$

Since V_B is a constant over well B, Eq. (14) reduces to the overlap of the two functions inside well B. This is an important conceptual point in that it makes apparent the means of understanding the orientation dependence of H_{BA} for two such states. The maxima, minima, and zeros of H_{BA} are all directly related to the change in overlap of the two functions with orientation, and these are themselves functions of the nodal structure and rate of decay of the wavefunctions.

The integral in Eq. (14) is a three-dimensional integral and was evaluated numerically (see Appendix C). We assume that there is a fixed set of coordinate axes in each well. Each eigenfunction is referenced to the set of axes in its respective well. The "relative orientation" of the spherical wells is then just the relative orientation of these sets of axes (see Fig. 1). For any given calculation, well A is identified as fixed and the position of the second well is specified by the vector connecting the origins of the two systems. The three Euler angles give the rotation of the B-well coordinate system from a set of axes in well B which are parallel to those in well A (cf. Appendix D).

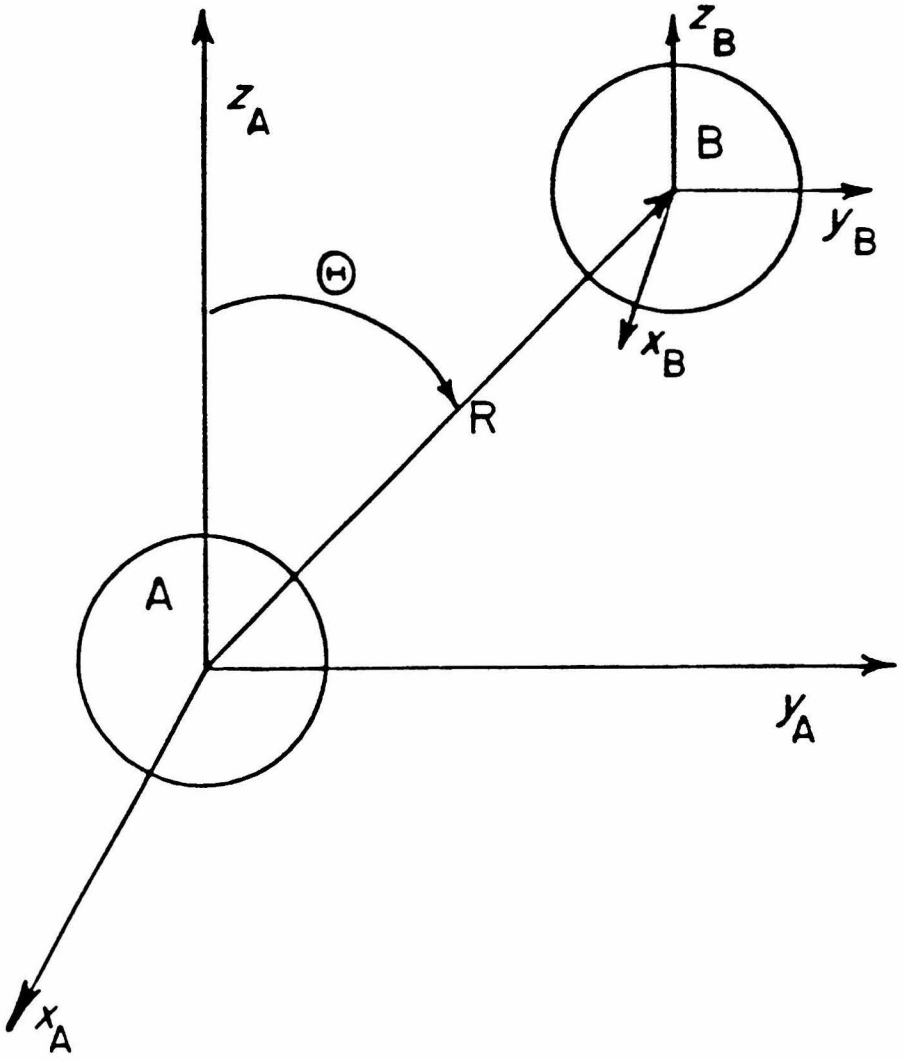

Fig. 1. Coordinate system used to specify the mutual orientation of wells A and B. The x-axes of the wells are assumed parallel and lie in the plane of the figure. For $\Theta = 0°$ the the z-axes of the wells lie along the same line.

IV. Results and Discussion of Calculations of H_{BA}

In this section five variables pertinent to the states of spherical wells are discussed in regard to their effects on the distance and orientation dependence of H_{BA}:

1. E, the binding energy of the electron at the site,
2. l and m, that is, the nodal structure of the wavefunctions,
3. r_0, crudely, the "size" of the molecule and therefore the molecular orbital considered,
4. the change in internuclear distance R between the wells, and
5. the orientation of the wells.

The discussion is not intended to be exhaustive; it is rather a survey of the qualitative effects of the above factors on T_{BA}. It is helpful at first to qualitatively examine the expression for H_{BA}. H_{BA} can be written in terms of ψ_A and ψ_B as

$$H_{BA} = -V_B \int_0^{r_0^B} \int_0^{\pi} \int_0^{2\pi} j_{l'}(k_i^B r_B) P_{l'}^{m'}(\theta_B) \Phi_{m'}(\varphi_B) k_l(k_o^A) P_l^m(\theta_A) \Phi_m(\varphi_A) \times r_B^2 \sin\theta_B dr_B d\theta_B d\varphi_B \quad (15)$$

where r_A, θ_A, and φ_A are implicit functions of r_B, θ_B, φ_B (see Appendix D). To a first approximation it can be seen that if the angular part of the integral remains approximately constant as a function of distance, the distance dependence of H_{BA} will arise predominantly from the radial portion; i.e.,

$$H_{BA} \approx -V_B C \int_0^{r_0^B} j_{l'}(k_i^B r_B) k_l(k_o^A r_A) r_B^2 dr_B. \quad (16)$$

From Eq. (16) it is apparent that H_{BA} should decay approximately exponentially with distance since the value of $r_B^2 j_{l'}(k_i^B r_B)$ at any point in

well B does not change as a function of R, but $k_l(k_o^A r_A)$ decays essentially exponentially with distance.

The orientation effects can be similarly analyzed by examining the form of the angular functions for a given (l,m) state. For spherically symmetric states there will be no dependence of T_{BA} on orientation. Consider, however, a state in well A with $l \neq 0$. The angle between R (cf. Fig. 1) and the positive Z axis in well A defines some $(\theta_A)_c$, around which the values of $P_l^m(\theta_A)$ are sampled in the integral for H_{BA}. As R increases in length at this $(\theta_A)_c$, the range of values of θ_A sampled decreases, as the solid angle subtended by well B at well A decreases. To see how this might affect H_{BA}, consider an $l=1, m=0$ state in each well for which $P_l^m(\theta_A) = \cos\theta_A$. For $(\theta_A)_c = 0$, $P_l^m((\theta_A)_c) = 1$, and values around $(\theta_A)_c$ are close to one. As R increases, and the range of θ_A sampled decreases, the values of $P_l^m(\theta_A)$ sampled in the integral become closer to one. Now consider $(\theta_A)_c = \pi/2$. $P_l^m((\theta_A)_c) = 0$ and as R increases the angles sampled in the integral approach $\pi/2$. Therefore, there is an extra decay with distance in the $(\theta_A)_c = \pi/2$ orientation induced by the angular part of the wavefunction. Specific cases are now considered quantitatively.

We first examine the lowest energy state for any V_0, having $l=m=0$. An expression for $H_{BA}(R)$ has been obtained[17] (cf. Chapter 3) and is given in Eq. (17).

$$H_{BA}(R) = -\frac{\hbar^2 A_0^2}{2m\alpha^2 R}\exp(-\alpha R). \tag{17}$$

m is the electron mass, A_0 a normalization constant, and $\alpha = [-2mE/\hbar^2]^{1/2}$. As expected, the rate decays approximately exponentially with distance, due to the fall-off of the radial wavefunctions outside their respective wells.

Eq. (17) also shows the behavior of H_{BA} as a function of orbital energy within the present model. As the electron becomes more tightly bound, α increases ($\alpha = (-2E)^{1/2}$); thus, H_{BA} will decrease. As with all square well models, the exponential decay constant for H_{BA} is proportional to $(-E)^{1/2}$. Interestingly, Eq. (17) shows no explicit dependence on the well size. This dependence is contained in the normalization constant A_0 which is a function of r_0 but it is interesting to note that changes in r_0 for a given E do not affect the rate of decay of H_{BA}. In fact, for two $l=m=0$ states, a change in r_0 merely amounts to a rescaling of $H_{BA}(R)$. This is easily understood by examining the form of H_{BA} in Eq. (15). This invariance of the rate of decay of T_{BA} for fixed l, m, and E also holds for higher l states.

Analytical expressions have been obtained for $l=1$, $m=0$ states in the two orientations $\Theta = 0°$ and $\Theta=90°$[17] (cf. Fig. 1). (Note the difference in notation between θ_A (θ_B) the azimuthal angle in the spherical polar coordinate system located at site A (B) and Θ, the orientational angle of Fig. 1. It is apparent that $\theta_A = \Theta$ for the present orientations.) For $\Theta = 0°$, $H_{BA}(R)$ is

$$H_{BA}(R) = \frac{3\hbar^2 A_1^2}{m\alpha^4 R^3}\left(1 + \alpha R + \frac{\alpha^2 R^2}{2}\right)\exp(-\alpha R). \tag{18}$$

For $\Theta = 90°$, $H_{BA}(R)$ is

$$H_{BA}(R) = \frac{-3\hbar^2 A_1^2}{2m\alpha^4 R^3}\left(1 + \alpha R\right)\exp(-\alpha R). \tag{19}$$

These expressions have a number of factors in common with that for $l=m=0$ states. First, the dependence on distance is still essentially exponential and the exponential decay constant is still proportional to

$(-E)^{1/2}$. The difference between Eqs. (18) and (19) and Eq. (17) occurs in the pre-exponential factor and is due to the angular functions $P_1^0(\theta) = \cos\theta$ of the $l=1, m=0$ wavefunctions. Most interesting is that H_{BA} for $\Theta = 90°$ has an extra factor of $1/R$ in the pre-exponential factor. Thus, it decays faster than H_{BA} for $\Theta = 0°$.This extra factor is due to the node in $P_1^0(\theta)$ at $\Theta=90°$, as outlined above.

Extrapolation of these results to higher l states is now reasonably straightforward. For the present model, the dominant decay will be exponential in the well separation distance and the exponential decay constant will be proportional to $(-E)^{1/2}$. The pre-exponential part of $H_{BA}(R)$ will decay at least as rapidly as $1/R$ depending on Θ and the nodal structure of the wavefunctions in question. Plots of H_{BA} vs. Θ at an edge-to-edge distance of 4Å are shown in Figs. 2 and 3 for $l=1, m=0$ and $l=5, m=4$ states respectively. The increased complexity of the $l=5, m=4$ results is mainly due to the $\Phi_4 = \cos4\varphi$ states used in each well, the overlap of which change quickly with Θ. It is apparent from these results that the assumption of a spherically symmetric H_{BA} for large molecules will generally be in error. The choice of an average value for H_{BA} may be sufficiently accurate for description of electron transfer between randomly distributed species, but for molecules which are rigidly oriented relative to one another serious errors can occur.

One interesting example of the effects of the nodal properties of the wavefunctions is found in comparing H_{BA} at fixed R for $\Theta = 0°$ and $\Theta = 90°$ as l increases for π-like states. That is, we consider H_{BA} for pairs of states such as $l=1, m=0$ states, $l=2, m=1$ states and so on ($l-m$ is the number of θ nodes occurring in P_l^m for θ between -1 and 1). As shown previously, H_{BA} is larger at $\Theta = 0°$ than at $\Theta = 90°$ for fixed R for

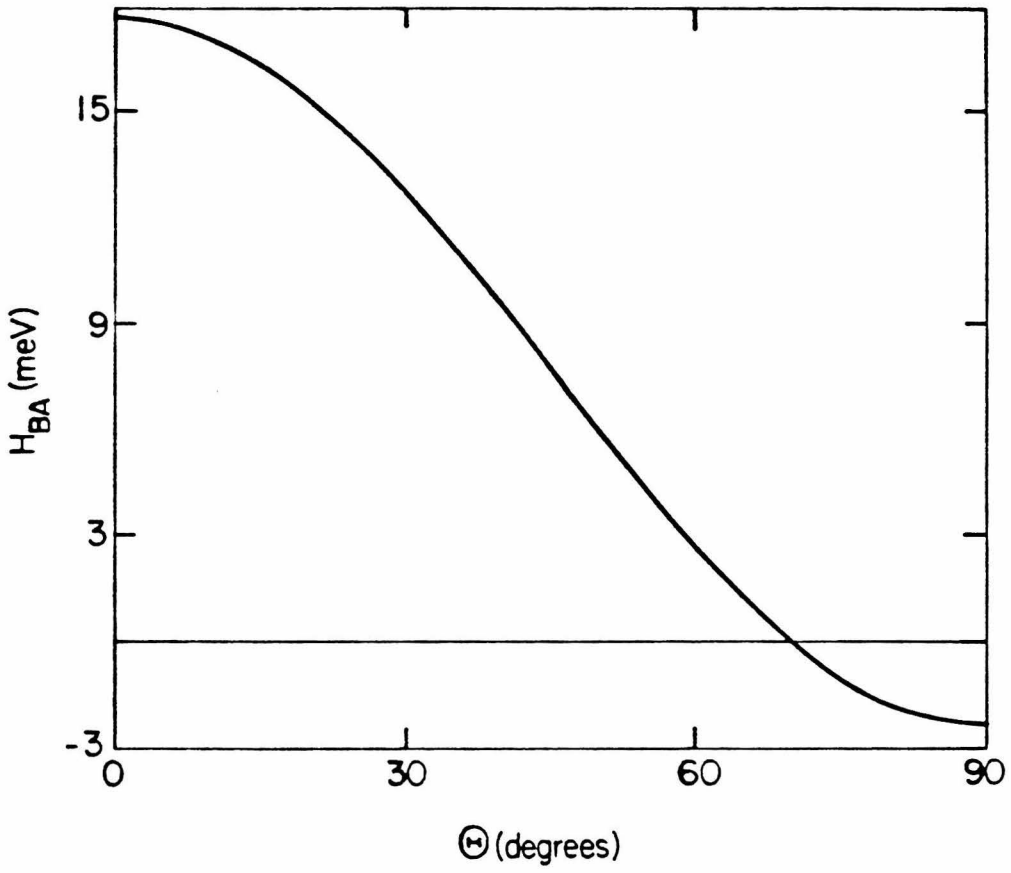

Fig. 2. The matrix element H_{BA} for two spherical wells as a function of Θ at R = 11.829Å (4Å edge-to-edge). For both states r_0 = 3.91448Å, l = 1, m = 0, V_0 = 4.19903eV, and E = −1.1525eV.

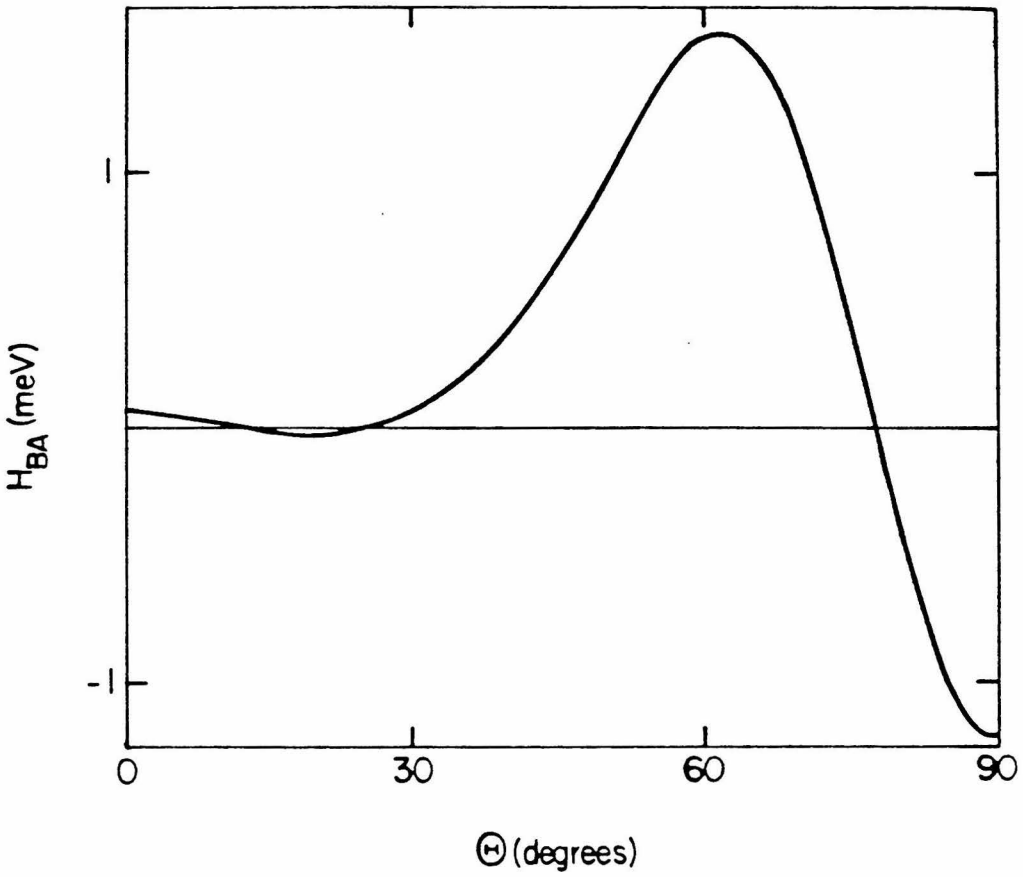

Fig. 3. The matrix element H_{BA} for two spherical wells as a function of Θ at R = 11.829Å (4Å edge-to-edge). For both states r_0 = 3.91448Å, l = 5, m = 4, V_0 = 18.0313eV, and E = −1.1525eV.

$l=1, m=0$ states since $P_1^0(\theta) = \cos\theta$ and $\theta_A = \Theta$. For $l=2, m=1$ states $P_2^1(\theta) = \sin\theta\cos\theta$ so that $P_2^1(\theta) = 0$ for both $\Theta = 0°$ and $\Theta = 90°$.[15] On this basis one would predict $H_{BA}(\Theta = 0°) = H_{BA}(\Theta = 90°)$, which is the case. H_{BA} for each of these angles decays more quickly than for all intermediate Θ. As a final example of this form of angle-dependence $l=5, m=4$ states are examined. For these states $P_5^4 = \sin^4\theta\cos\theta$, and the order of the zero in P_5^4 is much larger at $\Theta = 0°$ than that at $\Theta = 90°$. One would therefore expect $H_{BA}(R)$ for $\Theta = 0°$ to be much smaller than $H_{BA}(R)$ for $\Theta = 90°$. Fig. 4 shows that this is the case.

In addition to this behavior with Θ, Fig. 3 also exhibits several zeros as a function of Θ. This is due to a cancellation of positive and negative contributions to the overlap in well B and increases in frequency with increasing m. Since increasing m yields more nodes in ψ, this increase in the number of zeros of H_{BA} with m is not surprising.

It is of interest to ask how a change in energy of the states examined will affect the orientation dependence of H_{BA}. The orientation dependence will not be qualitatively affected by a change in orbital energy. Since the angular nodal structure is independent of energy one would expect the effects seen previously to be relatively general. It is reasonable, however, to expect some differences in relative values at two given orientations as a function of energy. The large R ratio of Eqs. (18) and (19) exemplifies this point, since as α increases the ratio of $H_{BA}(\Theta = 0°)$ to $H_{BA}(\Theta = 90°)$ increases for $l=1, m=0$ states. This effect is due to the increased decay of the radial function which inhibits contribution from non-θ=90° portions of the angular wavefunction. However, it is a second-order type of effect which should not be important for the energy ranges of interest to the present model. An example of this is shown in Fig. 5.

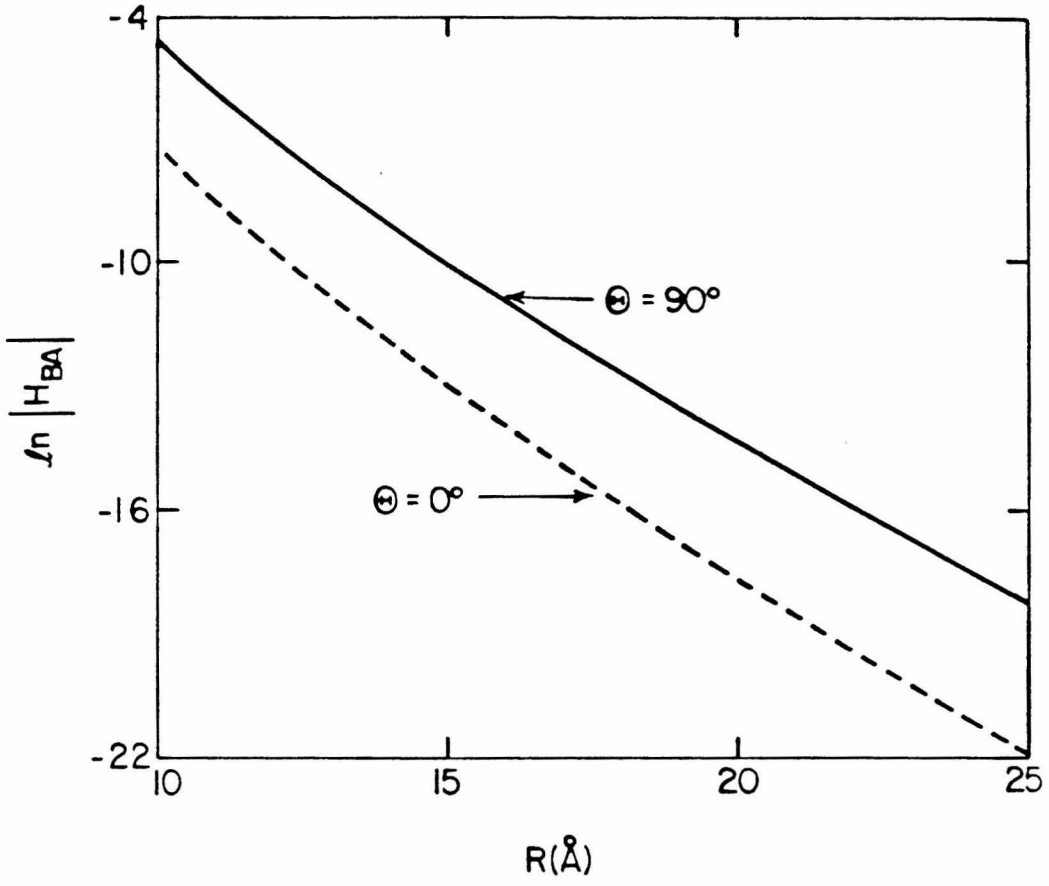

Fig. 4. ln $|H_{BA}|$ for two spherical wells as a function of R for $\Theta = 0°$ and $\Theta = 90°$. For both states $r_0 = 3.91448$Å, $l = 5$, $m = 4$, $V_0 = 18.0313$eV, and $E = -1.1525$eV.

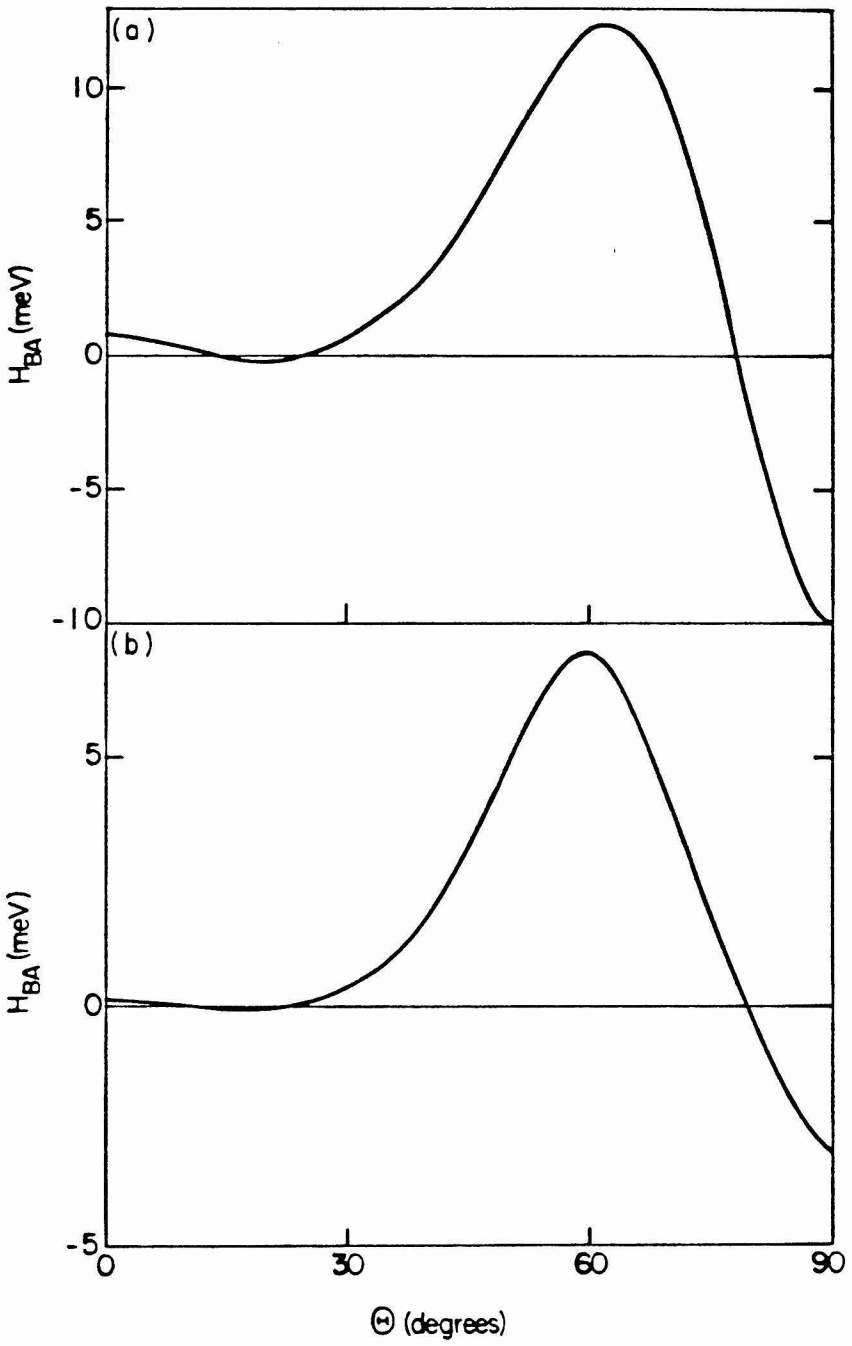

Fig. 5. The matrix element H_{BA} for two spherical wells as a function of Θ at R = 10Å. In both a) and b) r_0 = 3.91448Å, l = 5, and m = 4. In a) V_0 = 18.0313eV and E = −1.1525eV. In b) V_0 = 23.5303eV and E = −6.0001eV.

There, $H_{BA}(\Theta)$ is plotted for two different sets of energies. While there is a significant change in the size of H_{BA} it is rather uniform, thus preserving the shape of the curves.

V. Extensions

The above discussion points up the salient features we have examined in the calculations of H_{BA} using spherical wells. One could use such calculations as possible models of the electronic coupling in electron transfer events for weakly coupled systems. This spherical model may be appropriate to single atomic species, such as transfer between two metal atoms, or carbon atoms within a chain (of course, this requires the validity of the one-electron model). Such cases have also been modeled using Extended Hückel-type methods, where the interaction is taken as directly proportional to the overlap between the two wavefunctions. Our major interest is in examining biological and biominetic electron transfer events, say between pairs of porphyrins or between porphyrins and quinones. Such molecules are quite nonspherical however; thus, the model of the following chapter was developed. It uses potential wells of oblate-spheroidal shape. Nevertheless, many of the trends observed for the spherical wells carry over for obvious reasons. The value of H_{BA} still decays largely exponentially with distance and the exponential decay constant at large distances is proportional to $(-E)^{1/2}$. The oblate-spheroidal wavefunctions can be envisioned as arising from a continuous deformation of the spherical wavefunctions in the cases of interest to biological electron transfers and thus all the angular nodal function arguments carry over as before.

The major difference between the spherical and spheroidal cases is

due to the effect of the nonspherical potential shape on the decay distance of wavefunction A in the calculation of H_{BA}. At a given center-to-center distance between two spheroidal wells the edge-to-edge distance can change drastically as the orientation of the wells changes. Since the wavefunctions decay exponentially outside the wells, the shortest edge-to-edge separations will result in the largest values of H_{BA}, all other effects being equal. This aspect is discussed in the following chapter.

Appendix A: Calculation of $P_l^m(\theta)$, $j_l(r)$, and $k_l(r)$

These special functions were calculated using standard recursion relations.[15] The relations and error checking methods are summarized here.

The Associated Legendre polynomials obey the recursion relation

$$P_{l+1}^m(x) = \frac{\left[(2l+1)xP_l^m(x) - (l+m)P_{l-1}^m(x)\right]}{(l-m+1)} \tag{A1}$$

where, in the present case, $x = \cos\theta$. The procedure begins with $P_m^m(x) = \sin^m(\theta)$, $P_{m-1}^m = 0$ and recurs upwards to obtain the desired $P_l^m(\theta)$. The program used calculated the above in double precision arithmetic. Error accumulation was estimated using standard methods via the expression

$$R_{l+1} = \frac{\left[|(2l+1)xA_l| + |(l+m)A_{l-1}|\right]}{(l-m+1)|P_{l+1}^m|} \tag{A2}$$

where R_{l+1} is the relative error in P_{l+1}^m and A_n is the absolute error in P_l^m. The initial value of P_m^m was assumed to be accurate to 14 places and R_{l+1} checked at each recursion to be less than 10^{-7}. If this tolerance was exceeded, a parallel quadruple precision routine was called, thus extending the range of allowed P_l^m. In calculations for spherical wells the double precision routine was always sufficient, as the l values required were universally less than seven. For the spheroidal case higher l values were required and the quadruple precision routine was needed.

The calculation of the $j_l(k_i r)$ used the recursion relation

$$j_{l+1}(k_i r) = \frac{(2l+1)}{k_i r} j_l(k_i r) - j_{l-1}(k_i r) \tag{A3}$$

with error analysis computed analogously to that in Eq. (A2). For the spherical Bessel functions of the first kind recursion is stable when recurring downward. For some large N it is assumed that $j_{N+1} = 0, j_N = \varepsilon$ where ε is small and the recursion relation of Eq. (A3) is used to obtain the j_l of interest. Convergence is checked by incrementing N and redoing the calculation. Normalization is obtained by comparison with the easily calculated value of $j_0(k_i r)$. Again, the spherical calculations only required a double precision version of the routine but, due to the larger number of j_l's required, the spheroidal code was converted to quadruple precision.

Finally, the modified spherical Bessel functions of the second kind were calculated recurring upwards using the relation

$$k_{l+1}(k_o r) = -\frac{(2l+1)}{k_o r}\left[k_l(k_o r) + k_{l-1}(k_o r)\right]. \tag{A4}$$

In this case, $k_0(k_o r)$ and $k_1(k_o r)$ are known and since recursion is stable upwards there is no need for convergence checks on normalization. No numerical error accumulation checks were used.

Appendix B: Eigenenergy Computation

The solution of Eq. (12) of Chapter 2 must be obtained numerically due to the complicated nature of the functions involved. The procedure used is discussed here.

All functions are assumed to be evaluated at r_0; therefore, the r dependence of all functions will be neglected here. Rewriting Eq. (12) one obtains

$$\frac{1}{j_l(E)}\frac{d}{dr}j_l(E) - \frac{1}{k_l(E)}\frac{d}{dr}k_l(E) = 0 \ . \tag{B1}$$

The energy eigenvalue sought yields satisfaction of Eq. (B1). Since all functions are continuous functions of E a binary search procedure was used as a coarse technique for approximately locating the eigenvalues. In the binary search procedure Eq. (B1) is calculated at many closely spaced points. An E_0 which satisfied Eq. (B1) occurs between any two points between which there is a sign change. This approximate E is then used as an initial guess and Newton's method is employed to obtain a rapidly convergent value of E.

Newton's method[19] is a technique for obtaining the fixed point of the equation

$$g(x) = x - \frac{f(x)}{f'(x)} \tag{B2}$$

The fixed point, where $g(s)=s$, can occur only for $f(x)=0$.[19] Choosing $f(x)$ to be Eq. (B1) and using the initial guess obtained from the binary search procedure eigenvalues are easily obtained. One sets $g(x_n) = x_{n+1}$ and iterates to a desired degree of accuracy. Since the eigenvalues of the spherical wells are reasonably well spaced for a given l, one can fre-

quently bypass the binary search procedure. Newton's method was also used in Chapters 5 and 6 where again the roots of noninvertible equations were required.

Appendix C: Numerical integration scheme

The integral sought is that for H_{BA}

$$H_{BA} = -V_0^B \int_0^{r_0^B} \int_0^{\pi} \int_0^{2\pi} \psi_A(r,\theta,\varphi)\psi_B^*(r,\theta,\varphi) r^2 \sin\theta \, dr \, d\theta \, d\varphi. \qquad \text{(C1)}$$

The integral is over well B, and r, θ, and φ are assumed referenced to the center of well B. ψ_A is written as an explicit function of the coordinates of well B. For all but the simplest cases H_{BA} is not available in closed form. Therefore, numerical integration schemes were used to obtain H_{BA}.

A variety of techniques could be used such as the trapezoidal rule, Simpson's rule, each over subintervals of the region of interest of each integration variable in Eq. (C1). We chose to use Gaussian-Legendre quadrature, assuming that the integrand would be at least partially oscillatory.

For functions defined on the interval $[-1,1]$ the quadrature formula

$$\int_{-1}^{1} f(x)dx \approx \sum_{j=0}^{n} A_j f(x_j) \qquad \text{(C2)}$$

is exact if f is a polynomial of order $2n+1$ or less, when the x_j are the zeros of the orthogonal polynomial of order $n+1$ on $[-1,1]$, and the A_j are suitably chosen (tabulated) weighting factors.[19] The orthogonal polynomials on $[-1,1]$ are the Legendre polynomials, hence the name Gaussian-Legendre quadrature. When $f(x)$ is not a polynomial in x the value of the r.h.s. of Eq. (C2) can be shown to approach the l.h.s. as $n \to \infty$.[19]

Frequently, the region of integration is other than $[-1,1]$. In this case the region $[-1,1]$ is linearly mapped onto the region of interest,

$[a,b]$ via

$$x = \left[\frac{b-a}{2}\right]u + \frac{(b+a)}{2} \tag{C3}$$

where u is in the region [-1,1] and x is in the region $[a,b]$. Eq. (2) becomes

$$\int_a^b f(x)dx = \frac{(b-a)}{2}\int_{-1}^{1} g(u)du \approx \frac{(b-a)}{2}\sum_{j=0}^{n} A_j g(u_j) \tag{C4}$$

where $g(u) = f(x(u))$.

Finally, in the case of multidimensional integrals, integration over each variable was performed using Gaussian-Legendre formulae in a nested expression as in Eq. (C5).

$$H_{BA} \equiv \int_0^{r_0^B}\int_0^{\pi}\int_0^{2\pi} F(r,\theta,\varphi)dr d\theta d\varphi = \frac{r_0^B \pi^2}{4}\sum_{j=0}^{n_1}\sum_{k=0}^{n_2}\sum_{l=0}^{n_3} A_j A_k A_l G(u_j,v_k w_l). \tag{C5}$$

The number of integration points in such an expression equals $n_1 \times n_2 \times n_3$, and thus increases rapidly with the n_i. However, convergence to three places in H_{BA} could be obtained with an average of 10–15 points per dimension.

Occasionally, there was a need to calculate integrals over infinite ranges, such as the radial part of an overlap integral. In this case a similar scheme, Gaussian-Laguerre quadrature can be used. The Laguerre polynomials are orthogonal polynomials defined in $[0,\infty]$ and the integrand weighting function is a decaying exponential, which is convenient due to the decaying nature of the radial wavefunctions outside the wells.

Appendix D: Coordinate transformation between spheres

In defining the relative orientation of the two wells, well A was assumed fixed, its center located at the origin of a set of coordinate axes denoted (X_A, Y_A, Z_A). The center of well B is translated by the distance (X_0, Y_0, Z_0) relative to the origin of coordinate system A. Well B also has a local set of coordinate axes, the origin of which is located at the center of well B. The orientation of these axes relative to those in well A are defined by the Euler angles[20] (α, β, γ) as rotations relative to a set of axes centered at well B which are parallel to those of well A.

In performing an integral over well A, a point $(r_A, \theta_A, \varphi_A)$ in well A is generated by the numerical integration routine. Ψ_A can be immediately evaluated. To evaluate Ψ_B one needs the coordinates of this point relative to the coordinate axes of well B, which are the natural axes for Ψ_B. The steps followed to obtain the coordinates of the point are:

1. Convert $(r_A, \theta_A, \varphi_A)$ to Cartesian coordinates $\equiv (X_A, Y_A, Z_A)$.

2. Obtain the coordinates of (X_A, Y_A, Z_A) in the coordinate system of well B parallel to that in well A by

$$\begin{aligned} X_B &= X_A - X_0 \\ Y_B &= Y_A - Y_0 \\ Z_B &= Z_A - Z_0. \end{aligned}$$

3. Obtain the coordinates in the rotated coordinate system in well B by multiplying the vector (X_B, Y_B, Z_B) by the Eulerian rotation matrix.[20]

4. Convert (X'_B, Y'_B, Z'_B) into the appropriate spherical polar coordinates of well B, $(r_A, \theta_A, \varphi_A)$.

When performing integrals over the mobile well, well B, the coordinates of a point in well B can be obtained relative to the coordinate system in well A by reversing the above four steps.

References

1. D. DeVault, Q. Rev. Biophys. **13,** 387 (1980).

2. N. Sutin, Prog. Inorg. Chem. **30,** 441 (1983).

3. V. G. Levich, in *Physical Chemistry: An Advanced Treatise*, Vol. IX, H. Eyring, D. Henderson, and W. Jost, eds. (Academic, New York, 1970), p. 986.

4. G. Binnig and H. Rohrer, Helv. Phys. Acta, **55,** 726 (1982).

5. R. P Feynmann, *The Feynmann Lectures on Physics, Vol. III* (Addison-Wesley, Reading, 1965), Chapter 10.

6. M. D. Newton, Int. J. Quantum Chem.: Quantum Chem. Symp. **14,** 363 (1980).

7. D. Rising, A. F. Voter and W. A. Goddard, unpublished results.

8. J. D. Petke and G. M. Maggiora, Chem. Phys. Lett. **97,** 231 (1983).

9. J. R. Bardeen, Phys. Rev. Lett. **6,** 57 (1961).

10. D. N. Beratan and J. J. Hopfield, J. Am. Chem. Soc. **106,** 1584 (1984).

11. S. Larsson, J. Phys. Chem. **88,** 1321 (1984).

12. C. Cohen-Tannoudji, B. Diu, and F. Laloe umlaut, *Quantum Mechanics* (Wiley, New York, 1977).

13. B. Brocklehurst, J. Phys. Chem. **83,** 536 (1979).

14. L. I. Schiff, *Quantum Mechanics*, 3rd ed. (McGraw Hill, San Francisco, 1968), p. 83.

15. G. Arfken, *Mathematical Methods for Physicists*, 2nd ed. (Academic, San Francisco, 1970).

16. I. S. Gradshteyn and I. M. Ryzhik, *Tables of Integrals, Products, and Series* (Academic, New York, 1980).

17. P. Siders, R. J. Cave, and R. A. Marcus, J. Chem. Phys. **81,** 5613 (1985).

18. J. V. Beitz and J. R. Miller, J. Chem. Phys. **71,** 4579 (1979).

19. L. W. Johnson and R. D. Riess, *Numerical Analysis* (Addison-Wesley, Reading, 1977), p. 129.

20. J. B. Marion, *Classical Dynamics of Particles and Systems* (Academic, New York, 1970), p. 384.

Chapter 3

A Model for Orientation Effects in Electron Transfer Reactions

I. Introduction

The mutual orientation of the donor and acceptor in an electron transfer reaction may have observable effects on the electron transfer rate in certain systems. For example, the primary photoinduced electron transfer in photosynthetic reaction centers may be influenced by the orientation of the reactants. In plant photosystem II the electron acceptor is probably a pheophytin[1,2] and the donor may be a substituted chlorophyll *a* monomer.[2,3] Both of these molecules are large and nonspherical, suggesting that there may be one or more preferred orientations for electron transfer. Another biologically important electron transfer, that between hemes in cytochromes, may also depend on the mutual orientation of the porphyrin rings of the hemes.[4]

Orientation effects are beginning to be examined experimentally in model systems. For example, electron transfer between cofacial porphyrins has been studied and was observed to be rapid.[5,6] Systems involving porphyrins held in other orientations are under study.[7] In these systems the electron transfer is between sites that are chemically linked. When the pi-type orbitals at the donor and acceptor sites are largely electronically independent, the electron transfers may be treated using the usual outer-sphere formalism. It is with systems such as these in mind that we have set out to develop a model theoretical system within which to examine the nature and magnitude of orientation effects on electron-transfer rates.

The rate constant for nonadiabatic electron transfer between reactants A and B at fixed separation and orientation has been examined within the Golden Rule formalism; e.g.,[8-10]

$$k = \frac{2\pi}{\hbar} |T_{BA}|^2 \; F.C. \tag{1}$$

The Franck-Condon sum (here denoted F.C.) has been discussed in detail elsewhere, e.g..[10-12] In this paper we consider the dependence, within the theoretical model described below, of the electronic matrix element T_{BA} on the mutual orientation and separation distance of A and B.

The matrix element T_{BA} depends on the electronic wavefunctions localized on sites A and B. An isolated electronic site A or B (at infinite separation, say) is modeled in this paper as an oblate spheroid, and the potential for the electron is set equal to a negative constant inside the well and zero outside. It may be recalled that an oblate spheroid can be obtained by rotating an ellipse about its minor axis.

The volume of the spheroidal potential well is supposed to enclose the carbon skeleton of an aromatic system. The circle of revolution generated by the major axis when the spheroid is rotated about its minor axis is imagined to lie in the plane of the carbon skeleton. Other models have similarly exploited the delocalized character of the pi electrons in aromatic systems. In the Free Electron Molecular Orbital model[13] for example, the electron is free to move in one dimension on a ring or intersecting rings, but has zero probability density off the ring. In another model introduced by Schmidt[14] and developed by Platt[15] to calculate electron densities and electronic spectra of aromatics, the electron is free to move in a plane in a region bounded by infinite potential walls. In contrast, in the present paper the electronic wavefunction is three-dimensional and is not confined to a well, because the potential used is finite. The wavefunctions therefore have long-range tails which are important in describing electron transfer.

The present model yields a predominantly exponential dependence of the rate on separation distance, a dependence used or found in various

experimental studies.[16] The molecular basis of this model may actually be an exchange mechanism involving orbitals of adjacent molecules or atoms.[17]

There have been previous discussions of orientation effects in the context of the tunneling of trapped electrons in glassy matrices. Rice et.al.[18] considered orientation effects in a qualitative way, and concluded that orientation dependence in the electron tunneling rate would be equivalent to a reduced concentration of electron acceptors, and thereby reduce the tunneling relative to an analogous system with no orientation dependence. Brocklehurst[19] examined the orientation dependence of the overlap of electronic wavefunctions for spherically symmetric sites. He considered both hydrogenic and spherical-well potentials. The electronic matrix element was assumed by Brocklehurst to be proportional to the overlap of the wavefunctions, an approximation which we consider using states of spherical wells in Appendix B. He concluded that the orientation effect on the electron-transfer rate constant can be as large as 10^3. Doktorov et al.[20] considered an angular factor, $\cos^n\Theta$, in the unimolecular rate constant for electron tunneling between spherical sites. For $n \leq 4$ the effect of this angular dependence was to reduce the overall rate constant. The present paper considers sites that are asymmetric which presumably better represent the shapes of the aromatic systems toward which this study is aimed.

Spectral properties of porphyrin compounds have been examined by numerous workers using semi-empirical electronic structure methods.[21] *Ab initio* techniques have also been used to examine porphyrin electronic structure.[22,23] Calculations on diporphyrin systems and their low-lying charge transfer states have been reported recently.[24] Electronic struc-

ture techniques have been used to study orientation and distance effects for a model transition metal redox pair[25] as well as for face-to-face porphyrins at small separation distances using both semi-empirical and *ab initio* methods.[26,27] For porphyrin electron transfers *ab initio* calculations of the electronic matrix element are extremely lengthy. Moreover, *ab initio* techniques which employ Gaussian basis functions are better suited to describe wavefunctions inside molecules than to depict the long-range tails of the wavefunctions. While our model is significantly less detailed than that on which these wavefunctions are based, the present aim is to include the general features of the problem. In fact, it is the simplicity of the model which facilitates the calculations presented here.

The paper is organized as follows. In Sec. II the model for the potential and the wavefunctions used are briefly described, the calculation of the electron transfer matrix element is outlined, and results from calculations of the matrix element are presented. In Sec. III a more detailed description of the calculation of the single-site wavefunctions is given. The results for the electron transfer matrix element calculations are discussed in Sec. IV. Concluding remarks are given in Sec. V. The relation between the Golden-Rule rate expression and the matrix element is given in Appendix A. Expressions for the matrix element for states of spherical wells are derived in Appendix B. Applications to molecules of experimental interest will be presented in a subsequent article.

II. Wavefunctions and Results

A. The model

The model involves the interaction of two sites, labeled A and B (e.g.,molecules or electronically isolated chromophores). The single-site wavefunctions are taken to be one-electron wavefunctions; that is, only

the transferable electron is considered explicitly. The potential in which the electron moves is modeled as an oblate spheroidal well. A cross section of the potential is sketched in Fig. 1. The potential is independent of φ, the angle of rotation about the z axis. The cross section is an ellipse having semi-major axis a, semi-minor axis b, and eccentricity $e \equiv \sqrt{1 - b^2/a^2}$. The potential V is zero outside the well and has a constant negative value inside. Actually, there will also be a Coulombic term when the molecule is charged,[28] but it is assumed, for the present, that in a medium with some polarity this contribution is small relative to the values of V_0 used below.

It is convenient to use oblate spheroidal coordinates (ξ, η, φ), defined by

$$x = \frac{1}{2}d[(1 + \xi^2)(1 - \eta^2)]^{1/2} \cos \varphi \,, \quad y = \frac{1}{2}d[(1 + \xi^2)(1 - \eta^2)]^{1/2} \sin \varphi \,,$$
$$z = \frac{1}{2}d\xi\eta \quad , \tag{2}$$

where $0 \le \xi, \; -1 \le \eta \le 1 \,, \; 0 \le \varphi \le 2\pi$. The scale factor d has been chosen so that the surface of the potential well is described by the single radial-like coordinate ξ. With $d = 2\sqrt{a^2 - b^2}$, V is defined as

$$V = \begin{cases} -V_0 \,; & \xi \le \xi_0 \equiv 2b/d \\ 0 \,; & \xi > \xi_0 \end{cases} \quad . \tag{3}$$

Contours of the coordinate system are presented in Fig. 2. (The angular coordinate φ, not shown, is defined as for spherical coordinates.) The surface $\xi = 0$ is a disc of diameter d. The surface $\eta = 0$ is the xy plane minus this disc.

Spherical coordinates r and θ are given in terms of oblate spheroidal coordinates :

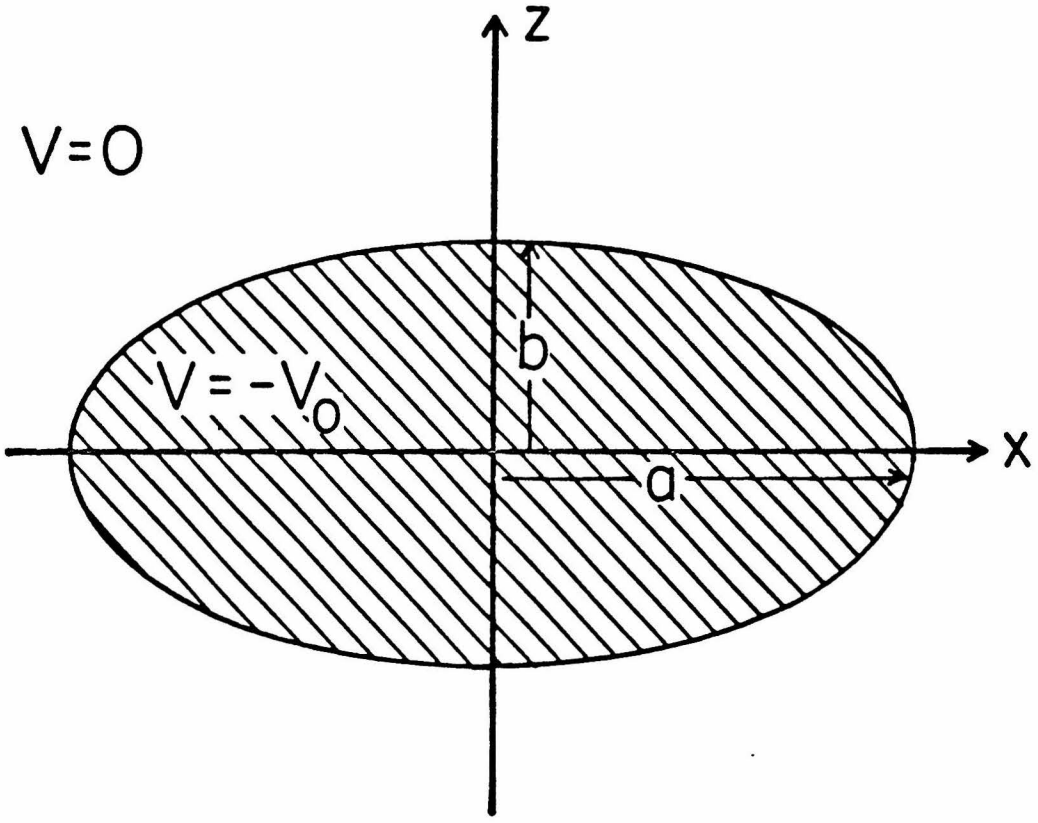

Fig. 1. Potential well for a single site. There is cylindrical symmetry about the z axis.

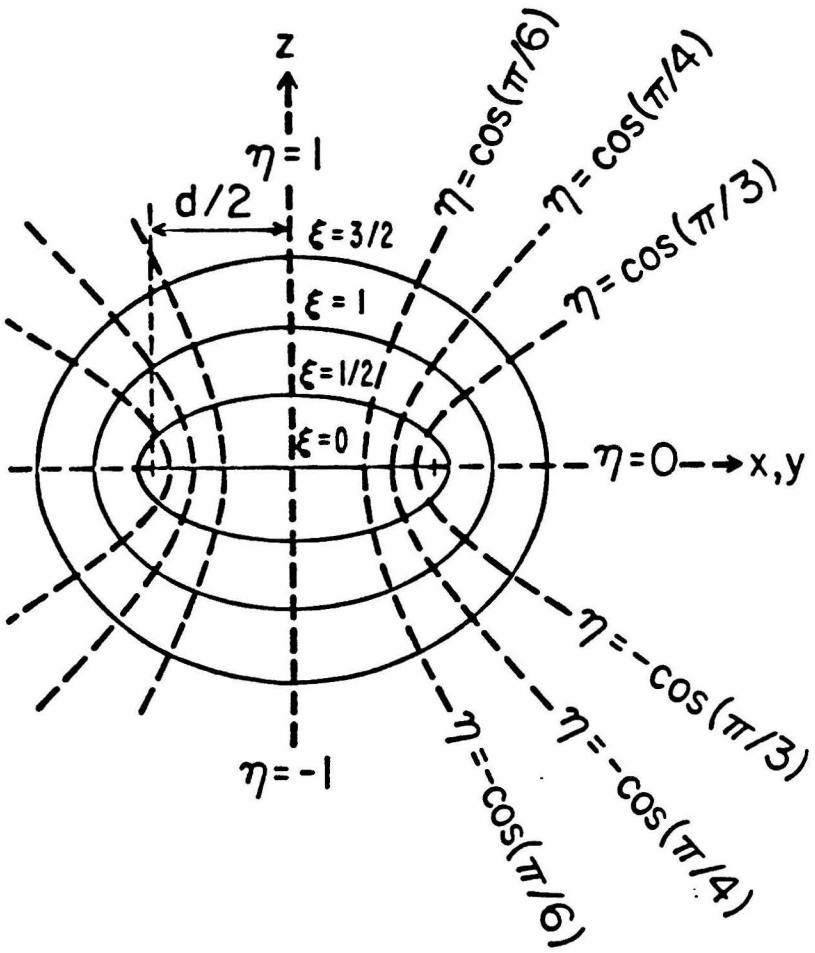

Fig. 2. Oblate-spheroidal coordinate system. Contours of constant ξ are indicated by solid lines. The dashed lines are contours of constant η. The contours of constant η on the right are for $\varphi = 0$, on the left for $\varphi = \pi$.

$$r = \frac{d}{2}(1 + \xi^2 - \eta^2)^{\frac{1}{2}}, \quad \cos\theta = \xi\eta(1 + \xi^2 - \eta^2)^{-\frac{1}{2}} . \tag{4}$$

It is clear that the oblate spheroidal coordinates become spherical coordinates at asymptotically large distances from the potential, in the sense that $\xi \to 2r/d$ and $\eta \to \cos\theta$ as $r \to \infty$.

The single-site wavefunctions sought are bound-state solutions to the Schrodinger equation with the potential of Eq. (3). The Schrodinger equation may be written as a pair of Helmholtz's equations, one satisfied inside the well and one outside, i.e.,

$$(\nabla^2 + k^2)\Psi = 0 \tag{5}$$

with $k^2 = 2m(E + V_0)/\hbar^2$ when $\xi \leq \xi_0$ and $k^2 = 2mE/\hbar^2$ when $\xi > \xi_0$, m being the electronic mass. The value of V_0 affects the eigenvalue E and hence controls the rate of decay of the wavefunction with distance and ultimately the decay of the thermal matrix element.

In Sec. III it is shown that the wavefunction may be written as

$$\Psi_{mtu} = \begin{cases} \Psi^i_{mtu}(\xi,\eta,\varphi) \equiv A_{mtu} \sum_{r=0}^{\infty} C^i_n \psi^i_{mn} \; ; \; \xi \leq \xi_0 \\ \Psi^o_{mtu}(\xi,\eta,\varphi) \equiv A_{mtu} \sum_{r=0}^{\infty} C^o_n \psi^o_{mn} \; ; \; \xi \geq \xi_0 \end{cases} \tag{6}$$

$$n = 2r + m + s \quad .$$

The value of s determines the parity of the wavefunction relative to the xy plane of the potential, Ψ_{mtu} being even when $s = 0$ and odd when $s = 1$. The superscript i or o denotes the wavefunction inside or outside the well, respectively.

The functions ψ^i_{mn} and ψ^o_{mn} are solutions of the Schrodinger equation in oblate spheriodal coordinates when the potential is a constant over all space and is equal to its inner or outer value, respectively. Quantization

in the case of a finite depth well is accomplished by requiring continuity of the wavefunction Ψ_{mtu} and its derivative at the boundary, i.e., at $\xi = \xi_0$.

The functions $\psi^{i,o}_{mn}$ are separable in oblate spheroidal coordinates and may be written as

$$\psi^{i}_{mn}(\xi,\eta,\varphi) = R^{i}_{mn}(\xi;k_i^2)\, S^{i}_{mn}(\eta;k_i^2)\, \Phi_m(\varphi), \quad \xi \le \xi_0 \tag{7a}$$

$$\psi^{o}_{mn}(\xi,\eta,\varphi) = R^{o}_{mn}(\xi;k_o^2)\, S^{o}_{mn}(\eta;k_o^2)\, \Phi_m(\varphi), \quad \xi \ge \xi_0. \tag{7b}$$

$\Phi_m(\varphi)$ may be written as a linear combination of $\sin m\varphi$ and $\cos m\varphi$ and the number of nodes in $\Phi_m(\varphi)$ is equal to $2m$. The index n has been chosen to have the possible values $n = m, m+1, m+2\ldots$.

The quantum numbers t and u in Eq. (6) will be described as follows: t is the number of nodal lines in the two-dimensional $\xi\eta$ subspace and u orders states of equal t by energy (u = 1,2,...). At fixed V_0, a, and b, a wavefunction can usually be specified using m, t, and u. (Near an avoided crossing the nodal lines become increasingly complicated, however. When the nodal structure is not too distinct one could simply use m and a parameter which orders states of the given m by energy.)

Contour plots of wavefunctions for several states having m=0 are shown in Figs. 3-5. Energy levels[29] for several states are shown in Fig. 6 as a function of eccentricity at constant volume for the infinite potential case (Fig. 6a) and for V_0 = 10 eV (Fig. 6b). Energy levels are shown as a function of V_0 in Fig. 7.

For calculations of T_{BA} most of the states we have studied have one nodal line in the $\xi\eta$ subspace (i.e., t = 1) and s = 1. Such wavefunctions provide the closest analog to $2p\,\pi$ electron systems, s = 1 being appropriate to π-like symmetry, since these functions are odd with respect to the xy plane. For simplicity we will use the notation (m,π) to denote a state

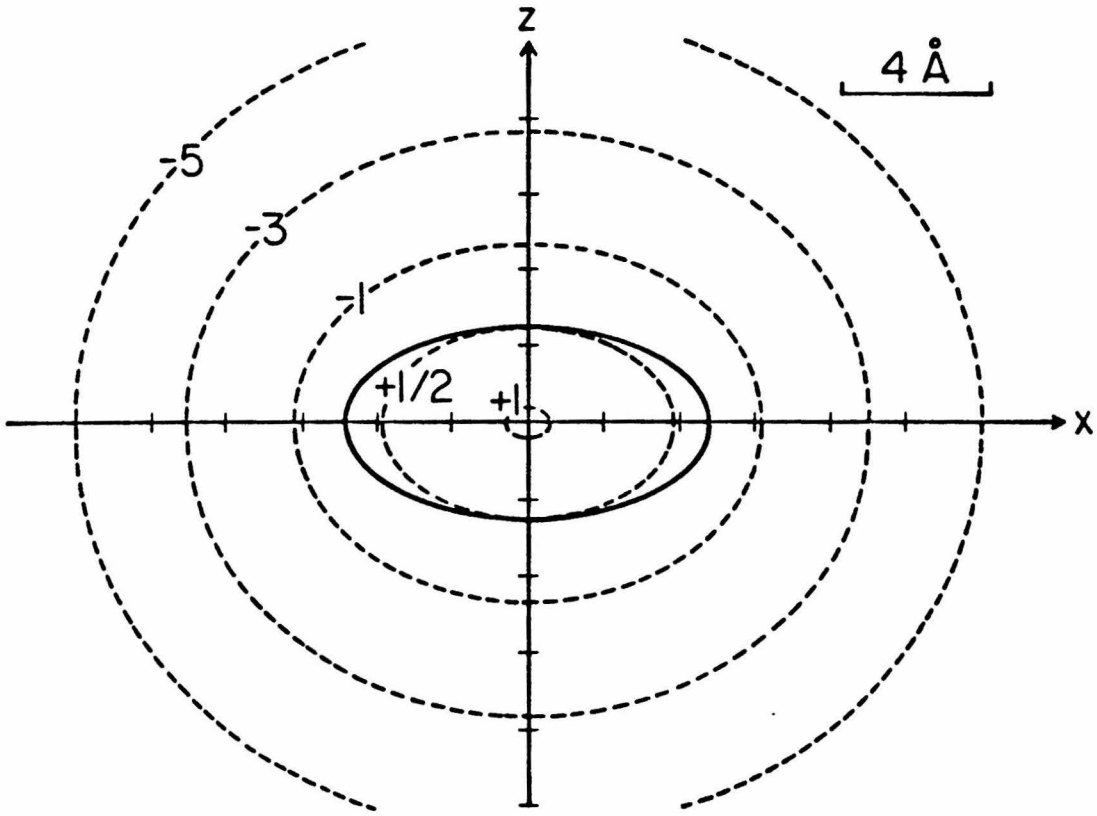

Fig. 3. Contours of Ψ for a state with $(m,t,u) = (0,0,1)$, $V_0 = 10$ eV, $E = -7.98$ eV, $a = 4.85$ Å, $b = 2.55$ Å. The heavy line is the well boundary. The contours are labeled with values of $\log_{10} |\Psi|$. This state is referred to later as a $(0,\sigma)$ state.

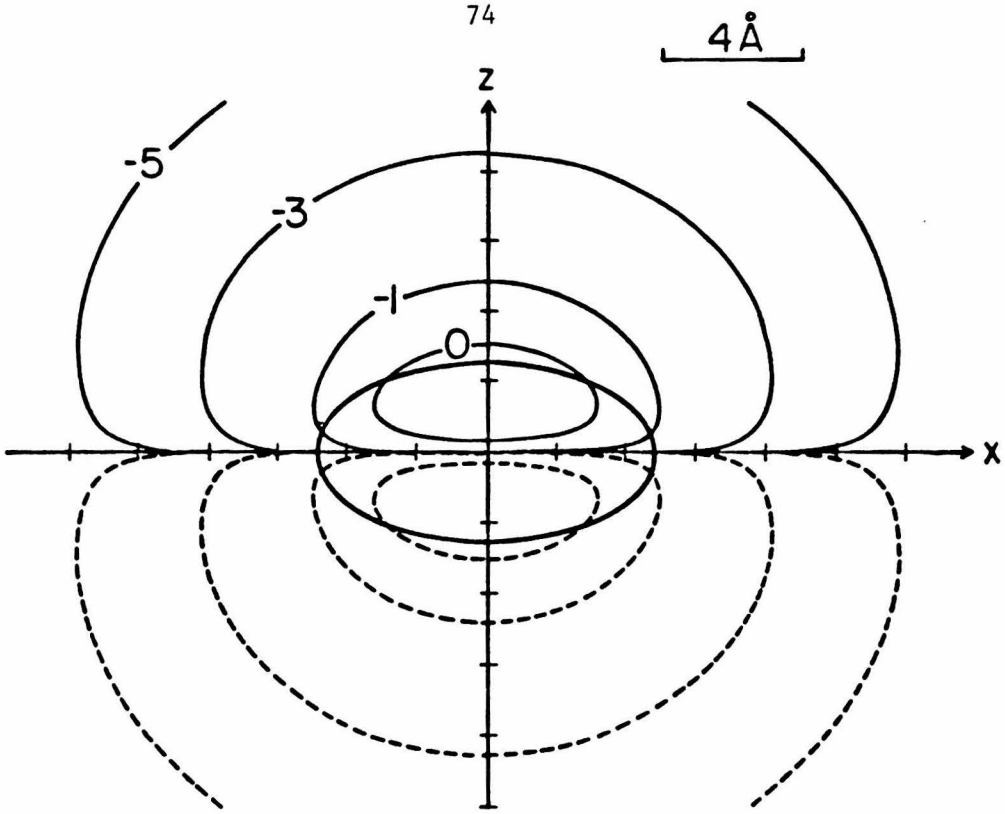

Fig. 4. Contours of Ψ for a state with $(m,t,u) = (0,1,1)$. a, b and V_0 are as in Fig. 3. E = -4.70 eV. The heavy line is the well boundary. The contours are labeled with values of $\log_{10} |\Psi|$. Dashed contours indicate $\Psi < 0$. Solid contours are for $\Psi > 0$. This state is referred to later as a $(0,\pi)$ state.

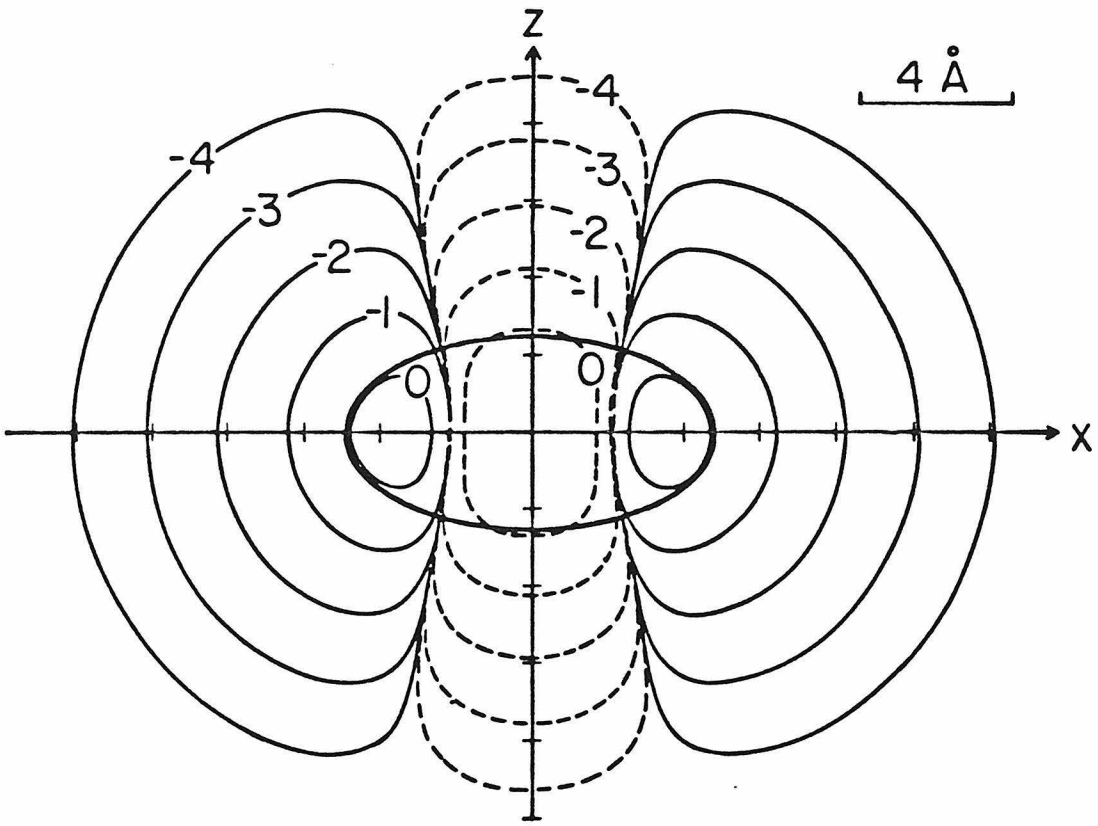

Fig. 5. Contours of Ψ for a state with $(m,t,u) = (0,1,2)$. a, b and V_0 are as in Fig. 3, E = -4.44 eV. The various lines are as in Fig. 4.

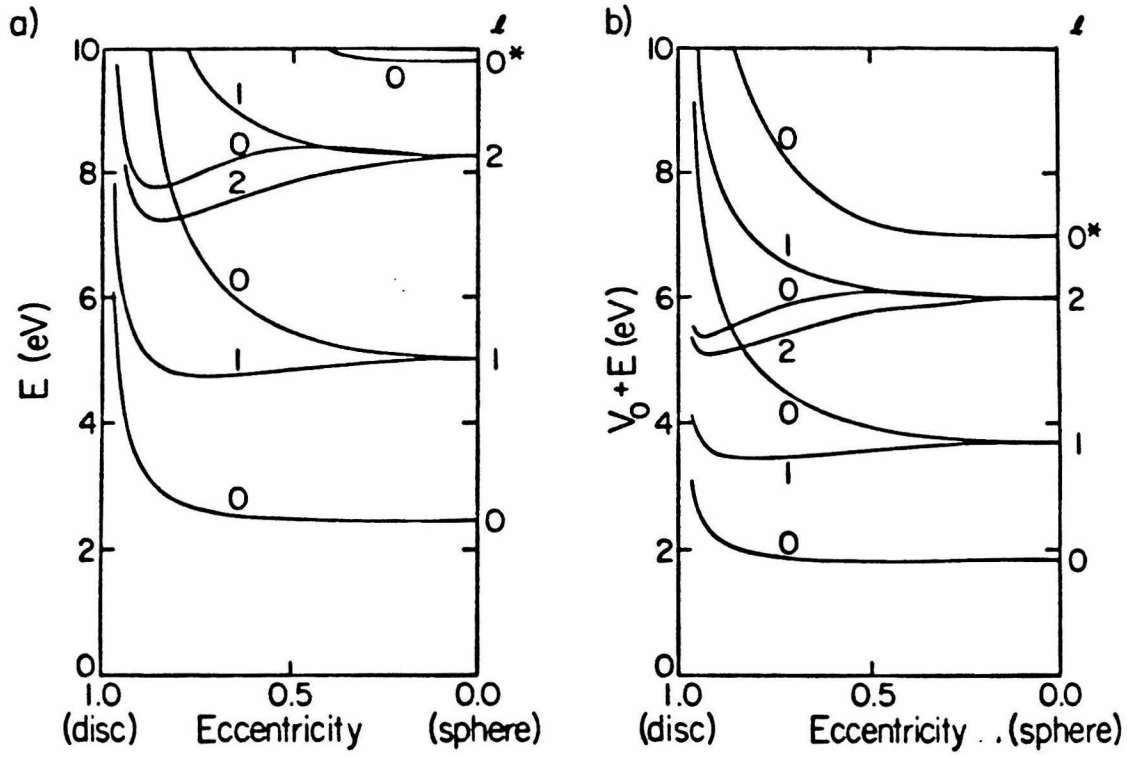

Fig. 6. Energies relative to the bottom of the potential well versus eccentricity. In both (a) and (b) the wells have a constant volume of 251.25 Å^3. The effective spherical radius R_{eff} ($\equiv (a^2b)^{1/3}$) for these results is 3.9145 Å. Energy levels are labeled with l on the right-hand side of the figure and m above individual curves, where l and m are the total angular momentum and its z projection of the state of the spherical well to which a given spheroidal state correlates. The m and l quantum numbers of the states in Figs. 3-5 are (m,l) = (0,0), (0,1), and (0,2), respectively. An asterisk indicates the presence of a radial nodal surface in the spherical wavefunction. V_0 equals ∞ in (a) and 10 eV in (b). In both cases only those spheroidal states which correlate to the four lowest distinct spherical energy eigenvalues are shown.

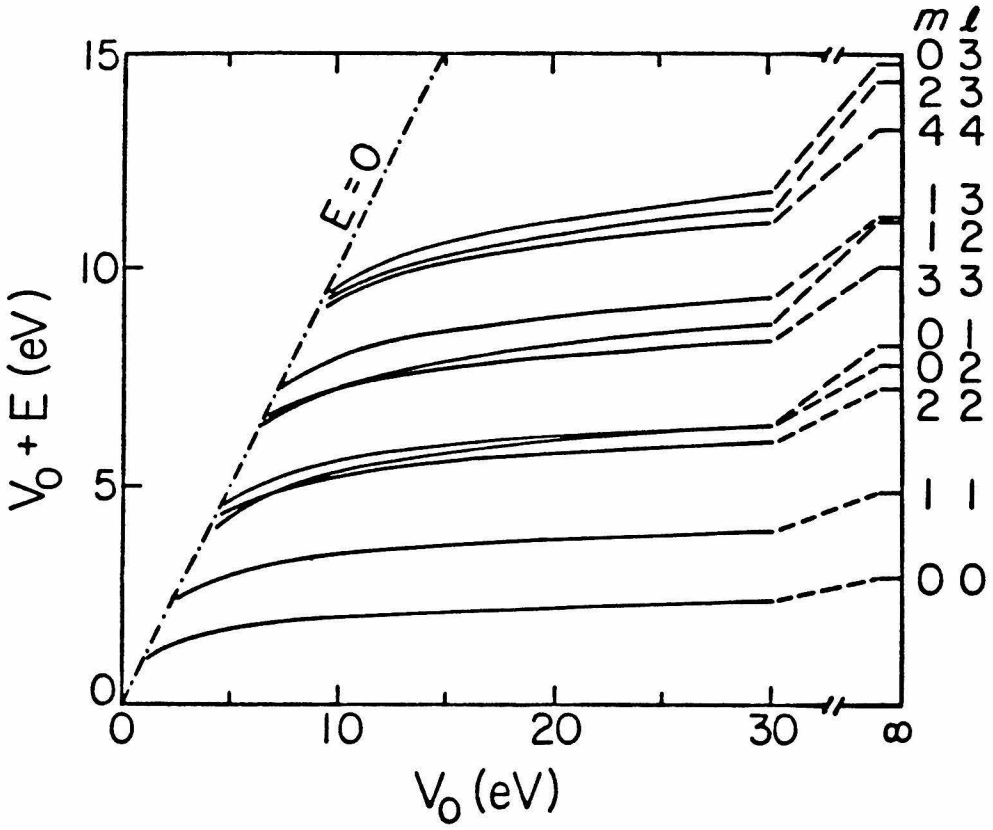

Fig. 7. Energies relative to the bottom of the well versus well depth. a and b as in Fig. 3, volume = 251.25 Å^3. m and l are indicated on the right-hand side of the figure and are defined as for Fig. 6.

with $t = 1$ and $s = 1$ for a given m for the rest of the article, π denoting odd symmetry with respect to reflection in the xy plane. The π-like nature of the $(0,\pi)$ state is apparent in Fig. 4. For comparison with experimental systems designed to assess orientation and distance effects we note that a $(1,\pi)$ state has the same nodal structure as the HOMO in benzene. A $(4,\pi)$ state has the same nodal structure as the HOMO in porphine, as determined in *ab initio* calculations.[22] To illustrate a particular geometrical effect we have also given some results for states with zero nodes. We will refer to them as $(0,\sigma)$ states, since m is zero and, like σ states, they are even with respect to reflection in the xy plane of the potential.

B. Electron transfer between sites

The system used to model electron transfer between a pair of molecules A and B consists of two wells (site A and site B), each of the type described previously, and one electron (the "transferable" electron). The rate constant for the electron transfer reaction

$$A^- + B \rightarrow A + B^- \tag{8}$$

is given by (1), using the Golden Rule and Condon approximations. That rate constant is for transfer between sites having specific and fixed mutual orientations and fixed relative separation distance. In order to use Eq. (1), nuclear coordinates and an associated set of vibrational states have been assumed to be present in the wells and in the intervening medium (along with solvent orientational states), but will not be dealt with explicitly in this paper. Recent reviews on this aspect of the electron transfer problem are given in Ref. 30.

The zeroth-order problem is that in which the two wells do not

interact (e.g., the infinite-separation limit). The following two zeroth-order states are considered:

1) the electronic state at site A, uninfluenced by site B: The wavefunction for this state, denoted by Ψ^A_{mtu}, is given by Eq. (6), with the origin of the coordinates at the center of well A and with ξ_0 defining the boundary of well A. The V_0 appearing in Eq. (3) and appropriate to site A is denoted by V_0^A.

2) the electronic state at site B, uninfluenced by site A, which has as its wavefunction $\Psi^B_{m't'u'}$, given by (6), but centered now on site B, and having $V_0 = V_0^B$.

The electronic matrix element T_{BA}, described in Appendix A for the present model, is

$$T_{BA} = (H_{BA} - S_{AB}H_{AA})/(1 - |S_{AB}|^2) \ , \tag{9}$$

where

$$H_{BA} = -V_0^B \int \Psi^{B*}_{m't'u'} \Psi^A_{mtu} \, d\tau_B \ , \quad H_{AA} = -V_0^B \int \Psi^{A*}_{mtu} \Psi^A_{mtu} \, d\tau_B \ , \tag{10a}$$

$$S_{AB} = \int \Psi^{A*}_{mtu} \Psi^B_{m't'u'} \, d\tau \tag{10b}$$

The integrals in (10a) are over well B, and that in (10b) is over all space.

C. Results of calculations of the electron transfer matrix element

Calculations of the electron transfer matrix element were performed with various eigenstates of each of the two separated wells with specific fixed mutual orientations. The states and orientations chosen illustrate some general effects of the shape of the potential well and orientation on the matrix element.

Mutual orientations of the two wells are defined using the coordinate system in Fig. 8. Well A was assumed fixed and well B was positioned at various values of R and Θ. In the calculations given here the x-axes of the

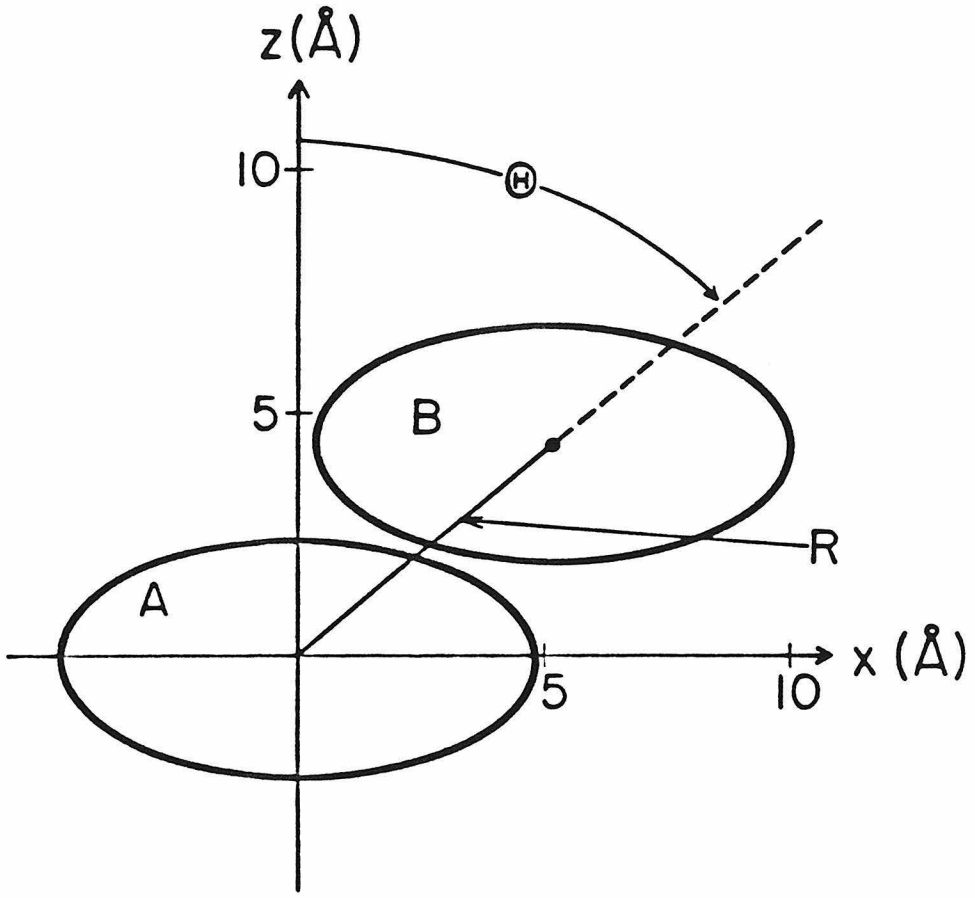

Fig. 8. Coordinate system used to specify the mutual orientation of well A and well B. The x-axes of the wells are assumed parallel and lie in the plane of the figure in all geometries. $\Theta = 0°$ corresponds to the z axes of the wells being superimposed.

wells are parallel, as are the y-axes. $\Theta = 0^{\circ}$ corresponds to the wells being displaced along the z axis, and so being in a "face-to-face" configuration. $\Theta = 90^{\circ}$ corresponds to displacement along the x axis, i.e., in an "end-to-end" arrangement.

The values of a and b used (apart from those in Fig. 6) were chosen as follows: a was an estimate of the in-plane radius of porphine, and is the same a as that used by Platt[15] to treat porphine as a $2a$ x $2a$ square using the Schmidt box model. The value of b was chosen so that the average thickness of the well ($= 4b/3$) corresponded to the interplane spacing in graphite, 3.4 Å.[31] Other values of b are, of course, possible. The general features of the orientation dependence are not qualitatively affected by the choice of b.

T_{BA} and H_{BA} are compared for the wells at contact for various states and various angles Θ in Table I. It can be seen that typically T_{BA} and H_{BA} agree to within 5%. The agreement becomes even better with increased separation. The calculation of H_{BA} is much less time-consuming than T_{BA}, and only values of H_{BA} are given in the rest of the article. The trends seen are unaffected.

Results as a function of distance and orientation are plotted in Figs. 9 to 11 for pairs of $(0,\sigma)$ and $(0,\pi)$ states. In Figs. 9-12 V_0 was chosen so that each state, independently of m and of the parity, has an energy E = -1.1525 eV. This value of E yields states which cause $|H_{BA}|^2$ to have an (approximately) exponential decay whose slope of a $ln\ |H_{BA}|^2$ vs. R plot is from 1.4 to 1.7 depending on the states involved. These are in the range of some experimental estimates for the decay of the electronic matrix element with distance for aromatic molecule-aromatic anion systems.[16] (The rate in Ref. 16a is proportional to exp (-2αR), where 2α is

TABLE I. Comparison of H_{BA} and T_{BA} at selected angles Θ for potential wells at contact. [a, b]

State	Θ (degrees)	H_{BA} (eV)	H_{BA}/T_{BA}
$(0, \sigma)$	0	-0.263	1.000
	30	-0.229	1.000
	45	-0.182	1.006
	60	-0.121	1.008
	90	-0.045	1.004
$(0, \pi)$	0	0.666	1.084
	30	0.474	1.092
	45	0.267	1.074
	60	0.077	1.025
	90	-0.015	1.000
$(2, \pi)$	0	0.481	1.007
	30	0.040	1.069
	45	0.109	1.029
	60	0.299	1.035
	90	-0.062	1.002
$(4, \pi)$	0	0.246	1.001
	30	-0.079	1.012
	45	0.113	1.013
	60	0.279	1.019
	90	-0.066	1.002

[a]The wells have a = 4.85 Å, b = 2.55 Å, and V_0 such that E = -1.1525 eV. For $(0, \sigma)$, $(0, \pi)$, $(2, \pi)$ and $(4, \pi)$, states, V_0 = 2.5937, 5.6540, 10.6541 and 17.3530 eV, respectively. In the worst case H_{BA} is converged to within 2% of the exact value. In general, the convergence is much better.

[b]$\Phi_m(\varphi) = \cos m\varphi$. Similar agreement of H_{BA} and T_{BA} is seen for $\Phi_m(\varphi) = \sin m\varphi$ or any linear combination of $\sin m\varphi$ and $\cos m\varphi$.

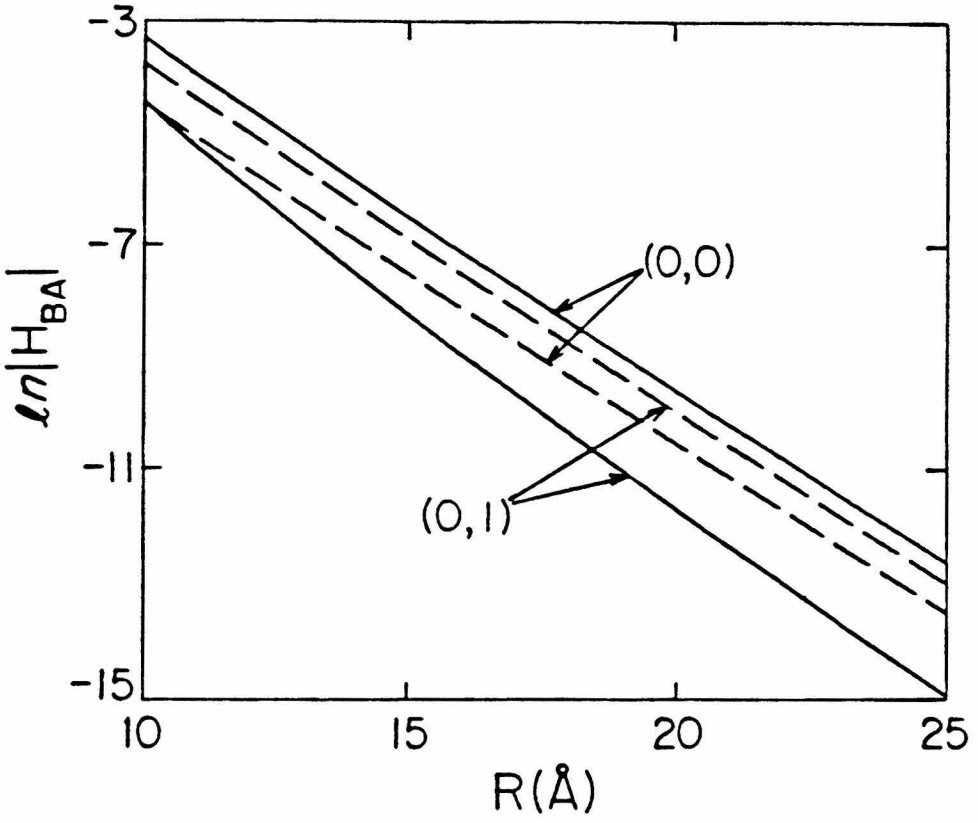

Fig. 9. $ln\ |H_{BA}|$ as a function of center-to-center separation for a pair of $(0,\sigma)[=(0,0)]$ states in each well and for a pair of $(0,\pi)$ states. a and b are as in Fig. 3. E = -1.1525 eV; V_0 is 2.5937 eV for the $(0,\pi)[=(0,1)]$ states and 5.6540 eV for the $(0,\pi)$ state. Solid lines are for $\Theta = 90^0$ and dashed lines for $\Theta = 0^0$.

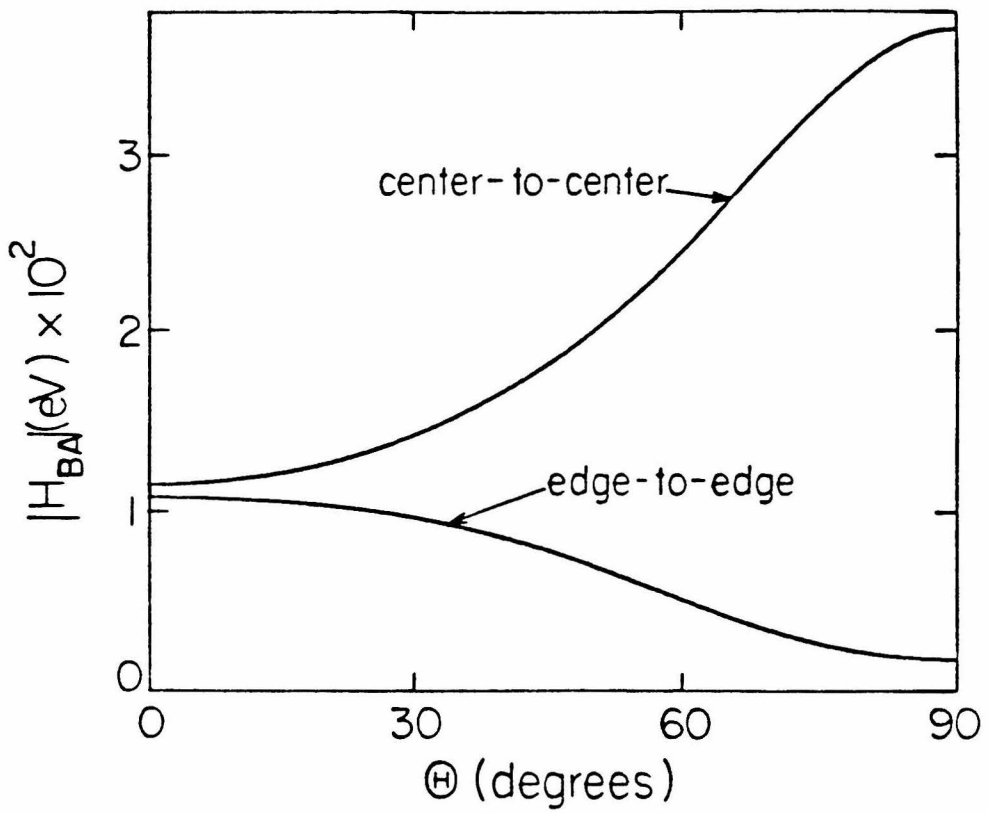

Fig. 10. $|H_{BA}|$ as a function of Θ for a pair of $(0,\sigma)$ states. a, b and V_0 and E are as in Fig. 9 for the $(0,\sigma)$ states. Shown are results for a constant center-to-center distance of 10 Å and for a constant edge-to-edge distance of 5 Å.

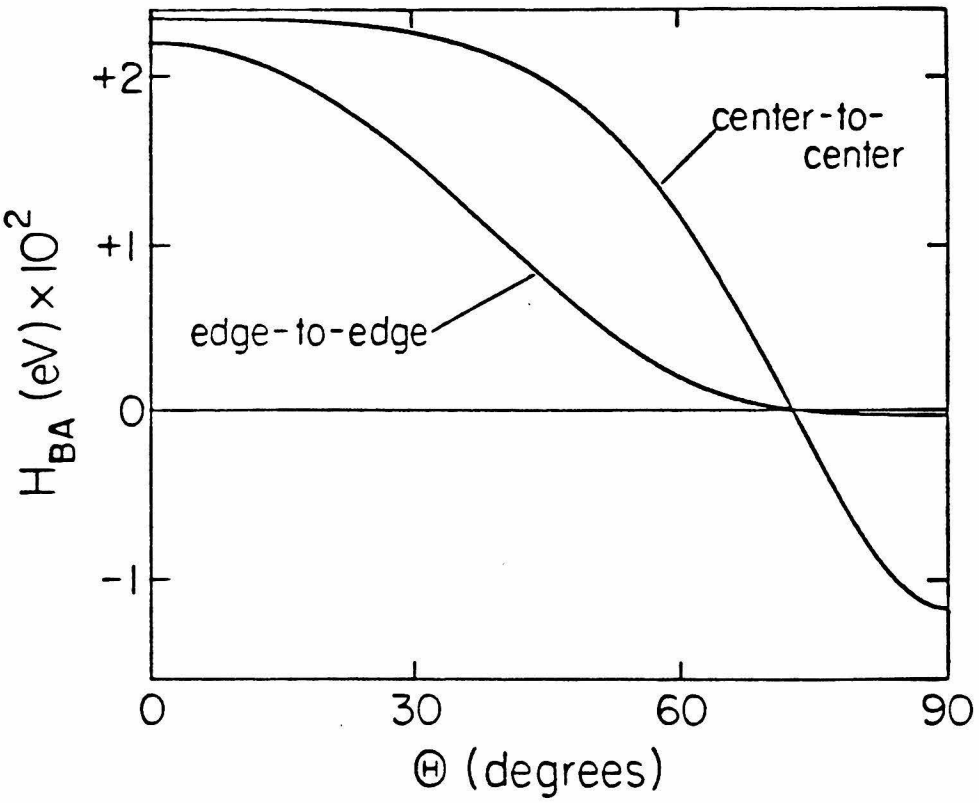

Fig. 11. H_{BA} as a function of Θ for $(0,\pi)$ states. a, b, V_0 and E are as in Fig. 9 for the $(0,\pi)$ states. Shown are results for a constant center-to-center distance of 10 Å and for a constant edge-to-edge distance of 5 Å.

roughly 1.1 $Å^{-1}$.)

In Table II H_{BA} is given as a function of distance for $\Theta = 0°$ and 90° for the $(1,\pi)$, $(2,\pi)$ and $(4,\pi)$ states. Each eigenvalue of states with $m > 0$ is two-fold degenerate. The functions $\cos m\varphi$ or $\sin m\varphi$ or any linear combination of them are eigenfunctions of the φ portion of the Schrodinger equation and H_{BA} will in general depend on which of these functions is chosen, as well as on the relative orientation of the wells. In actual molecules of current interest, deviations from cylindrical symmetry can remove this degeneracy. The value of H_{BA} for any arbitrary Φ_m (i.e., any linear combination of $\cos m\varphi$ and $\sin m\varphi$) for parallel xy planes may be obtained from the H_{BA}^{cc} and H_{BA}^{ss} in Table II using a standard formula.[32] For brevity of graphical presentation the dependence on distance for states with $m \neq 0$ is given in Fig. 12 as a root mean square average of H_{BA} over γ_A and γ_B, the angles of rotation of Ψ_{mtu}^{A} and Ψ_{mtu}^{B} relative to a fixed set of axes located in well A or well B, respectively:[32]

$$(H_{BA})_{AV} = \left[\frac{1}{4\pi^2}\int_0^{2\pi}\int_0^{2\pi} H_{BA}^2(\gamma_A,\gamma_B)\, d\gamma_A d\gamma_B\right]^{1/2} = \frac{1}{2}\left[|H_{BA}^{cc}|^2 + |H_{BA}^{ss}|^2\right]^{1/2}. \quad (11)$$

Nonaveraged H_{BA}'s are also given in Table I for spheroids in contact.

III. Quantization and Single-Site Wavefunctions

The method used to obtain the wavefunctions of Sec. II is described next.

A. Expansion for the separated wavefunctions

The functions sought are solutions to Eq. (5), valid both inside and outside the spheroidal well. Neglecting the boundary conditions at $\xi = \xi_0$

TABLE II. H_{BA} as a function of center-to-center distance for various (m, π) states at $\Theta = 0°$ and $90°$.[a]

State	R(Å)	$H_{BA}^{cc,\,ss}(\Theta = 0°)$[b]	$H_{BA}^{cc}(\Theta = 90°)$	$H_{BA}^{ss}(\Theta = 90°)$
$(1, \pi)$	10	1.02 (-2)	4.16 (-2)	-4.78 (-3)
	15	2.69 (-4)	6.89 (-4)	-6.33 (-5)
	20	9.16 (-6)	1.97 (-5)	-1.46 (-6)
	25	3.60 (-7)	7.06 (-7)	-4.39 (-8)
$(2, \pi)$	10	3.81 (-3)	-4.49 (-2)	1.76 (-2)
	15	6.08 (-5)	-4.76 (-4)	1.61 (-4)
	20	1.45 (-6)	-1.10 (-5)	3.10 (-6)
	25	4.36 (-8)	-3.49 (-7)	8.35 (-8)
$(4, \pi)$	10	3.77 (-4)	-4.29 (-2)	3.68 (-2)
	15	2.02 (-6)	-1.29 (-4)	1.09 (-4)
	20	2.24 (-8)	-1.48 (-6)	1.17 (-6)
	25	3.76 (-10)	-3.00 (-8)	2.19 (-8)

[a]The states and wells used are the same as those in Table I. H_{BA}^{ss} is H_{BA} calculated using $\Phi_m(\varphi) = \sin m\varphi$ in each well. H_{BA}^{cc} is for $\Phi_m(\varphi) = \cos m\varphi$ in each well. The number in parentheses is the power of 10 to be multiplied by the number preceding it.

[b]In the $\Theta = 0^0$ orientation $H_{BA}^{cc} = H_{BA}^{ss}$.

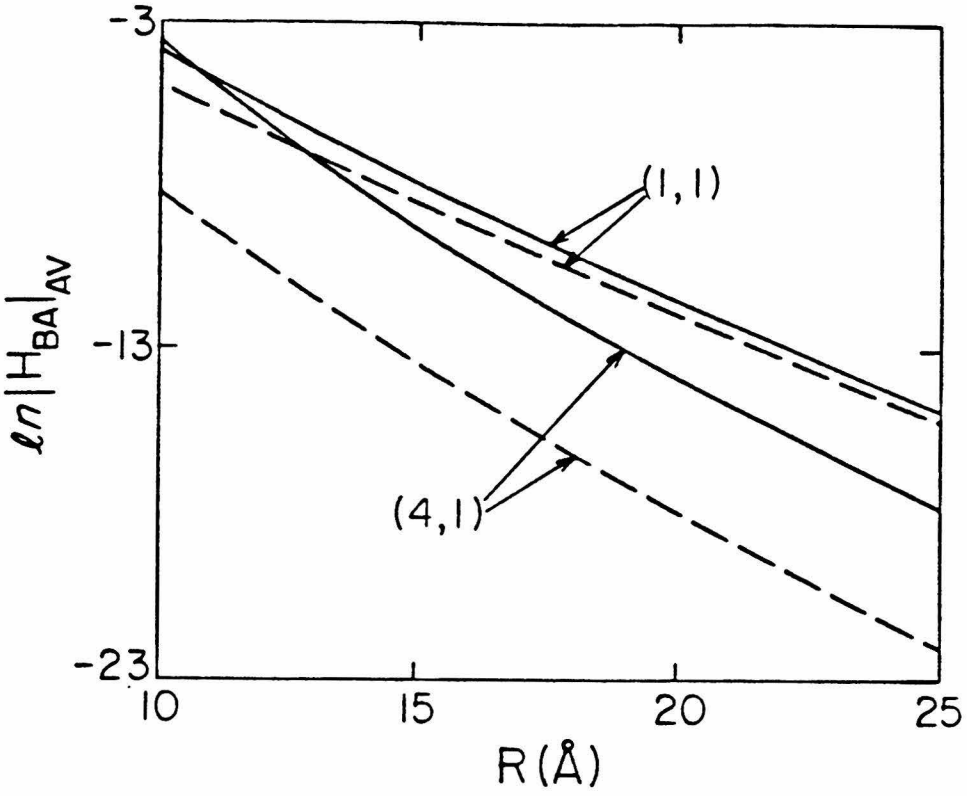

Fig. 12. $ln\ (H_{BA})_{AV}$ as a function of center-to-center distance for a pair of $(1,\pi)$ states in each well and for a pair of $(4,\pi)$ states. In all cases a, b and E are as in Fig. 9. V_0 for the $(1,\pi)$ states is 7.9296 and for the $(4,\pi)$ states is 17.3530 eV. Solid lines are for $\Theta = 90°$ and dashed lines for $\Theta = 0°$.

the wavefunction inside the well can be separated as in Eq. (7a), yielding

$$\frac{d^2\Phi_m^i}{d\varphi^2} + m^2\Phi_m^i = 0 \tag{12}$$

$$\frac{d}{d\eta}\left\{(1-\eta^2)\frac{dS_{mn}^i}{d\eta}\right\} + \left\{\frac{d^2}{4}\eta^2 k_i^2 - \frac{m^2}{1-\eta^2} + \lambda_{mn}^i\right\} S_{mn}^i = 0 \tag{13}$$

$$\frac{d}{d\xi}\left\{(1+\xi^2)\frac{dR_{mn}^i}{d\xi}\right\} + \left\{\frac{d^2}{4}\xi^2 k_i^2 + \frac{m^2}{1+\xi^2} - \lambda_{mn}^i\right\} R_{mn}^i = 0 \tag{14}$$

for the separated equations.

Any choice of k_i^2 (that is, of energy for fixed V_0) yields a sequence of discrete eigenvalues λ_{mn}^i. The subscript m describes the eigenvalue in Eq. (12). The subscript n orders the eigenvalues λ_{mn}^i and was defined in Sec. II. The $\psi_{mn}^{i,o}$ are odd or even with respect to reflection in the xy plane as $n-m$ is odd or even.

Equations (12) through (14) for a given k_i^2 yield a particular set of solutions ψ_{mn}^i of the form shown in Eq. (7a). The function ψ_{mn}^o, neglecting the boundary conditions at $\xi = \xi_0$, can similarly be separated as in Eq. (7b). The related separated differential equations are identical to Eqs. (12) to (14), with i replaced by o. The angle function $\Phi_m(\varphi)$ is the same both inside and outside the well so the superscripts i and o are suppressed in Eq. (7).

The inner and outer radial functions $R_{mn}^i(\xi;k_i^2)$ and $R_{mn}^o(\xi;k_o^2)$ were evaluated through their expansions in spherical and modified spherical Bessel functions, $j_n(dk_i\xi/2)$ and $k_n(d\,|k_o|\,\xi/2)$, respectively. The angular functions $S_{mn}^i(\eta;k_i^2)$ and $S_{mn}^o(\eta;k_o^2)$ were evaluated through their expansions in the associated Legendre functions $P_n^m(\eta)$. The radial and angular functions R_{mn} and S_{mn} in Eq. (7), their expansion coefficients, and the

eigenvalues λ_{mn} are discussed by Flammer,[33] who presents tables of both. Hodge[34] has given an algorithm for obtaining them which was easily programmed and was used for the calculations in the present paper.[35] The radial and angular functions were converged to at least four significant figures in all cases.[36]

B. Quantization in the limit $V_0 \to \infty$

In this case the sum for Ψ in Eq. (6) reduces to a single term and the allowed energy levels are those for which k_i^2 yields

$$R^i_{mn}(\xi_0; k_i^2) \ , \tag{15}$$

since the wavefunction must vanish for $\xi \geq \xi_0$. In the spherical limit $(b \to a)$ the energy eigenvalues given in Fig. 6a, are simply those for which bk_i is a zero of the lth-order Bessel function. An oblate spheroidal square well has been used as a model for the potential in which a nucleon moves in the nucleus.[37] In this context the energy levels have been calculated previously in the limit $V_0=\infty$.[38]

C. Quantization for finite V_0

The wavefunctions in this case must be written as a sum of inner or outer functions because both the angular and radial parts of the wavefunctions depend on the energy. Quantization is accomplished by requiring that the wavefunction and its normal derivative be continuous at $\xi = \xi_0$, i.e.,

$$\lim_{\xi \to \xi_o^-} \Psi^i_{mtu}(\xi,\eta,\varphi;k_i^2) = \lim_{\xi \to \xi_o^+} \Psi^o_{mtu}(\xi,\eta,\varphi;k_o^2) \tag{16}$$

$$\lim_{\xi \to \xi_o^-} \frac{\partial \Psi^i_{mtu}}{\partial \xi}(\xi,\eta,\varphi;k_i^2) = \lim_{\xi \to \xi_o^+} \frac{\partial \Psi^o_{mtu}}{\partial \xi}(\xi,\eta,\varphi;k_o^2) \ . \tag{17}$$

Continunity of $\partial\psi/\partial\eta$ at the boundary $\xi = \xi_o$ is ensured by Eq. (16).

The following method was used to determine the energy eigenvalues E_{mtu} for which Eq. (16) and (17) are satisfied. Each outer angular function $S^o_{mn}(\eta;k_o^2)$ was expanded in the complete set of inner angular functions $S^i_{mn}(\eta;k_i^2)$, thereby yielding Ψ_{mtu} as an expansion in $S^i_{mn}(\eta;k_i^2)$ for both $\xi \leq \xi_0$ and for $\xi \geq \xi_0$. Equating the two expansions term by term at $\xi = \xi_0$ yields

$$\mathbf{C}^i = \mathbf{M}\mathbf{C}^o \quad . \tag{18}$$

In (18) $\mathbf{C}^i$ denotes the column vector with elements $(C^i_{m+s}, C^i_{m+s+2} \ldots)$ and $\mathbf{C}^o$ denotes $(C^o_{m+s}, C^o_{m+s+2} \ldots)$, the C^i_n's and C^o_n's being the coefficients appearing in Eq. (6). Both vectors are of infinite dimension but are truncated in practice. The elements of the matrix $\mathbf{M}$ depend on the energy and on the quantum number m, and are given by

$$M_{kj} = \frac{<S^i_{mq} \mid S^o_{mp}> R^o_{mp}(\xi_0;k_o^2)}{<S^i_{mq} \mid S^i_{mq}> R^i_{mq}(\xi_0;k_i^2)} \tag{19a}$$

where

$$p = m + 2(j-1) + s \ , \quad j \geq 1 \ ; \quad q = m + 2(k-1) + s \ , \quad k \geq 1 \ . \tag{19b}$$

Similarly, continuity of the normal derivative at $\xi = \xi_0$ yields the matrix equation

$$\mathbf{C}^i = \mathbf{M}'\mathbf{C}^o \tag{20}$$

where

$$M'_{kj} = \frac{<S^i_{mq} \mid S^o_{mp}> dR^o_{mp}(\xi_0;k_o^2)/d\xi_0}{<S^i_{mq} \mid S^i_{mq}> dR^i_{mq}(\xi_0;k_i^2)/d\xi_0} \tag{21}$$

and p and q are again given by Eq. (19b). Equations (18) and (20) yield

$$\mathbf{C}^o = \mathbf{M}^{-1}\mathbf{M}'\mathbf{C}^o \quad . \tag{22}$$

Thus, $\mathbf{C}^o$ is an eigenvector of the matrix $\mathbf{M}^{-1}\mathbf{M}'$ having a unit eigenvalue. An energy eigenvalue and eigenvector $\mathbf{C}^o$ is found by iterating the energy in Eq. (22) to obtain an eigenvector with unit eigenvalue. The inner expansion coefficients $\mathbf{C}^i$ are then obtained using Eq. (18) and this $\mathbf{C}^o$. The wavefunctions are normalized by the factor A_{mtu} in (6), A_{mtu} being $\langle\Psi^u_{mtu}|\Psi^u_{mtu}\rangle^{-\frac{1}{2}}$, where Ψ^u_{mtu} is the unnormalized solution.

IV. Discussion

In this section the dependence of H_{BA} on distance and the factors affecting the orientation dependence of H_{BA} are discussed.

Figures 9 and 12 give plots of $ln\,|H_{BA}|$ or $ln\,(H_{BA})_{AV}$ versus distance and it is seen that H_{BA} decreases, as expected, predominantly exponentially with distance for all the states considered. In Appendix B analytical expressions for H_{BA} as a function of distance are derived for certain states of spherical wells.[39] For spherical states analogous to the $(0,\sigma)$ states of spheroidal wells, we find (Eq. (B10))

$$H_{BA} = -\frac{\hbar^2 A_0^2}{2m\alpha^2 R}\exp(-\alpha R) \quad , \tag{23}$$

where A_0 is the radial normalization constant, given in Appendix B, for single-well wavefunctions. R is the distance between the well centers, and $\alpha = (-2mE/\hbar^2)^{\frac{1}{2}}$. It can be seen explicitly that the large-R asymptotic distance dependence of $ln\,|H_{BA}|$ is linear.

For spherical states analogous to the spheroidal $(0,\pi)$ states one has (Eqs. (B11) and (B12))

$$H_{BA} = -\frac{C}{\alpha}\left[\frac{1}{(\alpha R)^2} + \frac{1}{(\alpha R)^3}\right]\exp(-\alpha R) \quad , \quad (\Theta = 90^o) \tag{24}$$

and

$$H_{BA} = \frac{C}{\alpha}\left[\frac{1}{\alpha R} + \frac{2}{(\alpha R)^2} + \frac{2}{(\alpha R)^3}\right]\exp(-\alpha R) \quad , \quad (\Theta = 0^\circ) \ . \qquad (25)$$

The constant C is defined by comparing with Eq. (B11) and (B12) and using (B3).

In both orientations it is seen that $ln\ |H_{BA}|$ depends predominantly linearly on distance. In all cases the exponential dependence arises from the overlap of the radial part of Ψ^A, a modified spherical Bessel function, with Ψ^B. Since the outer spheroidal wavefunctions are composed of sums of modified spherical Bessel functions a similar distance dependence of H_{BA} is expected and is found.

In general, the functional form of the pre-exponential part of the distance dependence of H_{BA} is dependent on the potential functions at the two centers. For one-dimensional square wells H_{BA} is proportional to an exponential function of R.[40] For transfer of an electron between two protons H_{BA} is a polynomial in powers of R multiplied by an exponential.[41] The dominant part of H_{BA} in all these cases is a decaying exponential but the potential shape and nodal structure of the wavefunctions cause slowly varying deviations from purely exponential behavior.

In analyzing the orientation effects exhibited in Figs. 9 to 12, There are two principal factors to be considered, the well shape and the nodal structure. They are discussed below, initially for fixed center-to-center and then for fixed edge-to-edge distance:

1. In the $(0,\sigma)$ case (Fig. 9) there are no nodal complications, and the shape of the spheroidal well favors a larger $|H_{BA}|$ in the $\Theta = 90^\circ$ orientation than in the $\Theta = 0^\circ$ at fixed center-to-center distance.

2. (The following results are intended to refer only to (m,π) states.) For a fixed center-to-center distance, as the number of nodes in the φ

portion of the wavefunction increases, i.e., as m increases, the ratio $|H_{BA}(\Theta = 90°)| / |H_{BA}(\Theta = 0°)|$ increases (cf. Figs. 9 and 12). The pairs of $(0,\pi)$ states have larger $|H_{BA}|$'s at $\Theta = 0^0$ than at $\Theta = 90^0$, while all other (m,π) states have larger $|H_{BA}|$'s at $\Theta = 90°$. [Cf. Fig. 12, including the $(2,\pi)$ case of Table II.]

Result 1 is due to the smaller edge-to-edge distance occurring in the $\Theta = 90°$ configuration at a fixed center-to-center distance, and illustrates one geometrical shape effect. We have also observed result 2 for H_{BA} for spherical-well potentials.[42] To understand these results we consider the form of H_{BA} in the spherical case (cf. Appendix B). In essence, with increasing m the wavefunctions tend increasingly rapidly to zero along their z-axes, and so the face-to-face configuration becomes decreasingly favored. We have

$$H_{BA} = -\int_{wellB} V_0^B \Psi^{B*} \Psi^A \, d\tau_B$$
$$\propto \int_{wellB} j_{l'}(\beta_B r_B) P_{l'}^{m'}(\cos\theta_B) \Phi_{m'}^*(\varphi_B) V_0^B \, k_l(\beta_A r_A) P_l^m(\cos\theta_A) \Phi_m(\varphi_A) \, d\tau_B$$

where the subscripts A and B denote variables appropriate to the functions at site A and B, respectively. l is the total angular momentum quantum number. Spherical states which have similar nodal structures to the (m,π) spheroidal states considered have $l = m+1$. The variables (r_A,θ_A,φ_A) depend implicitly on (r_B,θ_B,φ_B). Since the integration is over well B the predominant angular dependence of H_{BA} on Θ for the orientations examined in this paper (xy planes of each well parallel) arises from the function $P_l^m(\cos\theta_A)$ which is of the form:

$$P_l^m(\cos\theta_A) \propto \sin^m\theta_A \cos\theta_A, \quad l = m + 1, m \geq 0 \ .$$

In the $\Theta = 0°$ orientation, the relevant θ_A approach zero as $R \to \infty$, for all

values of r_B, θ_B and φ_B in well B, and so $\sin^m \theta_A$ goes to zero increasingly rapidly with increasing m in the vicinity of well B. In the $\Theta = 90^\circ$ orientation, θ_A approaches 90° as $R \to \infty$ and $\cos \theta_A$ tends to zero in the vicinity of well B, but for all (m,l) spherical states considered $\cos \theta_A$ is always raised to the first power. Therefore, as m increases the $\Theta = 90^\circ$ orientation is increasingly favored over the $\Theta = 0^\circ$ orientation. For the $(m,l) = (0,1)$ state, only the $\cos\theta_A$ term occurs, and so the $\Theta = 0^\circ$ configuration is favored. Since the spheroidal wavefunctions are composed of sums of Legendre polynomials P_l^m, dominated by a few of them, and because of the correspondence between η and $\cos \theta$, this explanation is the anticipated one for this orientation dependence in the spheroidal case. Results 1 and 2 are thus at least qualitatively explained.

Although distances in experiments are often quoted as center-to-center distances it is useful, because of the exponential decay of the wavefunctions, to examine the results at constant edge-to-edge distances. The data presented are sufficient to make comparisons of H_{BA} for fixed edge-to-edge separation. Equal edge-to-edge separations in the two orientations are obtained by comparing H_{BA} for which the center-to-center separation is 4.6 Å $(= 2(a-b))$ larger in the $\Theta = 90^\circ$ orientation. For the systems examined in this paper, H_{BA} was always larger at $\Theta = 0^\circ$ than at $\Theta = 90^\circ$ for $m < 4$ and was roughly equal for $m = 4$ at the two Θ's.

The explanation presumably lies in a geometrical shape effect: In the $\Theta = 0^\circ$ configuration the spheroids present a larger cross section and smaller thickness to each other, thereby favoring a higher overlap. However, the difference in $|H_{BA}|$'s decreases with increasing m for the reason discussed above, and still larger m's may reverse the favored $\Theta = 0^\circ$ result.

While we have largely considered the orientations $\Theta = 90^0$ and $\Theta = 0^0$ in this article for purposes of illustration, other orientations are also of considerable interest. In fact, as m increases, maxima will occur in H_{BA} at Θ's other than $\Theta = 0^0$ (cf. $(2,\pi)$ and $(4,\pi)$ results in Table I). The angles at which these maxima occur are near the maxima in the angular function $P_l^m(\cos\theta)$ of the spherical state which has similar nodal structure to the spheroidal state in question ($\sim 55^0$ for the $(2,\pi)$ states and $\sim 63^0$ for the $(4,\pi)$ states). It can be seen in Fig. 6 that θ_A equals Θ and θ_B equals $\pi-\Theta$, where θ_A and θ_B are the spherical polar angles in each well, so the maxima of H_{BA} as a function Θ are related to maxima in $P_l^m(\cos\theta_A)$ and $P_l^m(\cos\theta_B)$. This analogy with spherical functions is adequate for the reasons stated previously.

We have also examined the angular dependence of the spheroidal wavefunctions at R = ∞. At a large radial distance each of the outer radial functions has the same asymptotic form, independently of m or n:

$$R^o_{mn}(\xi;k_o^2) \sim \frac{1}{\alpha r}\exp(-\alpha r)\,, \quad r \to \infty \tag{26}$$

where $\alpha \equiv |k_o| = (2m|E|/\hbar^2)^{1/2}$. Hence, the wavefunction Ψ_{mtu} at a fixed large r and fixed φ varies as

$$\Psi_{mtu} \sim \left[\sum_{n=0}^{\infty} C_n^o S_{mn}(\eta;k_o^2)\right]\exp(-\alpha r)/\alpha r \quad (r \to \infty)\,, \tag{27}$$

where in (27) we set $\eta = \cos\theta$.

To exhibit the angular dependence of Ψ_{mtu} at large r, Ψ_{mtu} in Eq. (27) was projected onto the associated Legendre polynomials $P_n^m(\cos\theta)$. If the angular probability distribution at large r were insensitive to the nonzero eccentricity of the spheroidal well one would find $|\langle P_n^m|\Psi_{mtu}\rangle|^2$ equal to zero except for a single value of n. Calculated projections, defined as

$$P_n^2 \equiv \frac{|\langle \Psi_{mtu} | P_n^m \rangle|^2}{|\langle P_n^m | P_n^m \rangle|^2} \Big/ \sum_k \frac{|\langle \Psi_{mtu} | P_k^m \rangle|^2}{|\langle P_k^m | P_k^m \rangle|^2}, \quad r = \infty \ , \tag{28}$$

are given in Table III for wells of three eccentricities, all with a volume of 251.25 Å^3. The data clearly indicate that even at r = ∞ the electron "sees" the nonsphericity of the potential well.

V. Conclusion

A model electron transfer system involving non-spherical (oblate spheroidal) donor and acceptor sites and a transferable electron has been presented. The wavefunctions for the isolated donor and acceptor sites and the matrix element for electron transfer have been described and the results of several calculations presented. Thus, a machinery has been developed for the calculation of orientation effects, especially for electron transfer between large aromatic molecules.

The sample calculations illustrate the effects of well shape and nodal structure on the orientation and distance dependence of the electron transfer matrix element. They indicate to a first approximation for the system and states studied, that the geometrical shape effect, for a constant edge-to-edge distance, causes $|H_{BA}|$ to be larger for $\Theta = 0^0$ ("face-to-face" configuration) than for $\Theta = 90^0$ ("end-to-end" arrangement). This effect is reduced with increasing m, a result explained by examining the long-range behavior of a pair of spherical wells. This increasing m effect is expected to apply to states similar to the HOMO or LUMO of large aromatic molecules.

When the results are presented instead at a given center-to-center separation they are significantly influenced by the greater edge-to-edge distance for the $\Theta = 0^0$ configuration ("face-to-face"), so that now $|H_{BA}|$ is largest at $\Theta = 90^0$ for most of the states considered.

TABLE III. Normalized projections P_n^2 of the $(m, t, u) = (0, 1, 2)$ state in limit $r \to \infty$[a]

n	e = 0.1	e = 0.5	e = 0.9
0	0.0003	0.2153	0.4045
2	0.9997	0.7825	0.5637
4	0.0000	0.0022	0.0315
6	0.0000	0.0000	0.0004

[a]The quantity P_n^2 is defined in Eq. (28); e is the eccentricity of the well at a constant volume of 251.25 Å^3. For these calculations, $V_0 = 10$ eV. Because $n - m$ is even, $P_n^2 \equiv 0$ for all odd n. The eccentricity of the wells in Figs. 3-5 and 9-12 is ~ 0.85.

Acknowledgments

It is a pleasure to acknowledge support of this research by the Office of Naval Research. RJC gratefully acknowledges the support of a National Science Foundation Pre-doctoral fellowship, 1979-1982.

The calculations reported in this paper made use of the Dreyfus-NSF theoretical chemistry computer which was funded through grants from the Camille and Henry Dreyfus Foundation, the National Science Foundation, and the Sloan Fund of the California Institute of Technology.

Appendix A: Golden Rule Rate Expression and Matrix Elements

The rate expression used to characterize electron transfer in this paper is a Golden Rule rate constant obtained by using a Born-Oppenheimer analysis by Holstein[43] and has been presented in a paper by Kestner, *et al.*[10] Another presentation of the derivation which corrects some typographical errors there is found in Ref. 44. The pertinent results are particularized below to the present model.

The rate expression for transfer of an electron from site A to site B when only a single electronic state is assumed on either site may be written in the Golden Rule and Condon approximations as

$$k_{B\leftarrow A} = \frac{2\pi}{\hbar} |T_{BA}|^2 \left(\frac{1}{Q_A} \sum_{\nu_A,\nu_B} e^{-E_{\nu_A}/kT} |<\nu_B|\nu_A>|^2 \delta(E_{\nu_B} - E_{\nu_A}) \right) . \quad \text{(A1)}$$

In Eq. (A1) ν_A denotes one of a set of nuclear wavefunctions appropriate to the electron being localized at site A, ν_B denotes a similar set for the electron localized at site B, and Q_A is the nuclear partition function appropriate to the electron being localized on site A. For the case of nonorthogonal electronic basis states, T_{BA} is equal to

$$T_{BA} = \frac{\int \Psi^{B*} V^B \Psi^A \, d\tau - (\int \Psi^{A*}\Psi^B \, d\tau)(\int \Psi^{A*} V^B \Psi^A \, d\tau)}{1 - |\int \Psi^{A*}\Psi^B \, d\tau|^2} . \quad \text{(A2)}$$

We define

$$H_{BA} \equiv \int \Psi^{0B^*} V^B \Psi^A \, d\tau \ , \quad S_{AB} = \int \Psi^{A^*}\Psi^B \, d\tau$$
$$H_{AA} \equiv \int \Psi^{A^*} V^B \Psi^A \, d\tau . \quad \text{(A3)}$$

For the type of potential used in this study, the integrals H_{BA} and H_{AA} over all space are reduced to integrals over well B, since V^B is zero outside well B. One thus obtains Eq. (9).

APPENDIX B: SPHERICAL WAVEFUNCTIONS AND THEIR ELECTRON TRANSFER MATRIX ELEMENTS Appendix B: Spherical Wavefunctions and their Electron Transfer Matrix Elements

(i) Spherical Wave Functions

In the spherical limit $a \to b$, the wavefunction of Eq. (6) assumes the simpler form given in Eq. (B1), where l is the total angular momentum quantum number.

$$\Psi_{ml}(r,\theta,\varphi;E) = A_l\ N_{ml}\ \Phi_m(\varphi)\ P_l^m(\cos\theta) \begin{cases} j_l(\beta r)k_l(\alpha b)/\, j_l(\beta b), & r \le b \\ k_l(\alpha r) & , r \ge b \end{cases} \quad \text{(B1)}$$

b is the radius of the spherical well, $\beta = [2m(V_0 + E)]^{1/2}/\hbar$, $\alpha = [-2mE]^{1/2}/\hbar$ and $\Phi_m(\varphi)$ is any linear combination of $\cos m\varphi$ and $\sin m\varphi$ with the absolute square of the coefficients equal to 1. The angular function P_l^m is an associated Legendre polynomial. We have used the definition of P_l^m given by Arfken.[45] The constants A_l and N_{ml} are normalization constants for the radial part of the wavefunction and for the (m,l) spherical harmonic, respectively:

$$A_l = \left\{ \frac{k_l^2(\alpha b)}{j_l^2(\beta b)} \int_0^b j_l^2(\beta r)\, r^2\, dr + \int_b^\infty k_l^2(\alpha r)\, r^2\, dr \right\}^{-1/2} \quad \text{(B2)}$$

$$N_{ml} = \left\{ \frac{2}{2l+1} \frac{(l+m)!}{(l-m)!} \nu \right\}^{-1/2}, \quad \text{(B3)}$$

where ν is 2π if $m = 0$ and π for $m \neq 0$. The Ψ_{ml} given by Eq. (B1) is clearly continuous at the boundary, $r = b$. The value of E in α and β was determined by making $\partial\Psi_{ml}/\partial r$ continuous there.[39] To compare the spherical (m,l) states with the spheroidal (m,π) states having similar nodal structure we use the relation $l = m+1$. Spherical $(m,l) = (0,0)$

states correspond to the $(0,\sigma)$ states used in Sec. II.

The integrals in (B2) can be evaluated in closed form to yield

$$A_l = \Big\{k_{l-1}(\alpha b)k_{l+1}(\alpha b) - [k_l^2(\alpha b)/j_l^2(\beta b)] \times j_{l-1}(\beta b)j_{l+1}(\beta b)\Big\}^{-\frac{1}{2}} (2/b^3)^{\frac{1}{2}} . \tag{B4}$$

(ii) Analytical Matrix Elements for Spherical Wavefunctions

It is possible to transform the matrix element H_{BA}, which is defined as a three-dimensional volume integral in Eq. (A3), to a two-dimensional surface integral. A method due to Bardeen[46] is used to effect the transformation.

For simplicity, the following discussion is restricted to the special case in which the same wavefunction is used in each well. That is, both wells have equal radius and depth, and (m,l) is the same for both Ψ^A_{ml} and Ψ^B_{ml}. For this case, H_{BA} is defined as in Eq. (B5).

$$H_{BA} \equiv - V_0 \int_{wellB} \Psi^A \Psi^{B*} d\tau_B \tag{B5}$$

In well B $-V_0\Psi^{B*}$ equals (E - T)Ψ^*_B and hence (B5) becomes

$$H_{BA} = \int_{wellB} \Psi^A (E - T) \Psi^{B*} d\tau_B . \tag{B6}$$

The subscripts ml on Ψ^A_{ml} and Ψ^B_{ml} have been suppressed. Here T is the kinetic energy operator, $-\hbar^2\nabla^2/2m$. It is assumed in what follows that the centers of the wells lie along the z axis of a right circular cylindrical coordinate system, well B at z = + R/2, and well A at z = -R/2. The region of integration may be extended beyond the boundary of well B since $(E-T)\Psi^{B*}$ vanishes outside well B. In particular, the region $z \geq 0$, will be used. Also, $\Psi^A E$ equals $T\Psi^A$ in any region that does not include well A,

so Eq. (B6) yields

$$H_{BA} = \frac{-\hbar^2}{2m}\int_{z\geq 0}(\Psi^{B*}\nabla^2\Psi^A - \Psi^A\nabla^2\Psi^{B*})d\tau \ . \qquad \text{(B7)}$$

Gauss' theorem applied to Eq. (B7) yields

$$H_{BA} = \frac{-\hbar^2}{2m}\int_{\varphi=0}^{2\pi}\int_{r=0}^{\infty}(\Psi^A \frac{\partial\Psi^{B*}}{\partial z} - \Psi^{B*}\frac{\partial\Psi^A}{\partial z})\, r dr d\varphi \ . \qquad \text{(B8)}$$

Gauss' theorem is applicable to Eq. (B7) because the discontinuity in $\nabla^2\Psi^B$ is merely a step discontinuity on the boundary of well B. The integral in Eq. (B8) is written in right circular cylindrical coordinates (r,φ,z). The surface of integration is the plane z=0, located midway between the two wells.

Equation (B8) can be further simplified by making use of the symmetry of the wavefunctions. In particular, $\Psi^A = (-1)^{l-m}\,\Psi^B$ and $\partial\Psi^A/\partial z = (-1)^{l-m+1}\,\partial\Psi^B/\partial z$ at z = 0. We have

$$H_{BA} = \frac{\hbar^2}{2m}\int_{\varphi=0}^{2\pi}\int_{r=0}^{\infty}(-1)^{l-m}(\Psi^A \frac{\partial\Psi^{A*}}{\partial z} + \Psi^{A*}\frac{\partial\Psi^A}{\partial z}) r dr d\varphi \ . \qquad \text{(B9)}$$

We have used Eq. (B9) to evaluate H_{BA} for three particular cases: (m,l) = (0,0), (0,1), and (1,1). Explicit expressions are given in Eqs. (B10)-(B12), wells B and A centered at $z = \pm R/2$, on the line x=y=0.

$$H_{BA} = -\frac{\hbar^2 A_0^2}{2m\alpha^2 R}\exp(-\alpha R), \quad m=0, l=0 \ , \qquad \text{(B10)}$$

$$H_{BA} = \frac{\hbar^2 3A_1^2}{m\alpha^4 R^3}\left[1 + \alpha R + \frac{\alpha^2 R^2}{2}\right]\exp(-\alpha R), \quad m=0, l=1 \ , \qquad \text{(B11)}$$

$$H_{BA} = -\frac{\hbar^2 3A_1^2}{2m\alpha^4 R^3}(1 + \alpha R)\exp(-\alpha R), \quad m=1, l=1 \ . \qquad \text{(B12)}$$

These choices for (m,l) correspond for $\mathbb{0} = 0°$ to spheroidal states

$(0,\sigma)$, $(0,\pi)$, and $(1,\sigma)$, respectively. (Θ is defined in Fig. 6.) For $\Theta = 90^0$, with parallel y axes, parallel z axes, and superimposed x axes in the two wells, Eq. (B10) corresponds to $(0,\sigma)$ states and (B12) to $(0,\pi)$ states. For $\Theta = 90^0$ and $(1,\sigma)$ states, Eq. (B11) applies if $\Phi_m(\varphi) = \cos m\varphi$, and Eq. (B12) applies if $\Phi_m = \sin m\varphi$. It is possible, in principle, to obtain analytical expressions for H_{BA} for states of higher m values. However, exact numerical results can be easily obtained for spherical wells and it was considered unnecessary to derive exact analytical ones for the present purposes. Approximate analytic ones will be given elsewhere.

(iii) Comparison of Electronic Matrix Elements to Overlap Integrals for Spherical Wells

In an earlier theoretical study of orientation effects[19] it was assumed that the matrix element H_{BA} is approximately proportional to the overlap integral S_{BA}. For $(m,l) = (0,0)$ states (i.e., states for which $l=m=0$ with spherical wells of radius b) the overlap is given by

$$S_{BA}(l=0) = \frac{A_0^2 \exp(-\alpha R)}{2\alpha^4 R} \times \left[\frac{4\alpha^2}{\alpha^2+\beta^2} + 1 - e^{-2\alpha b} + \alpha\left(R - 2b\right)\right]. \tag{B13}$$

Using Eq. (B10) for H_{BA}, one finds the ratio of S_{BA} to H_{BA} is given by

$$-\frac{V_0 S_{BA}}{2H_{BA}} = 1 + \frac{V_0}{4|E|}\left[1 - e^{-2\alpha b} + \alpha(R-2b)\right], \quad m=l=0 \ . \tag{B14}$$

For spherical $(m,l) = (0,1)$ states at orientations $\Theta=0^0$ and $\Theta=90^0$, H_{BA} is given by Eqs. (B11) and (B12). No closed form expressions for S_{BA} are available, but these overlap integrals are readily evaluated numerically. The results are shown in Fig. 13.

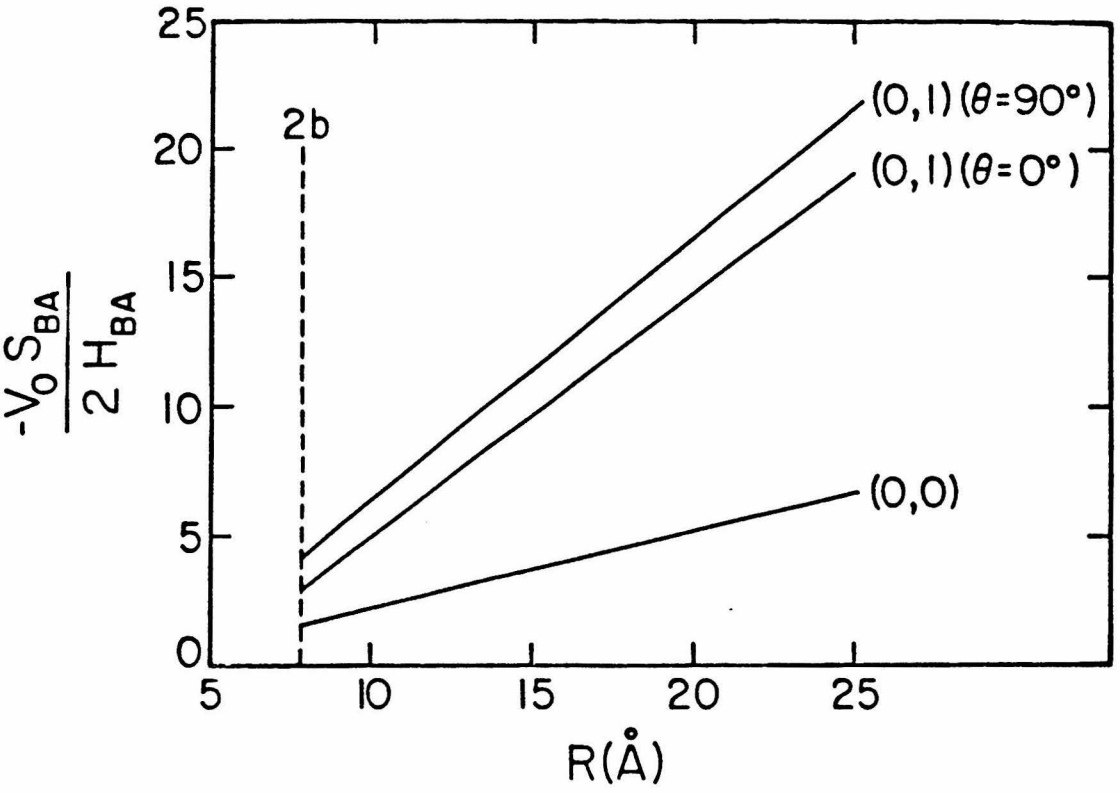

Fig. 13. Dependence of $-V_0 S_{BA} / 2H_{BA}$ for spherical wells on the separation distance R between the well centers. The well radius is 3.9145 Å and E = -1.1525 eV for all states. The spherical states are labeled as (m,l). V_0 = 2.48973 eV for (m,l) = (0,0), and V_0 = 4.19903 eV for (m,l) = (0,1).

Since H_{BA} is the overlap of the two functions in well B multiplied by V_0^B, the quantity plotted would be approximately constant if S_{BA} were proportional to H_{BA}. It is seen that the ratio grows linearly with distance and depends on orientation. Over short variations of distance proportionality may be an adequate approximation but for large variations it clearly breaks down.

On the basis of the spheroidal results in Table I we again expect $T_{BA} \approx H_{BA}$ to within 10%, at least for the results in Fig. 13, for which $R \geq$ 10 Å. On this basis, Fig. 13 also represents a plot of the ratio $S_{BA}/2T_{BA}$.

References

1. V. V. Klimov, A. V. Klevanik, V. A. Shuvalov, and A. A. Krasnovsky, FEBS Lett. **82** 183 (1977).

2. J. Fajer, M. S. Davis, A. Forman, V. V. Klimov, E. Dolan, and B. Ke, J. Amer. Chem. Soc. **102** , 7143 (1980).

3. M. S. Davis, A. Forman, and J. Fajer, Proc. Natl. Acad. Sci. U.S.A. **76,** 4170 (1979).

4. M. W. Makinen, S. A. Schichman, S. C. Hill, and H. B. Gray, Science **222** , 929 (1983).

5. T. L. Netzel, P. Kroger, C. K. Chang, I. Fujita, and J. Fajer, Chem. Phys. Lett. **67,** 223 (1979).

6. T. L. Netzel, M. A. Bergkamp, and C. K. Chang, J. Amer. Chem. Soc. **104,** 1952 (1982).

7. G. McLendon, private communication.

8. V. G. Levich and R. R. Dogonadze, Collect. Czech. Chem. Commun. **26,** 193 (1961); Translator, O. Boshko, University of Ottawa, Ontario, Canada.

9. R. R. Dogonadze, A. M. Kuznetsov, and M. A. Vorotyntsev, Phys. Status Solidi B (Ger.) **54,** 125, 425 (1972).

10. N. R. Kestner, J. Logan, and J. Jortner, J. Phys. Chem. **78,** 2148 (1974).

11. B. S. Brunschwig, J. Logan, M. D. Newton, and N. Sutin, J. Amer. Chem. Soc. **102,** 5798 (1980).

12. P. Siders and R. A. Marcus, J. Amer. Chem. Soc. **103,** 741 (1981).

13. K. Ruedenberg and C. W. Scherr, J. Chem. Phys. **21,** 1565 (1953), *ibid.* **22,** 151 (1954).

14. (a) O. Schmidt, Z. Physik. Chem. **B39,** 59 (1938); (b) *ibid.* **B42,** 83 (1939); (c) *ibid.* **B44,** 194 (1939); (d) *ibid.* **B47,** 1 (1940); O. Schmidt and H. Schmidt, Z. Physik. Chem. **B44,** 185 (1939).

15. J. R. Platt, J. Chem. Phys. **22,** 1448 (1954).

16. (a) I. V. Alexandrov, R. F. Khairutdinov, and K. I. Zamaraev, Chem. Phys. **32,** 123 (1978); J. V. Beitz and J. R. Miller, J. Chem. Phys. **71,** 4579 (1979); (b) In Alexandrov et al.[16a] the electron transfer between the biphenyl anion and napthalene had a $\beta(\equiv 2\alpha)$ of 1.2 $Å^{-1}$ and that between the same anion and phenylethylene had β = 1.0 $Å^{-1}$. In another study (J. R. Miller, private communication) the β for the same anion reacting with acridine was 1.1 $Å.^{-1}$ Electron transfer between tetramethylenediamine with a pyrene cation and with a biphenyl cation each had a β of 1.15 $Å^{-1}$ (J. R. Miller and L. V. Beitz, J. Chem. Phys. **74,** 6746 (1981)). The β inferred from conduction between two metals separated by monolayers of fatty acid salts of varying chain lengths varied between 1.0 and 1.5. [B. Mann and H. Kuhn, J. Appl. Phys. **42,** 4398 (1971); M. Sugi, T. Fukui and S. Iizima,

Appl. Phys. Lett. **27,** 559 (1975); E. E. Polymeropoulos, J. Appl. Phys. **48,** 2404 (1977)]. β's inferred from photoconduction involving excited chromophores separated from an acceptor by a fatty acid layer of known chain length were about 0.3 to 0.5 [M. Sugi, K. Nembach, D. Mobius and H. Kuhn, Solid State Commun. **15,** 1867 (1974); H. Killesreiter and H. Baessler, Chem. Phys. Lett. **11,** 411 (1971); H. Kuhn, J. Photochem. **10,** 111 (1979)].

17. Intramolecular exchange mechanisms involving intervening orbitals of atoms (or of molecules) have been examined in the literature [J. Halpern and L. E. Orgel, Disc. Faraday Soc. **29,** 32 (1960); H. M. McConnell, J. Chem. Phys. **35,** 508 (1961); S. Larsson, J. Am. Chem. Soc. **103,** 4034 (1981); S. Larsson, J. Chem. Soc. Faraday Trans. 2, **79,** 1375 (1983); S. Larsson, J. Phys. Chem. **88,** 1321 (1984); D. N. Beratan and J. J. Hopfield, J. Am. Chem. Soc. **106,** 1584 (1984).] In such models the transfer rate varies approximately as a power $1/x^{n-1}$, where n is the total number of orbitals in the shortest path from donor to acceptor which includes the donor, acceptor, and all intervening atomic or molecular centers, and $x > 1$ (cf. S. Larsson, 1984, *loc. cit.;* Beratan and Hopfield, *loc. cit.).* If each orbital occupies a length a, such a model yields a rate which is proportional to exp $[-(a^{-1} \ln x)r]$. Thus, these "exchange" models yield an exponential dependence of the rate on r. In such theories there will be differences of rate with exchange path, according as the paths are assumed to be composed of bonded species or of solvent molecules.

18. S. A. Rice and M. J. Pilling, Progr. React. Kinetics **9,** 93 (1978).

19. B. Brocklehurst, J. Phys. Chem. **83,** 536 (1979).

20. A. B. Doktorov, R. F. Khairutdinov, and K. I. Zamaraev, Chem. Phys. **61,** 351 (1981).

21. G. H. Loew, in *Iron Prophyrins, Part I,* A.B.P. Lever and H.B. Gray eds. (Addison-Wesley, Reading, MA, 1983), p. 1.

22. D. Spangler, G. M. Maggiora, L. L. Shipman, and R. E. Christoffersen, J. Amer. Chem. Soc. **99,** 7470 (1977); *ibid.* 7478 (1977).

23. A. Dedieu, M.-M Rohmer, and A. Veillard. Adv. Quant. Chem. **16,** 43 (1982).

24. J. D. Petke and G. M. Maggiora, Chem. Phys. Lett. **97,** 231 (1983).

25. Newton has performed *ab initio* calculations of the thermal matrix element for the $Fe(H_2O)_6^{3+}/Fe(H_2O)_6^{2+}$ self-exchange reaction reaction for Fe-Fe separation distances up to 10 Å. (cf. M. D. Newton, Intl. J. Quant. Chem: Quant. Chem. Symp. **14,** 363 (1980)).

26. M.-H Whangbo and K. R. Stewart, Isr. J. Chem. **23,** 133 (1983).

27. W. J. Pietro, D. E. Ellis, T. J. Marks, and M. A. Ratner, Mol. Cryst. Liq. Cryst. **105,** 273 (1984).

28. E. g., J. R. Miller and J. V. Beitz, J. Chem. Phys. **74,** 6746 (1981).

29. In all cases, energies were obtained iteratively and are accurate to not fewer than five digits.

30. Recent reviews include those of N. Sutin, Progr. Inorg. Chem. **30,** 441 (1983); L. Eberson, Adv. Phys. Org. Chem. **18,** 79 (1982); R. D. Cannon, *Electron Transfer Reactions* (Butterworths, Boston, 1980); D. DeVault, Quart. Rev. Biophys. **13,** 387 (1980); J. Ulstrup, *Charge Transfer Processes in Condensed Media, Lecture Notes in Chemistry, No. 10* (Springer-Verlag, New York, 1979). An early review is given in R. A. Marcus, Annu. Rev. Phys. Chem. **15,** 155 (1964).

31. R. T. Morrison and R. N. Boyd, *Organic Chemistry* (Allyn and Bacon, Boston, 1973) 3rd ed., p. 968.

32. Let the x-axes of the two wells both be in the plane of Fig. 6. Rotation of an eigenfunction in well A, $\Psi^A_{mtu}(\xi_A,\eta_A)\cos m\varphi_A$ by an angle γ_A about the fixed z axis yields a rotated function $\Psi^A_{mtu}(\xi_A,\eta_A)\cos m(\varphi_A-\gamma_A)$. A rotated $\Psi^B_{mtu}(\xi_B,\eta_B,\varphi_B)$ may be obtained analogously and one obtains for $H_{BA}(\gamma_A,\gamma_B)$,

$$H_{BA}(\gamma_A,\gamma_B) = \int d\tau_B \Psi^A_{mtu}(\xi_A,\eta_A)\cos m(\varphi_A-\gamma_A) \times V_0^B\,\Psi^B_{mtu}(\xi_B,\eta_B)\cos m(\varphi_B-\gamma_B)\ .$$

Introducing the addition formulae for $\cos m(\varphi_A-\gamma_A)$ and for $\cos m(\varphi_B-\gamma_B)$ into this expression and using Eq. (11) one sees that due to symmetry, only terms involving $\cos m\varphi_A\cos m\varphi_B$ and $\sin m\varphi_A \sin m\varphi_B$ are nonzero. Then, $H_{BA}(\gamma_A,\gamma_B)$ becomes $[H^{cc}_{BA}\cos m\gamma_A\cos m\gamma_B + H^{ss}_{BA}\sin m\gamma_A\sin m\gamma_B]$. $(H_{BA})_{AV}$ is as given in the second half of Eq. (11).

33. C. Flammer, *Spheroidal Wave Functions* (Stanford U. P., Stanford, California, 1957).

34. D. B. Hodge, J. Math. Phys. **11,** 2308 (1970).

35. The eigenvalues $\lambda^{i,o}_{m,n}$ were obtained using Hodge's algorithm, trivially modified as follows: The set $\Lambda = \{\lambda_{mn}; n = m + s, m + s + 2, \cdots\}$ contains the eigenvalues of a matrix that is, in principle, of infinite dimension. Hodge[34] presents a prescription for constructing the elements of the matrix so that the matrix eigenvalues are the eigenvalues of Eqs. (13) and (14). In practice, the matrix must be truncated. The eigenvalues of the truncated matrix are not, in general, equal to the eigenvalues λ_{mn} of the differential equations. In order to obtain a finite set $\Lambda_N = \{\lambda_{mn}; n = m + s, m + s + 2, \cdots, m + 2N + s - 2\}$ of true eigenvalues (i.e., eigenvalues of the differential equations), a larger set Λ_N' of approximate eigenvalues λ_{mn} was constructed, where $N' > N$ and λ_{mn} is an eigenvalue of the $N' \times N'$ truncated matrix. N' was then increased until every element of the subset $\Lambda_N \quad \Lambda_{N'}$ was constant to eleven significant digits upon successive increases of N'. At that point it was assumed that the first N true eigenvalues λ_{mn} had been obtained.

36. In cases when the expansions did not yield satisfactory convergence the functions were obtained by numerical integration of the appropriate differential equations, e.g., Eq. (13) for S^i_{mn}.

37. J. Rainwater, Phys. Rev. **79,** 432 (1950).

38. S. Granger and R. D. Spence, Phys. Rev. **83,** 460 (1951).

39. For spherical wells, the method of solution for the single site wavefunctions may be found in L. I. Schiff, *Quantum Mechanics* (McGraw-Hill, New York, 1968), 3rd ed., pp. 83-88.

40. M. Redi and J. J. Hopfield, J. Chem. Phys. **72,** 6651 (1980).

41. J. C. Slater, *Quantum Theory of Matter* (McGraw-Hill, New York, 1968), 2nd ed., p. 417.

42. R. J. Cave, P. D. Siders, and R. A. Marcus, to be published.

43. (a) T. Holstein, Ann. of Phys. (N.Y) **8,** 325 (1959); (b) *ibid.* **8,** 343 (1959).

44. P. D. Siders, Ph.D. Thesis, California Institute of Technology, Pasadena, California (1983), Chap. 5, Appendix A. Available from University Microfilms, Ann Arbor, MI, No.83-22, 674.

45. G. Arfken *Mathematical Methods for Physicists* (Academic Press, New York, 1970), 2nd ed., Chap. 12, p. 559.

46. J. R. Bardeen, Phys. Rev. Lett. **6,** 57 (1961).

Chapter 4

Mutual Orientation Effects in Electron Transfers Between Porphyrins

I. Introduction.

As increasingly detailed information is obtained on the rates and mechanisms of electron-transfer reactions it has become evident that a more complete understanding is desirable of how the separation distance and mutual orientation of a reactant pair affect the rate. This is especially true for biological and biomimetic electron-transfer pairs.[1]

For example, cytochrome *c* is a widely studied biological electron-transfer agent.[2] The heme is oriented with respect to the protein and has one edge exposed to the solution environment. Its reactions have been discussed in this context.[3] Many other biological electron transfers occur between molecules held rigidly at fixed distances and orientations. The electron-transfer rate has been measured for a [Zn^{II}, Fe^{III}] hybrid hemoglobin, for which both the orientation and separation distance of the porphyrins are known.[4] Relative orientations of biological electron-transfer pairs are under study: It has been reported that the molecular planes of the heme *c* and d_1 groups in cytochrome cd_1 of *Pseudomonas aeruginosa* are perpendicular to one another in both the reduced and oxidized forms of the protein.[5] Also, the relative orientations of the initial charge-transfer agents of photosynthetic reaction centers[6] have been determined.

Synthetic systems have also exhibited possible orientation-dependent electron transfers. Photoexcited electron transfer has been observed in the cofacial diporphyrins of Chang[7] and it has been found to proceed rapidly in the forward direction and considerably slower in the reverse.[8-10] Systems that are similar, but where the transition moments of the two porphyrin subunits are oriented perpendicularly, rather than parallel, have been examined by Overfield *et al.*[11,12] and show much

slower forward transfer than those of Refs. 7-10.[11,12] Orientation and separation-distance effects have also been examined in rigidly linked porphyrin-quinone systems,[13] so chosen because biological electron transfers frequently involve aromatic donors and acceptors such as porphyrins, porphyrin derivatives, and quinones. Also, it has been proposed that electron-transfer fluorescence quenching of Chl *a* by quinone multilayer arrays requires a favorable orientation of reactants and products.[14]

Orientation effects have been studied theoretically using a variety of models[15-21] to examine qualitative effects. Orientation effects have also been examined in studies of the ordering of spin states in bimetallic compounds,[22-24] a problem analogous to intramolecular electron transfer.[25] We have recently described a simple model for orientation effects[26] based on the delocalized nature of π electrons in aromatic systems. It is a one-electron model in which the transferable electron is assumed to be bound at an oblate-spheroidal potential well of specified depth. Electron transfer was modeled between two such non-penetrating sites, and the effects of orientation on the thermal matrix element (the electronic matrix element appearing in theories of non-adiabatic electron transfer,[27-29]) were examined for various separation distances.

In the present paper the model of Ref. 26 is applied to a number of systems of experimental interest, both biological and synthetic. The aim of the model is to illustrate possible effects of orbital and potential shape on the rate of electron transfer at fixed distances and orientations. Such calculations, to the extent that they are applicable, can reveal ways in which the architecture of individual electron-transfer pairs may help control electron-transfer rates. In particular, orientation effects are exam-

ined for the forward reaction $A^* + B \rightarrow A^+ + B^-$ for several systems, A^* denoting a photoexcited molecule, and for the highly exothermic reverse reaction $A^+ + B^- \rightarrow A + B$. The systems for which calculations are reported are (a) synthetic face-to-face porphyrins, including an open-jawed configuration, (b) porphyrin-like systems in an edge-to-edge configuration, (c) porphyrin systems comparing edge-to-edge and face-to-face as well as intermediate configurations, and (d) a photosynthetic system, involving a dimeric photoexcited chlorophyll molecule.

The actual experimental results for which orientation effects have been explicity studied are comparatively few. In particular, there are the results of Chang *et al.*[7-10] and of Overfield *et al.*[11,12] The present results will be compared with these below.

The present article is organized as follows: The model is summarized and the methods of choosing states and energies for given systems are discussed in Sec. II. Calculated results for several physical systems are given in Sec. III and they are discussed in Sec. IV.

II. Theoretical Model.

In current theories of nonadiabatic electron transfer[27-29] the rate constant for electron transfer between two reactants, A and B, at a given fixed separation distance and orientation is given by

$$k_{B<-A} = \frac{2\pi}{\hbar^2} |T_{BA}|^2 F.C. . \qquad (1)$$

In Eq. 1, *F.C.* is a sum of thermally-weighted Franck-Condon factors for the nuclear vibrational, librational, and rotational coordinates of the two reactants and the surrounding medium.[27-33] The distance and orientation dependence of the rate constant occurs mainly in the factor T_{BA},

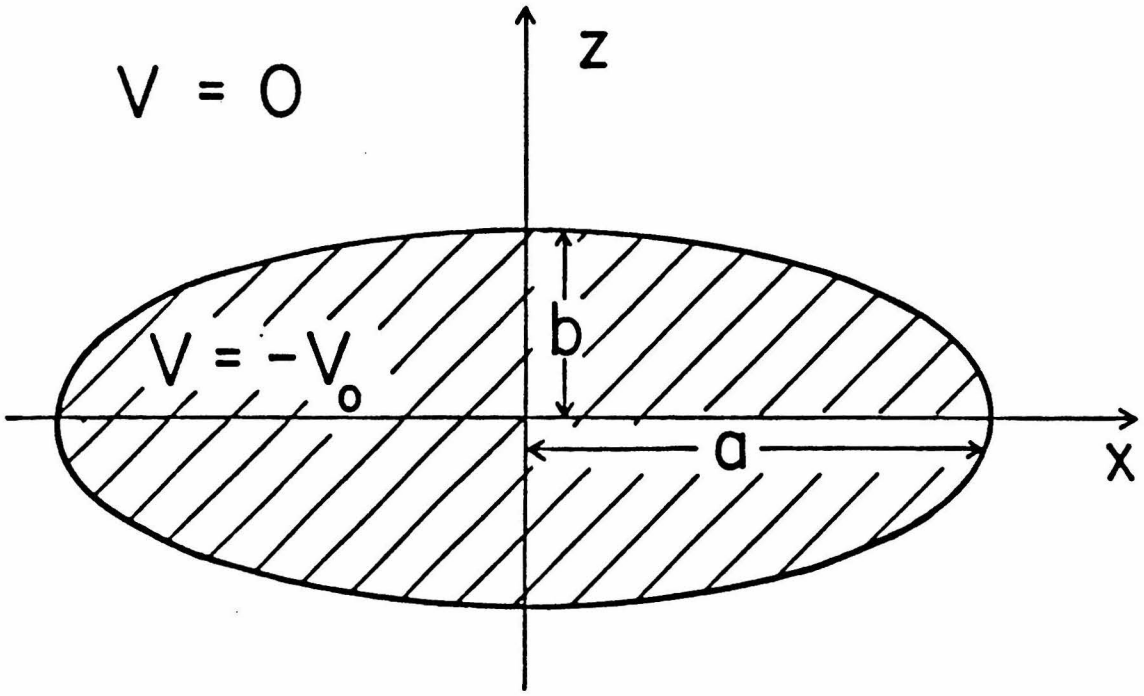

Fig. 1. Potential well for a single site. There is cylindrical symmetry about the z axis.

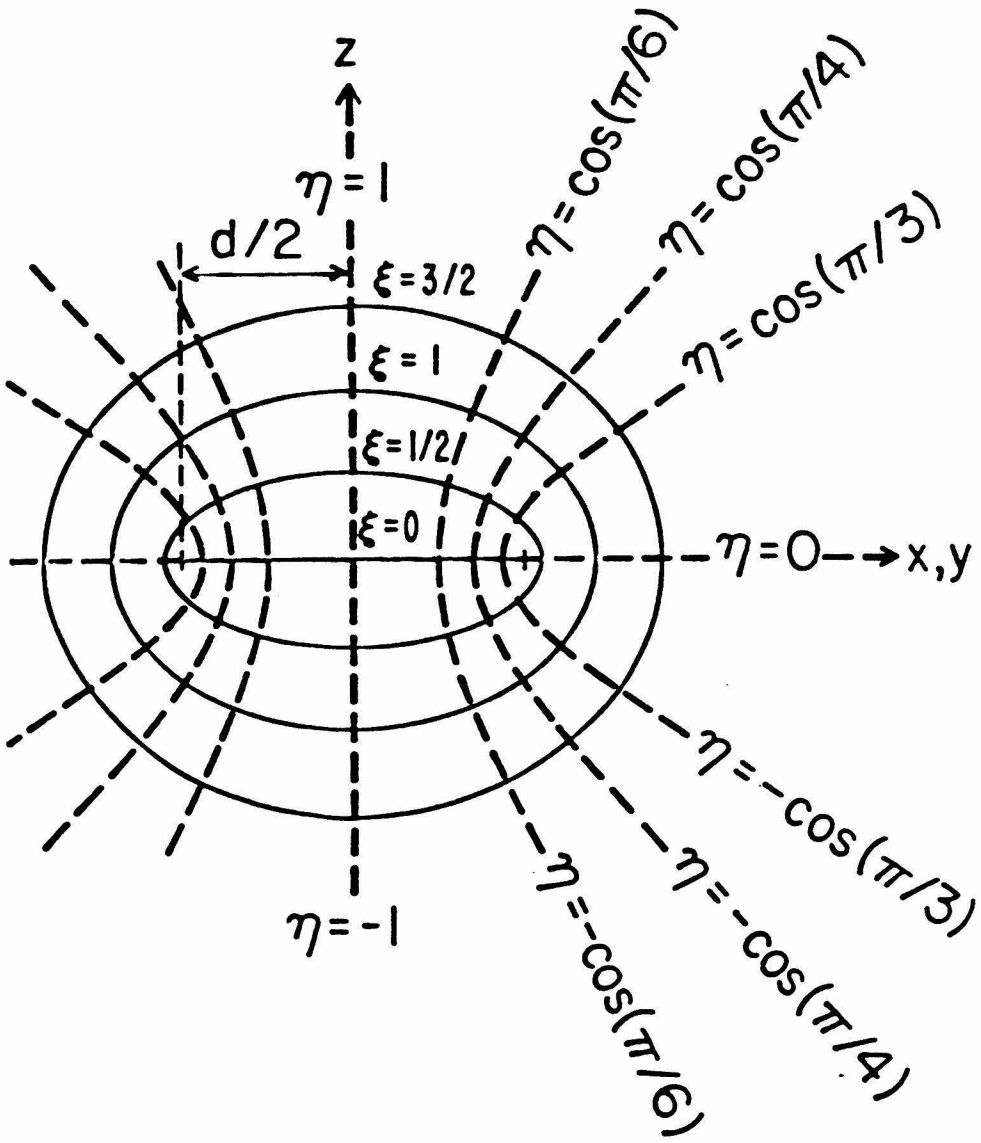

Fig. 2. Oblate-spheroidal coordinate system. Contours of constant ξ are indicated by solid lines. The dashed lines are contours of constant η. The contours of constant η on the right are for $\varphi = 0$, on the left for $\varphi = \pi$.

given by[26,28]

$$T_{BA} = (H_{BA} - S_{AB} H_{AA}) / (1 - |S_{AB}|^2) \tag{2}$$

where

$$H_{BA} = \langle \Psi_B | H_A' | \Psi_A \rangle \ , \ H_{AA} = \langle \Psi_A | H_A' | \Psi_A \rangle \ , \tag{3}$$

$$S_{AB} = \langle \Psi_A | \Psi_B \rangle \ . \tag{4}$$

The matrix element T_{BA} is calculated below within a simple one-electron model, and examined as a function of reactant separation and orientation. Ψ_A denotes the one-electron wave function associated with the electron's being localized at site A in the absence of site B; Ψ_B is analogously defined. H_A' is the difference between the actual electronic Hamiltonian of the system and the Hamiltonian for site A. A detailed description of the model and wave functions is given in Ref. 26. Several elements are briefly reviewed below.

An oblate-spheroidal square well of constant depth was chosen to model the single-site potential experienced by the single transferable electron localized at a molecule such as a porphyrin or quinone. The potential is illustrated in Figure 1. The plane of the molecule lies in the xy plane. The potential V is a negative constant, $-V_0$, inside the well and zero outside. The single-site Hamiltonian is then (in atomic units)

$$H_A = -\frac{1}{2}\nabla^2 + V_A \ . \tag{5}$$

Exact (three-dimensional) eigenfunctions were calculated for this Hamiltonian. Oblate-spheroidal coordinates[34] (ξ,η,φ) (Figure 2) were used to solve the Schroedinger equation. The coordinate φ is the angle of rotation about the z-axis. The wave function $\Psi(\xi,\eta,\varphi)$ can be written as

$\Psi(\xi,\eta)\Phi(\varphi)$. The Schroedinger equation can then be separated with respect to φ and one obtains $c_1 \cos m\varphi + c_2 \sin m\varphi$ for $\Phi_m(\varphi)$. The separation constant m depends on the given quantum state of interest. The function $\Psi(\xi,\eta)$ is even or odd with respect to reflection in the xy plane. There are three types of possible nodal surfaces, roughly corresponding to constant-coordinate surfaces for the three coordinates ξ, η and (exactly) φ. An ξ-type nodal surface is radial-like. Wave functions with one η-type node have, by symmetry, the xy plane of the potential as a nodal surface; i.e., they have π symmetry with respect to the xy-plane. Higher numbers of η-type nodes are symmetrically placed about the xy plane. The φ-type nodal surfaces are planes through the origin, perpendicular to the molecular xy plane.

When two oblate-spheroidal potential wells are chosen at a given separation distance and orientation, each with a specific single-site wave function, the various integrals in Eqs. 3 and 4 can be evaluated and T_{BA} obtained. Since the total Hamiltonian for the system, H_{TOT} is

$$H_{TOT} = -\frac{1}{2}\nabla^2 + V_A + V_B = H_A + V_B = H_B + V_A \ , \tag{6}$$

one has

$$H_A' = V_B \ . \tag{7}$$

Due to the definition of V_B the expressions in eq 3 reduce to

$$H_{BA} = -V_0^B \langle \Psi_B | \Psi_A \rangle_B \ , \ H_{AA} = -V_0^B \langle \Psi_A | \Psi_A \rangle_B \ , \tag{8}$$

where the subscript B on the integrals indicates that integration is only over well B. It was found that in all cases tested T_{BA} was equal to H_{BA} to within at least 10% and that the accuracy increased with separation distance. Accordingly, only values of H_{BA} are presented in this paper. In

Appendix A a method is shown for converting H_{BA} to a two-dimensional integral which reduces the computation time for H_{BA} significantly. The numerical results are the same as those from the direct three-dimensional integration over well B and were used here. Conceptually, it is perhaps easier to envision the three-dimensional integral, and for that reason, the discussion of the results given below is in terms of the three-dimensional expression.

The states chosen for a given calculation of H_{BA} are dependent upon the molecular system being modeled. Since the present article is concerned with electron transfers involving porphyrins and related compounds, the method of selecting the states appropriate to these systems is discussed. In all cases it is assumed that the transferable electron is localized on the porphyrin ring and does not have significant density on any central metal atom. A similar rationale could be applied to other cyclic aromatics.

The visible spectra of free-base and magnesium-containing porphyrin exhibit a characteristic set of absorptions, the Q and B bands, the B band occurring at higher energies and being much more intense.[35] The Q bands are believed due to the lowest-energy π electronic transitions of the ring.[35] Since little electronic rearrangement of the remaining electrons upon electron transfer is expected, these orbitals will be assumed to approximate the donor and acceptor orbitals in porphyrin electron transfers.

In one early theoretical attempt to understand porphyrin spectra the π- electrons were treated as being confined to a one-dimensional ring.[36] Within this treatment, the eigenfunctions are of the form $\exp(\pm m\varphi)$, the highest occupied pair of orbitals having $m = 4$; the lowest unoccupied

pair having $m = 5$.[36] The characteristics of the B and Q bands were explained as arising from allowed and forbidden transitions, respectively, between these states.[36] Later theoretical work by Gouterman[37] united the ring model description with a molecular orbital approach in what has become known as the "Four Orbital Model."[37]

The wavefunctions obtained in the molecular orbital approach[38] are real, the HOMO and HOMO-1 resembling $\cos 4\varphi$ and $\sin 4\varphi$, and the LUMO and LUMO+1 resembling $\cos 5\varphi$ and $\sin 5\varphi$. However, all four excited states generated from single excitations within these orbitals are dipole-allowed, in disagreement with experiment. Gouterman[37] showed that for a D_{4h} system with an accidental degeneracy between the HOMO and HOMO-1, configuration interaction mixes the x-polarized single excitation amongst themselves, and the y-polarized excitations amongst themselves, yielding an allowed and forbidden transition in each case. Furthermore, the states involved in the forbidden transitions were predicted to have large average values of angular momentum. The allowed and forbidden transitions were identified with the B and Q bands, respectively. For deviations from D_{4h} symmetry and/or nondegeneracy of the HOMO and HOMO-1, the Q bands are predicted to gain intensity at the expense of the B bands. Nevertheless, the Q band states are still qualitatively described in linear combinations of single excitations among the above four orbitals. Later *ab initio* calculations[39-42] have further supported the general predictions of the Four Orbital Model as to the shapes of the four orbitals, their energetic separation from other states, and the basic description of the Q band states[42]. Also, the prediction of large average angular momentum values in the the Q band states has been borne out experimentally in magnetic circular dichroism and Zeeman experiments[43-45].

(Evidence suggests that the B band states may be more complicated than the states predicted by the Four Orbital Model.[42])

In this article, states with one η-type node (i.e., π-states) and with m = 4 or 5 (designated $(4,\pi)$ and $(5,\pi)$, respectively) were chosen to qualitatively reproduce the four orbital model states. Figures 3 and 4 show contour plots of $(4,\pi)$ and $(5,\pi)$ states. The nodal patterns are qualitatively similar to those of the HOMO and LUMO orbitals in *ab initio* calculations for porphyrin-like molecules.[39-41] Metallo- and free-base porphyrins, chlorophylls and bacteriochlorophylls were all treated as having the same HOMO's and LUMO's. In modeling the excited state of a given molecule, only the excited, transferable electron is considered. The extent of mixing of the possible single excitations will determine the fraction of mixing of $\cos 5\varphi$ and $\sin 5\varphi$ in the donor wavefunction. This will depend on the symmetry, substituents, and the environment of the molecule. Using the Four Orbital Model and semiempirical[46] or *ab initio*[42] Molecular Orbital calculations, the extent of mixing between the pair of single excitations which make up the Q band could be determined, thus yielding an approximate description of the given excited state within the present model.(see Appendix B). However, the results below are presented for $\Phi_m(\varphi) = \cos 5\varphi$ or $\sin 5\varphi$ to ensure that the orientation effects seen are not peculiar to a specific choice of $\Phi_m(\varphi)$. Any $\Phi_m(\varphi)$ can be generated as a linear combination of the above.

To represent the HOMO of a (metallo-) porphyrin anion $\Phi_m = \cos 5\varphi$ or $\sin 5\varphi$ was again chosen, on the assumption that the additional electron is placed in the LUMO of the neutral molecule. ESR data on bacteriochlorophylls and bacteriopheophytins indicate that the unpaired spin density is delocalized over the entire ring.[47] The spin densities

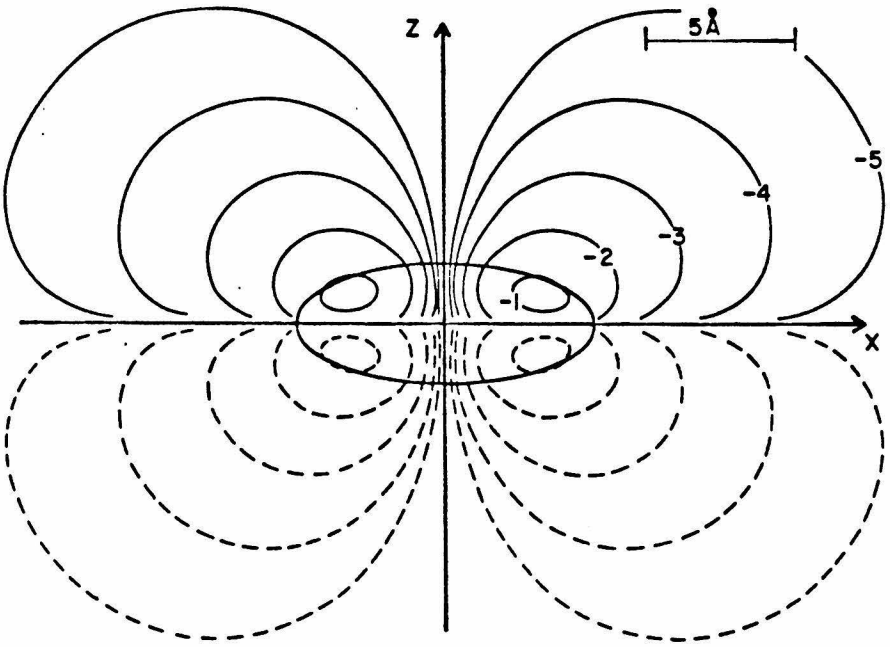

Fig. 3a. Contours of Ψ for a $(4,\pi)$ state for V_0 = 19.2227 eV, E = -0.4000 eV, a = 5 Å, b = 2 Å. The heavy line is the well boundary. The contours are labeled with values of $\log_{10}|\Psi|$. Dashed lines indicate $\Psi < 0$ and solid-line contours are for $\Psi > 0$. Contours of the wavefunction in the xz-plane are shown.

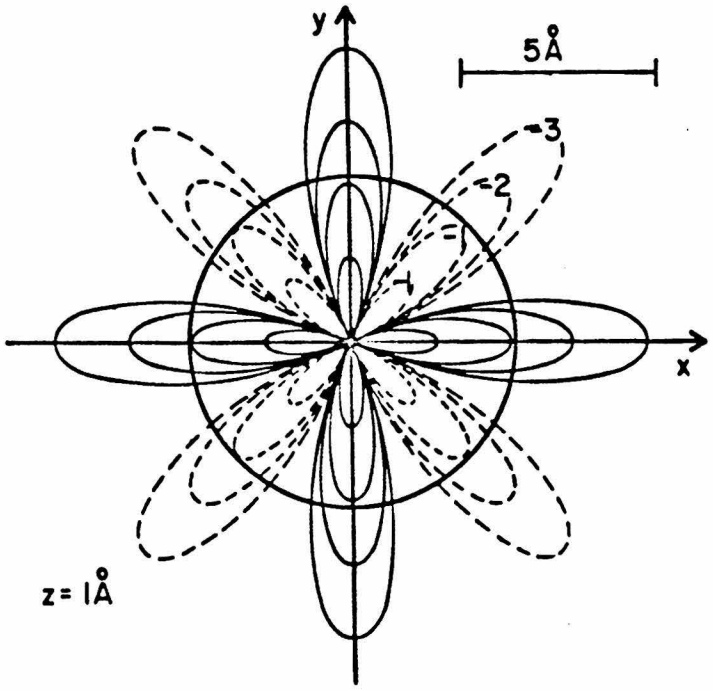

Fig. 3b. Contours of Ψ for a $(4,\pi)$ state for V_0 = 19.2227 eV, E = -0.4000 eV, a = 5 Å, b = 2 Å. The heavy line is the well boundary. The labeling conventions of Fig. 3a were used. Contours are shown of the wavefunction viewed looking down the $+z$ axis towards the origin in a plane 1Å above the xy-plane.

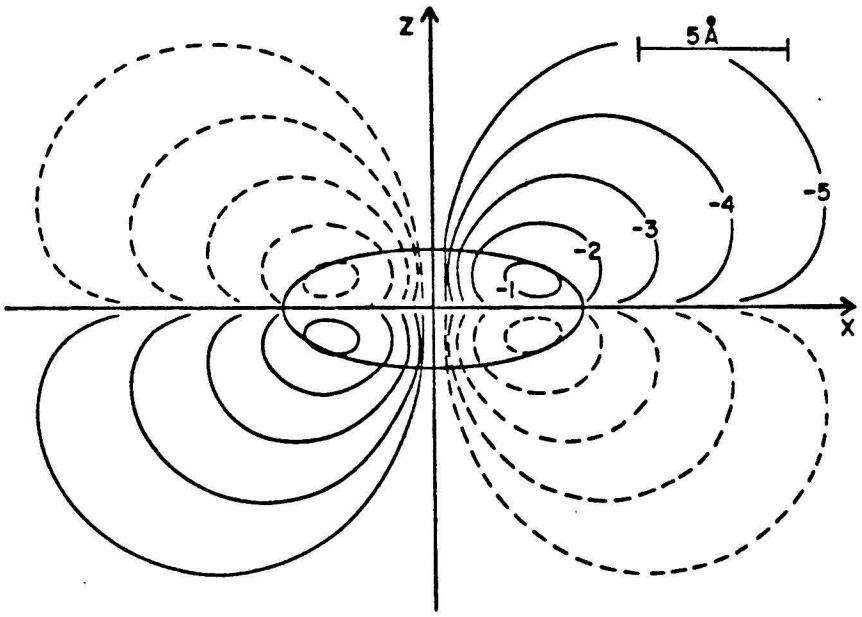

Fig. 4a. Contours of Ψ for a $(5,\pi)$ state V_0 = 23.4040 eV, E = -0.4000 eV, a = 5 Å, b = 2 Å. The labeling conventions of Fig. 3a were used. Contours of the wavefunction in the xz-plane are shown.

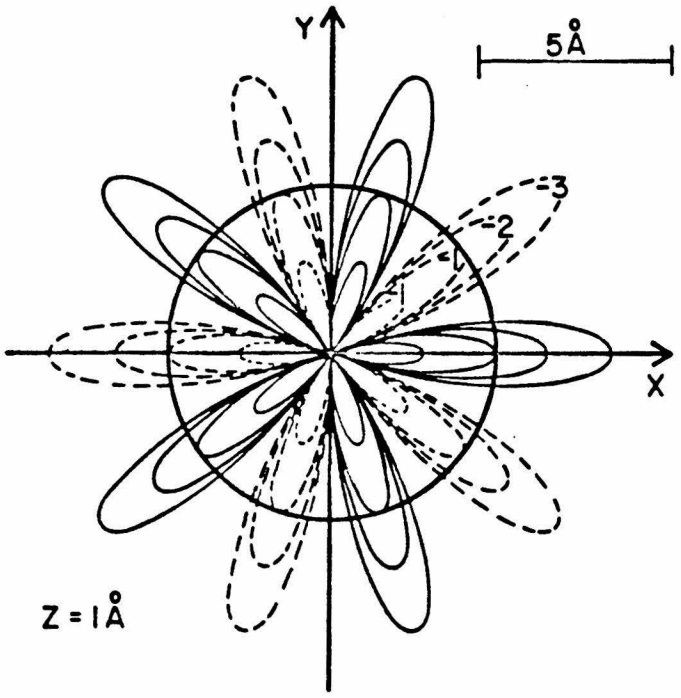

Fig. 4b. Contours of Ψ for a $(5,\pi)$ state V_0 = 23.4040 eV, E = -0.4000 eV, a = 5 Å, b = 2 Å. The labeling conventions of Fig. 3a were used. Contours of the wavefunction in the xz plane are shown. Contours are shown of the wavefunction viewed looking down the $+z$ axis towards the origin in a plane 1Å above the xy-plane.

obtained from *ab initio*[48] and semiempirical calculations[47] are in reasonable agreement with experimental results and can be approximately described as having the extra electron in the LUMO of the neutral molecule.[48]

Finally, in modeling the empty orbital in (metallo-) porphyrin cations $\Phi_m(\varphi) = \cos 4\varphi$ or $\sin 4\varphi$ $(4,\pi)$ states were selected. Evidence from comparisons of MO calculations with ESR measurements on porphyrins suggest that these cations can be described qualitatively by such localized, single-electron hole descriptions.[47]

In summary, in the results of the following section H_{BA} is examined as a function of orientation for transfer of an electron initially localized in a $(5,\pi)$ state transferring to a $(5,\pi)$ state $[(5,\pi) \rightarrow (5,\pi)]$ and for transfer of an electron initially localized in a $(5,\pi)$ orbital transfering to a $(4,\pi)$ state, $[(5,\pi) \rightarrow (4,\pi)]$. The $(5,\pi) \rightarrow (5,\pi)$ transfer can be viewed as "forward transfer" between a photo-excited molecule and a neutral acceptor. The $(5,\pi) \rightarrow (4,\pi)$ transfer can be viewed as "back transfer" from a reduced acceptor to an oxidized donor to yield the ground state species.

The sizes of the potential wells were chosen as follows. The semi-major axis a was chosen as 5 Å, an approximate in-plane radius of the porphine system.[49] The semi-minor axis b was chosen as 2 Å. This b yields an average thickness of 2.7 Å for the spheroidal well.[26] (This value represents approximately the "thickness" of the electron cloud obtained from *ab initio* calculations on a substituted porphyrin.[40] and allows approach of the "molecular" planes to distances close to those found in synthetic systems.[7,50,51]) As in Ref. 26, the trends in the results presented are not sensitive to the exact values of a and b.

E was chosen to make the decay of H_{BA} fall in the region of a number of experimental estimates.[52-56] In Ref. 26 it was shown that $H_{BA}(R)$ decayed approximately exponentially with increasing separation of the wells. The calculated decay constant β for ln $|H_{BA}|^2$ depends on what range of distances for H_{BA} were used, since H_{BA} is not a pure exponential. Here, the estimated β were obtained for edge-to-edge separations of between 10 and 20Å since several experimental studies have produced estimates of β for transfers at these distances.[55,56] In general, β decreases with increasing distance between the wells. Such distances are appropriate to those estimated in studies of tunneling in glassy matrices. Furthermore, β also depends on the orientation of the wells. The orientations chosen for estimating β were those of Figure 5d (shown below). The angles $\Theta = 0°, 60°$, and $90°$ were chosen as representative, $\Theta = 60°$ approximately corresponds to the maximum in H_{BA} as a function of Θ for a given edge-to-edge distance for this class of orientations. We have chosen $E = -0.400\,eV$ which, for $(5,\pi) \rightarrow (5,\pi)$ transfer, yields β's of $1.5Å^{-1}, 1.4Å^{-1}, 1.3Å^{-1}$ for $\Theta = 0°$, $60°$, and $90°$, respectively, over the above range of distances. Since $\Theta = 60°$ corresponds to the maximum in H_{BA} for the class of orientations, its decay should be most important in determining β when averaged over Θ. Other orientations may yield different β's but they are expected to fall in the range of the above values. In electron transfer reactions, the region of interest is that near the intersection of the reactants' and products' potential energy surfaces,[57] i.e., at the transition state for the reaction. In this region the reactants' and products' electronic energies are equal. The donor and acceptor potential depths are thus adjusted to make the energies equal to $-0.400\,eV$, for both forward and reverse transfer. The relative angular

dependence is largely unaffected by the orbital energies used.

III. Results.

Results are presented in this section for the set of orientations depicted in Figure 5. In Figure 5a the xy-planes of the two wells are assumed parallel and δ is the relative translation of the wells' z-axis in their common x-direction. The orientations in Figure 5b involve a jawing motion of the porphyrin through the angle α. At $\alpha = 0°$ the xy-planes of the wells are parallel. The interplane separation at the assumed hinge point is fixed at the value Δz. The orientations described in Figure 5c involve an edge-to-edge configuration of the wells. The wells are translated relative to one another along this common x-axis. One well is then rotated about its x-axis through an angle Γ. The parameter d (see below) is the edge-to-edge distance along the common x-axis. The orientations in Figure 5d involve wells with parallel xy-planes moved through the swing angle Θ. The parameter σ is the edge-to-edge separation distance. Finally, in Figure 5e, the types of orientations used to examine possible electronic effects in bacterial photosynthetic reaction centers are shown.

Values of H_{BA} are plotted in Figures 6 and 7 for the $(5,\pi) \rightarrow (5,\pi)$ and $(5,\pi) \rightarrow (4,\pi)$ transfer, respectively, between two porphyrins held at fixed interplane separation distance. The results are presented as a function of the slippage parameter δ defined in Figure 5a. The xy-planes are held at 4.2 Å in Figures 6a and 7a and at 5.4 Å in Figures 6b and 7b. These distances were chosen to model the interplane separations of the compounds of Chang.[7]

Calculations of H_{BA} for $(5,\pi) \rightarrow (5,\pi)$ and $(5,\pi) \rightarrow (4,\pi)$ transfers are

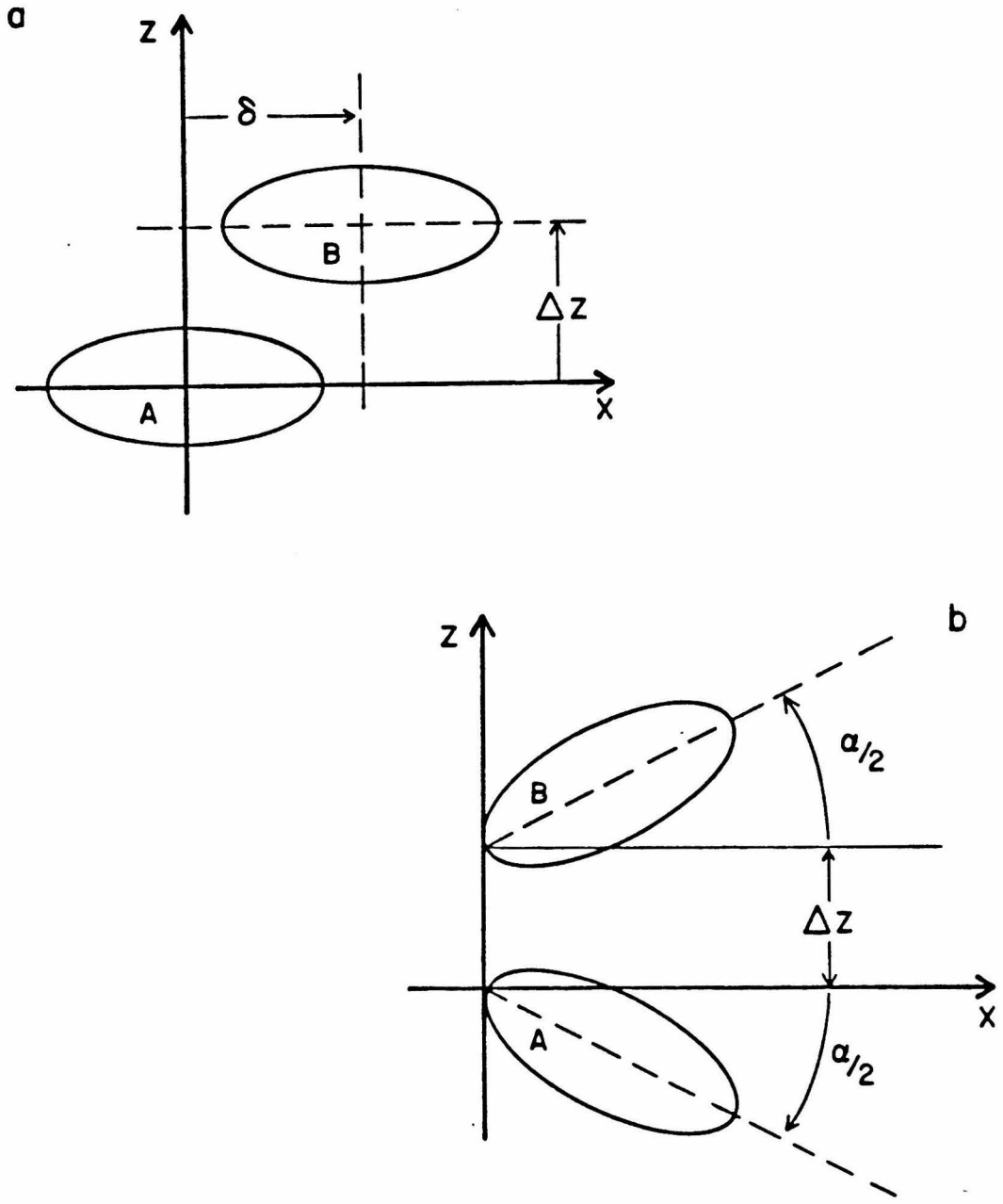

Figs. 5a, 5b. (a) Orientations examined in Figs. 6 and 7. $\delta = 0$ corresponds to superimposed z-axes at a given interplane separation, Δz. (b) Orientations examined in Fig. 8.

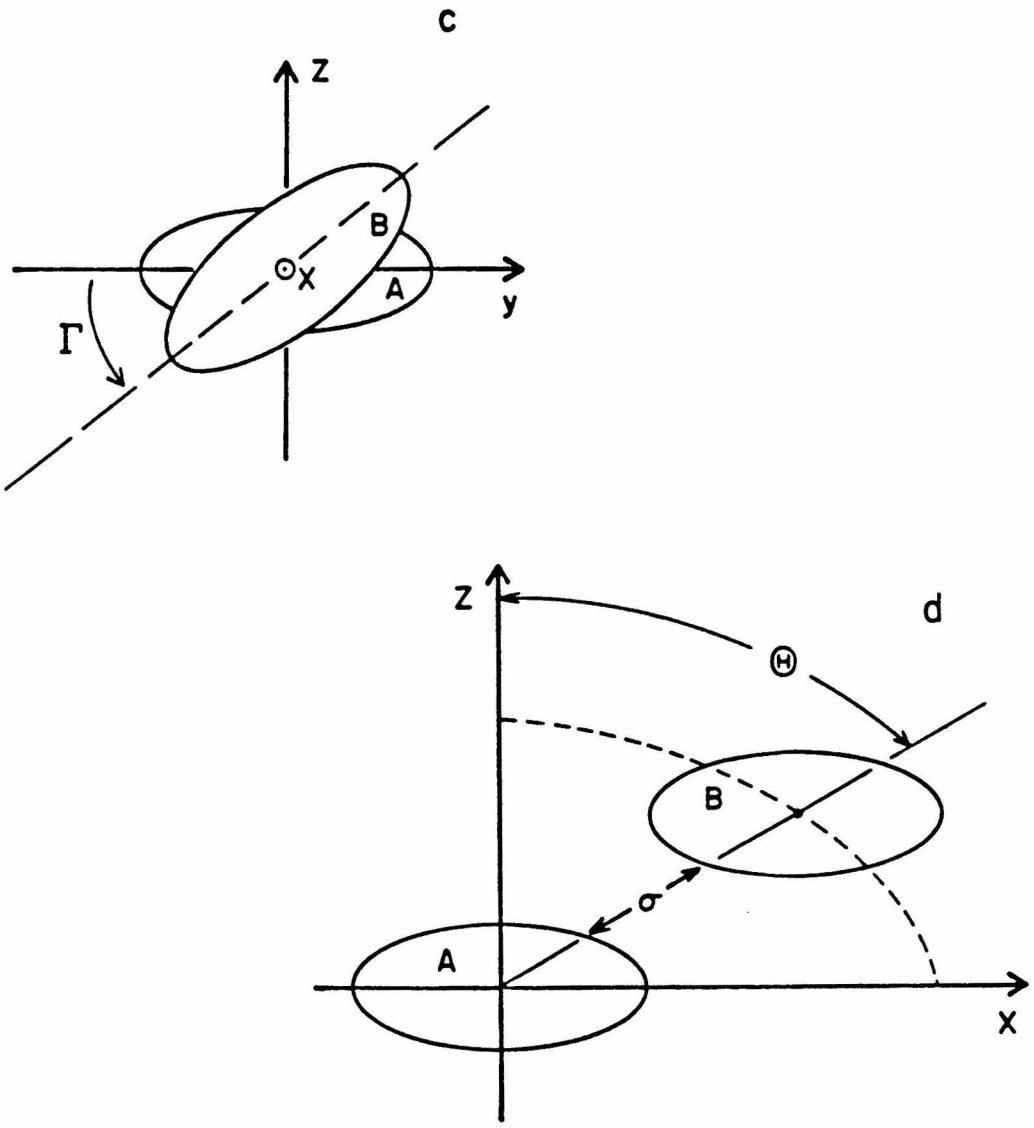

Figs. 5c, 5d. (c) End-on view of the mutual orientations of the xy-planes of the two wells for which results are presented in Fig. 9. The value $\Gamma = 0°$ corresponds to the z-axes of the wells being parallel. (d) Orientations examined in Figs. 10 and 11. The x-axes of the wells and lie in the plane of the figure in all geometries. $\Theta = 0°$ corresponds to the z-axes of the wells lying along the same line. σ is the edge-to-edge separation-distance.

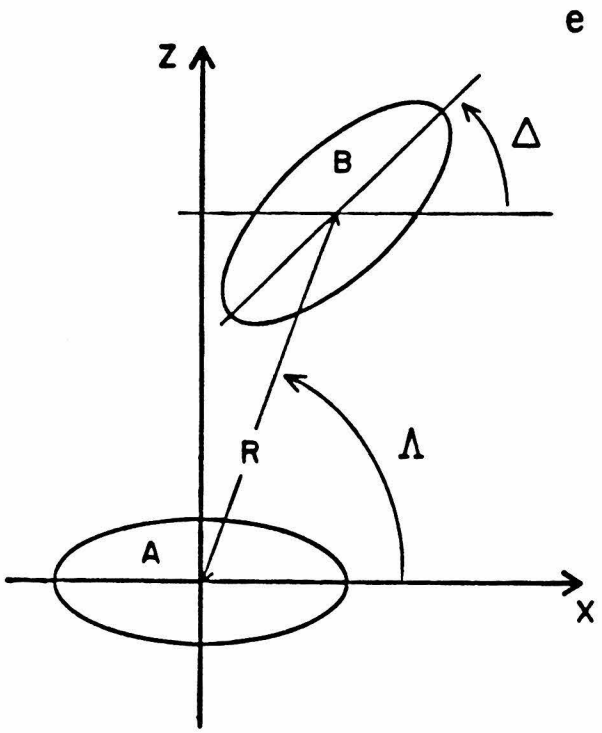

Figs. 5e. (e) Coordinate system used to describe the results presented in Figs. 12 and 13. The x-axes of the wells are in the plane of the figure. R is the center-to-center separation distance.

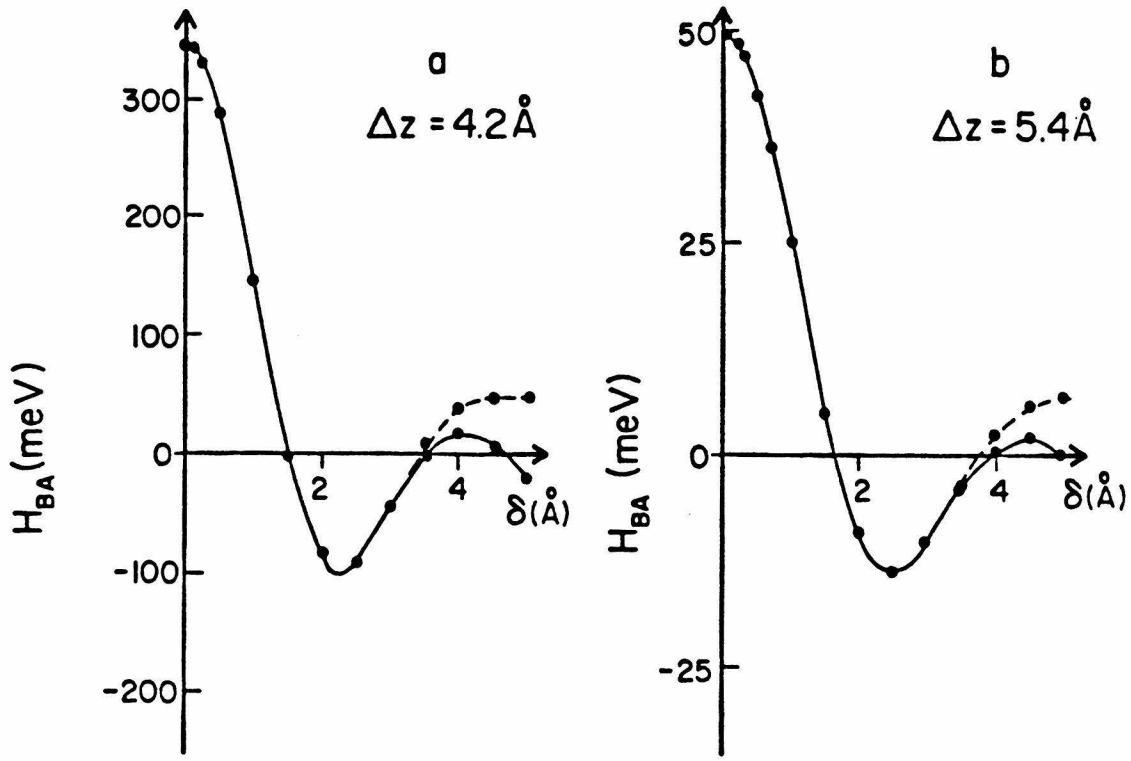

Fig. 6. Matrix element H_{BA} as a function of the slippage parameter δ defined in Fig. 5a at two fixed interplane separations for $(5,\pi) \rightarrow (5,\pi)$ transfer. For the donor and acceptor states a = 5 Å, b = 2 Å, E = -0.4000 eV, and V_0 = 23.4040 eV. The solid line indicates $\Phi_m(\varphi) = \cos m\varphi$ in each well; the dashed line indicates $\Phi m(\varphi) = \sin m\varphi$ in each well: (a) interplane spacing = 4.2 Å. (b) interplane spacing = 5.4 Å.

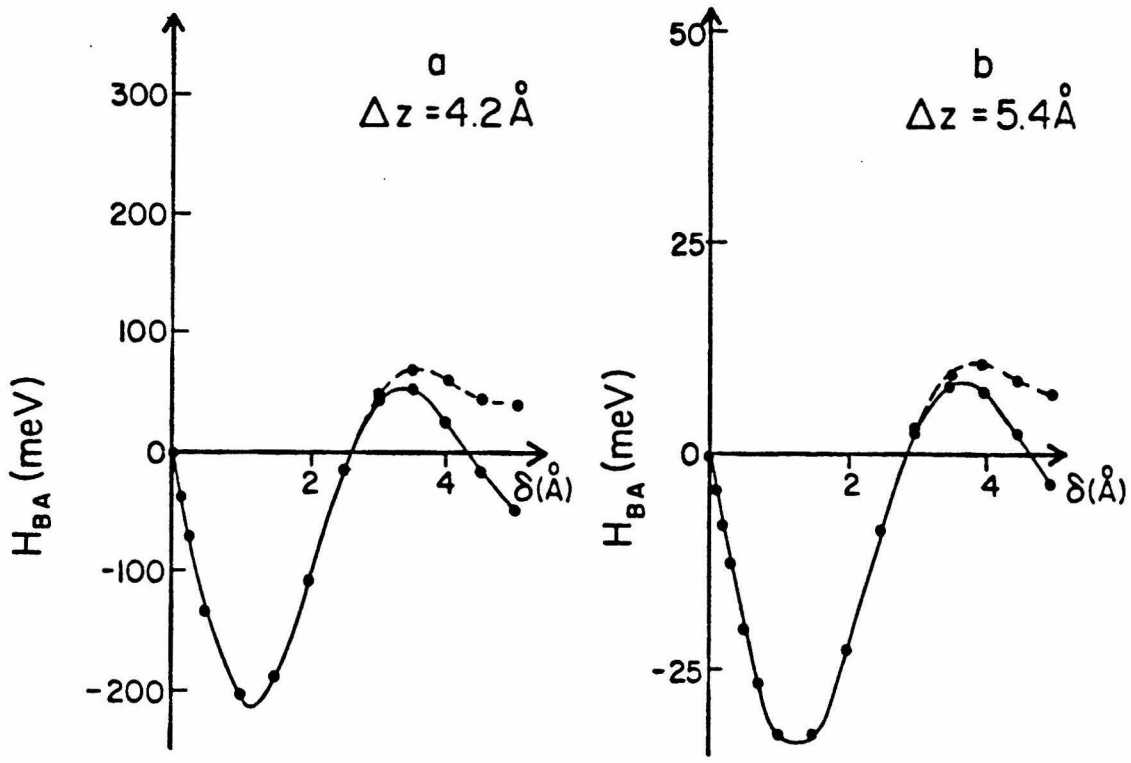

Fig. 7. Matrix element H_{BA} as a function of the slippage parameter δ defined in Fig. 5a at two fixed interplane separations for (5, π) → (4,π) transfer. For the donor and acceptor states a = 5 Å, b = 2 Å, and E = -0.4000 eV. For the donor, V_0 = 23.4040 eV. For the acceptor, V_0 = 19.2227 eV. The labeling convention of Fig. 6 was used: (a) interplane spacing = 4.2 Å. (b) interplane spacing = 5.4 Å.

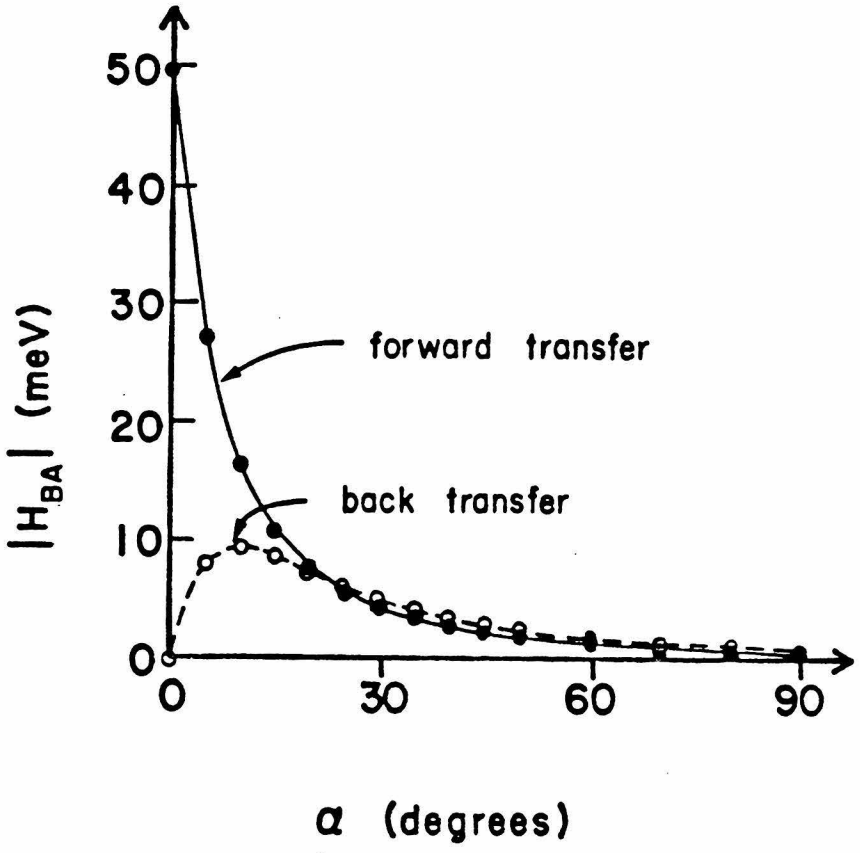

Fig. 8. Matrix element H_{BA} as a function of the jawing angle α defined in Fig. 5b between the two porphyrin planes. For $\alpha = 0$, the interplane spacing is 5.4 Å: (a) $(5,\pi) \rightarrow (5,\pi)$ transfer. For both states, $a = 5$ Å, $b = 2$ Å, E = -0.4000 eV, and $V_0 = 23.4040$ eV. (b) $(5,\pi) \rightarrow (4,\pi)$ transfer. For both states, $a = 5$ Å, $b = 2$ Å, and E = -0.4000 eV. For the donor $V_0 = 23.4040$ eV. For the acceptor $V_0 = 19.2227$ eV.

presented in Figure 8 as functions of the jawing angle α between the porphyrin planes (Figure 5b).

In Figure 9 H_{BA} is presented as a function of Γ at three different d's for the orientations shown in Figure 5c.

Values of H_{BA} calculated for the orientations of Figure 5d are presented in Figures 10 and 11. H_{BA} is shown in Figure 10 as a function of Θ for $(5,\pi) \rightarrow (5,\pi)$ transfer for three different edge-to-edge separations. Analogous results for $(5,\pi) \rightarrow (4,\pi)$ transfer are shown in Figure 11.

The class of orientations considered in Figure 5e is pertinent to the relative orientation of the special pair dimer and the Bchl *b* monomer, as presented in the recent reaction center crystal structure of *Rhodopseudomonas viridis*.[6] In modeling electron transfer between these centers it is assumed that the excited transferable electron is delocalized over a linear combination of the LUMO's of the two molecules which constitute the dimer. (In fact, its initial identification was based upon measurements indicating this delocalization.[1]) Since each Bchl *b* monomer is closely associated with only one of the two molecules in the dimer, it was assumed for simplicity that H_{BA} need only be calculated between the closest member of the dimer and the Bchl *b*.

H_{BA} as a function of Δ, with $\Lambda = \Delta$ is shown in Figure 12 for both $(5,\pi) \rightarrow (5,\pi)$ and $(5,\pi) \rightarrow (4,\pi)$ transfer. The experimental data indicate there is a 70° angle between donor and acceptor ring planes. The experimental orientation is approximated here by setting $\Delta = \Lambda = 70°$. In Figure 13 Δ is held fixed at 70° and Λ is varied from 30° to 90°.

IV. Discussion.

The results of the previous section are considered here in the order

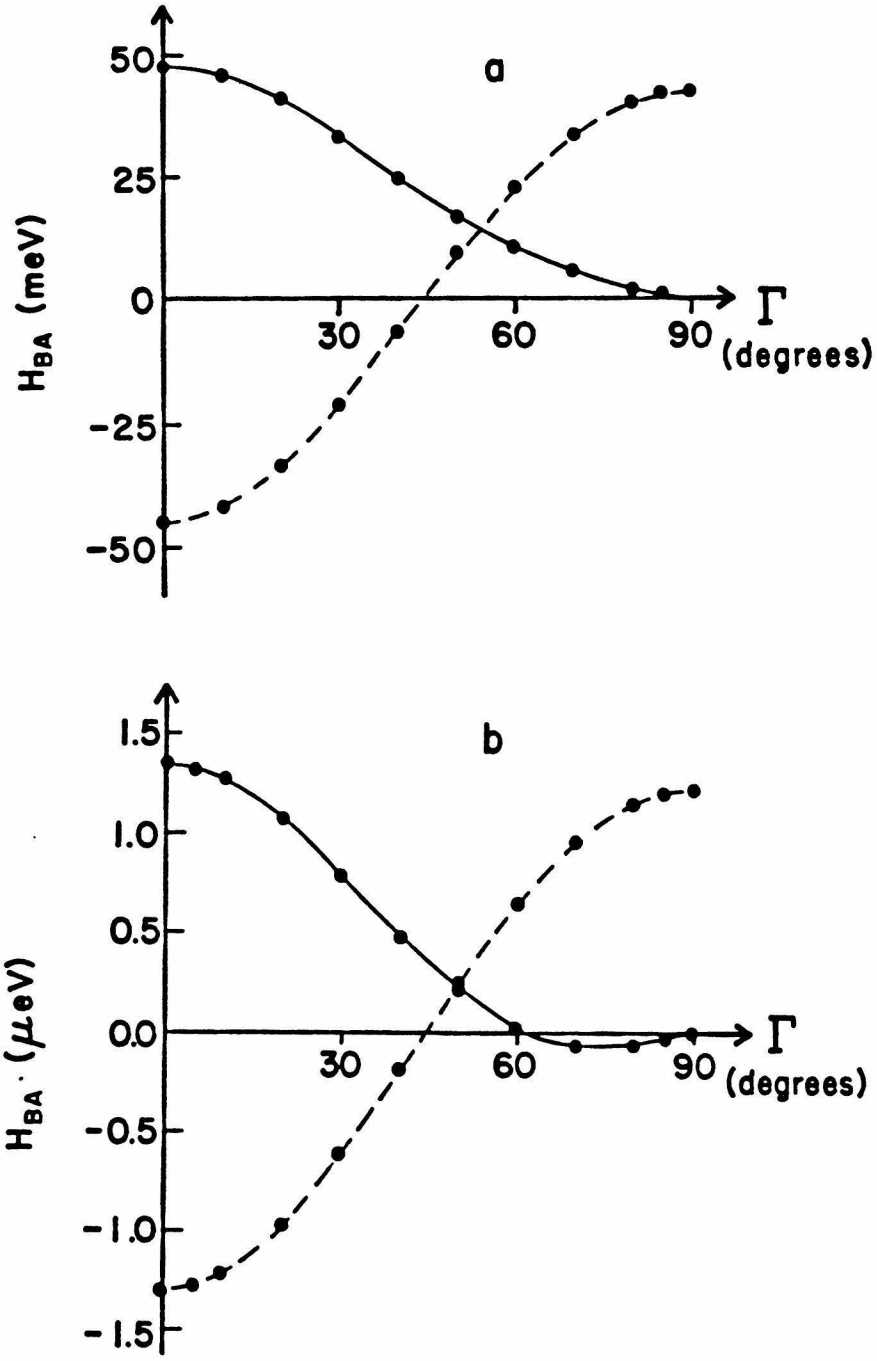

Fig. 9. Matrix element H_{BA} as a function of the twist angle Γ defined in Fig. 5c at several fixed edge-to-edge separations for $(5,\pi) \rightarrow (5,\pi)$ transfer. For the donor and acceptor states a = 5 Å, b = 2 Å, E = -0.4000 eV, and V_0 = 23.4040 eV. The labeling convention of Fig. 6 was used. (a) edge-to-edge separation = 0 Å (i.e., contact) (b) edge-to-edge separation = 10 Å.

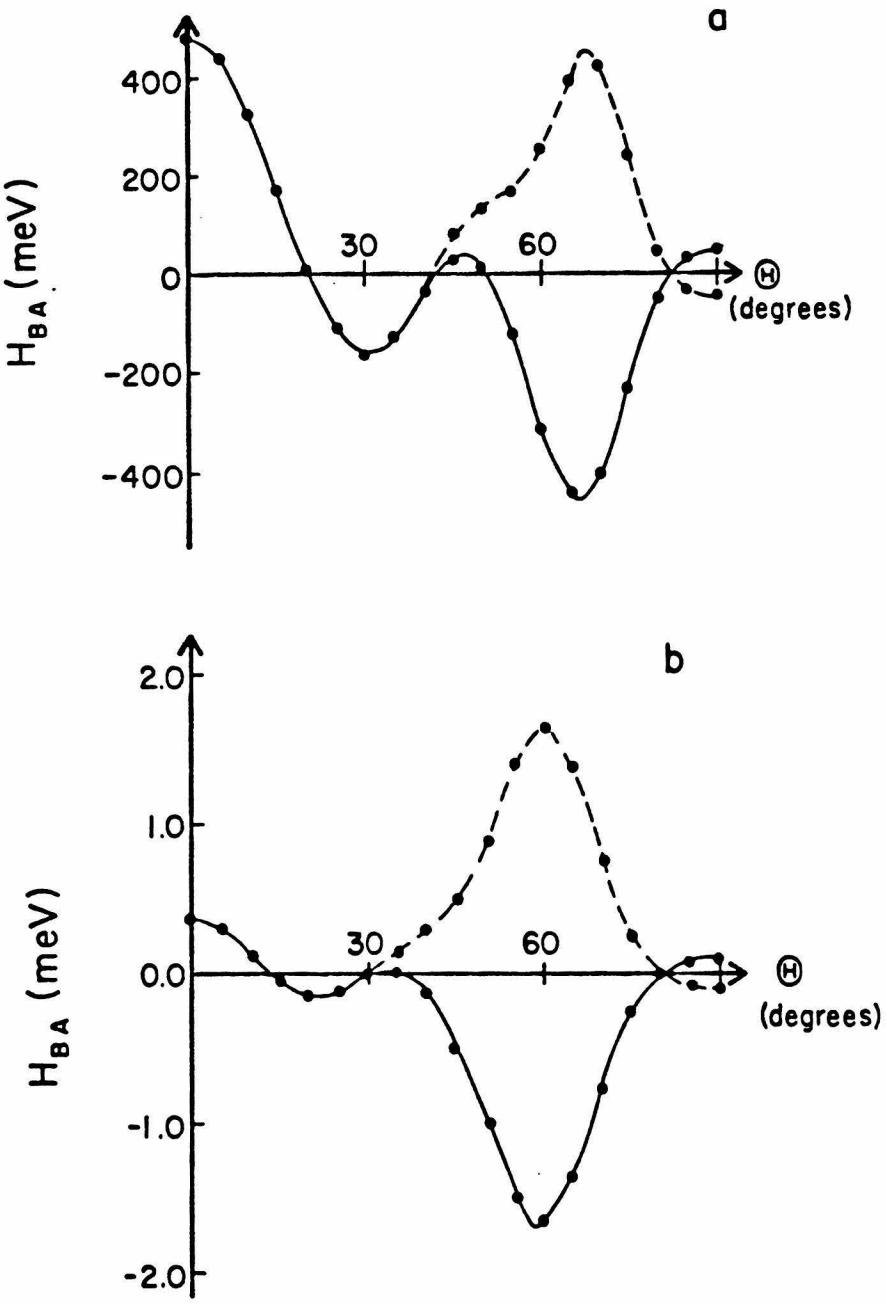

Fig. 10. Matrix element H_{BA} as a function of Θ (defined in Fig. 5d) at several fixed edge-to-edge separations for $(5,\pi) \rightarrow (5,\pi)$ transfer. For the donor and acceptor states, a = 5 Å, b = 2 Å, E = -0.4000 eV, and V_0 = 23.4040 eV. The labeling convention of Fig. 6 was used. (a) edge-to-edge separation = 0 Å (i.e., contact) (b) edge-to-edge separation = 5 Å.

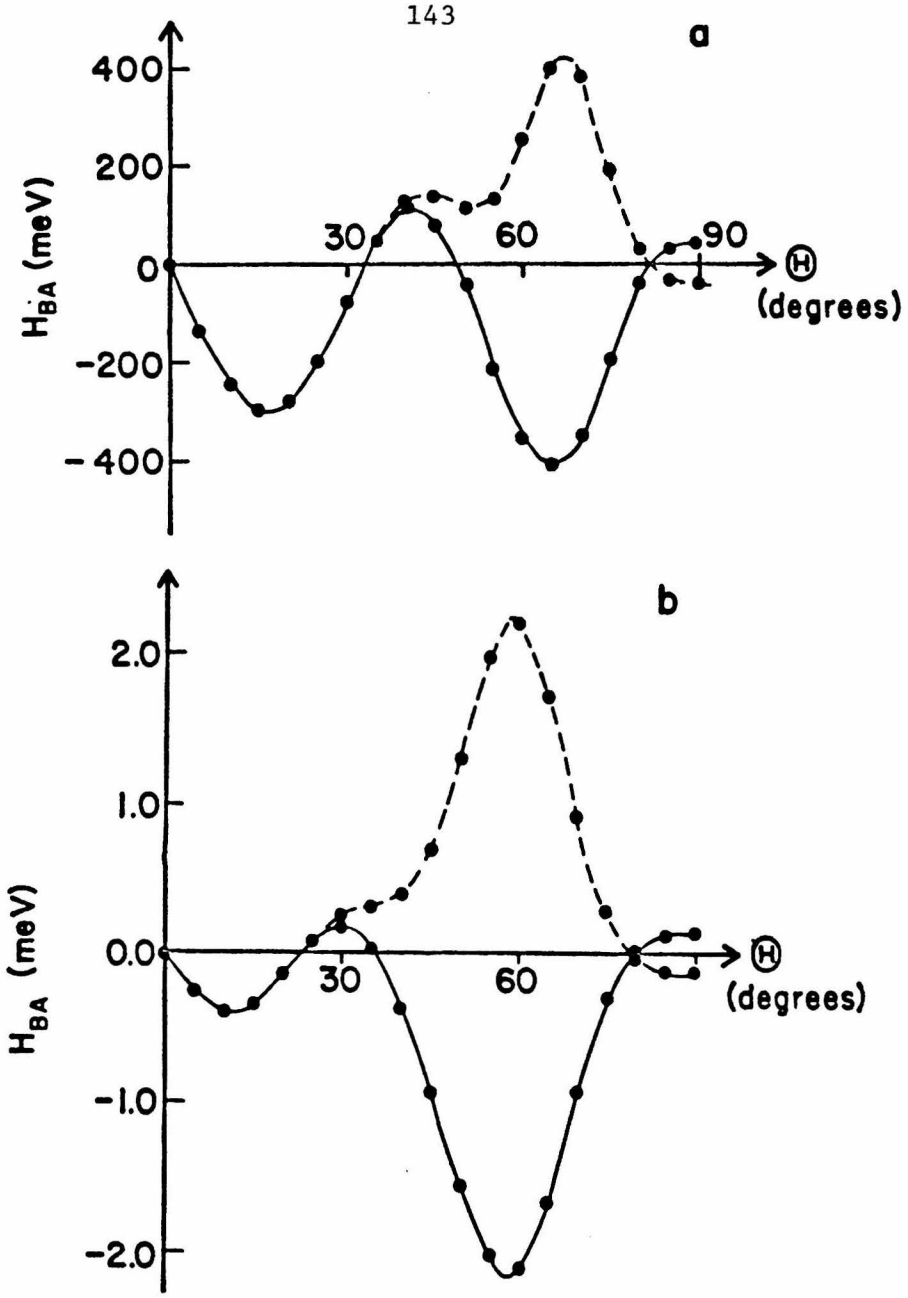

Fig. 11. Matrix element H_{BA} as a function of Θ defined in Fig. 5d at several fixed edge-to-edge separations for $(5,\pi) \rightarrow (4,\pi)$ transfers. For the donor and acceptor states a = 5 Å, b = 2 Å, and E = -0.4000 eV. For the donor V_0 = 23.4040 eV. For the acceptor, V_0 = 19.2227 eV. The conventions of Fig. 6 were followed in labeling the results. (a) edge-to-edge separation = 0 Å (i.e., contact). (b) edge-to-edge separation = 5 Å.

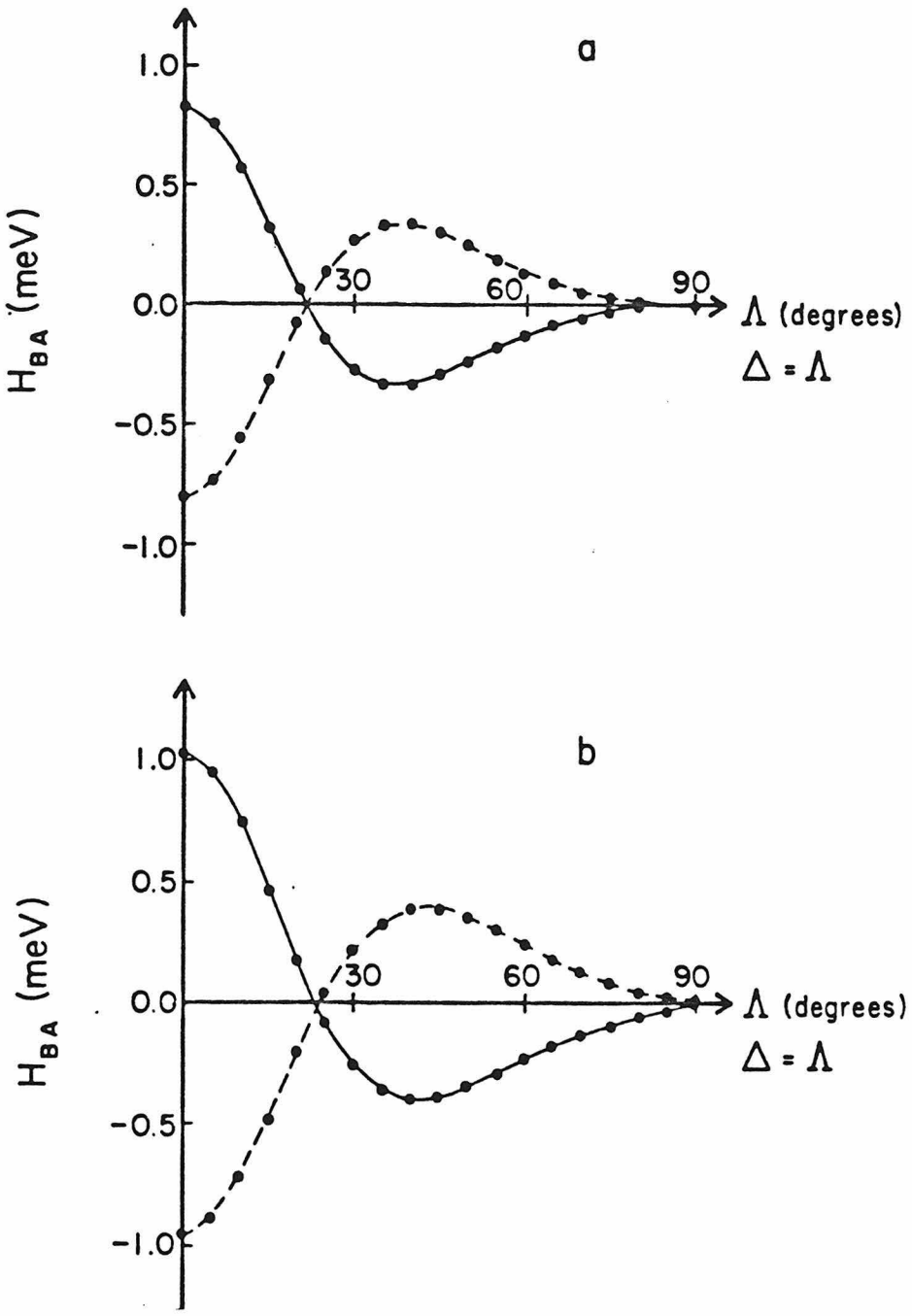

Fig. 12. Matrix element H_{BA} as a function of Δ for Δ= Λ where Δ and Λ are defined in Fig. 5e. The center-to-center separation is 13 Å. For both wells a = 5 Å, b = 2 Å. The labeling convention of Fig. 6 was used. (a) $(5,\pi) \rightarrow (5,\pi)$ transfer. E = -0.4000 eV and V_0 = 23.4040 eV. (b) $(5,\pi) \rightarrow (4,\pi)$ transfer. V_0 = 23.4040 eV for the donor and V_0 = 19.2227 eV for the acceptor, E being -0.4000 eV for both.

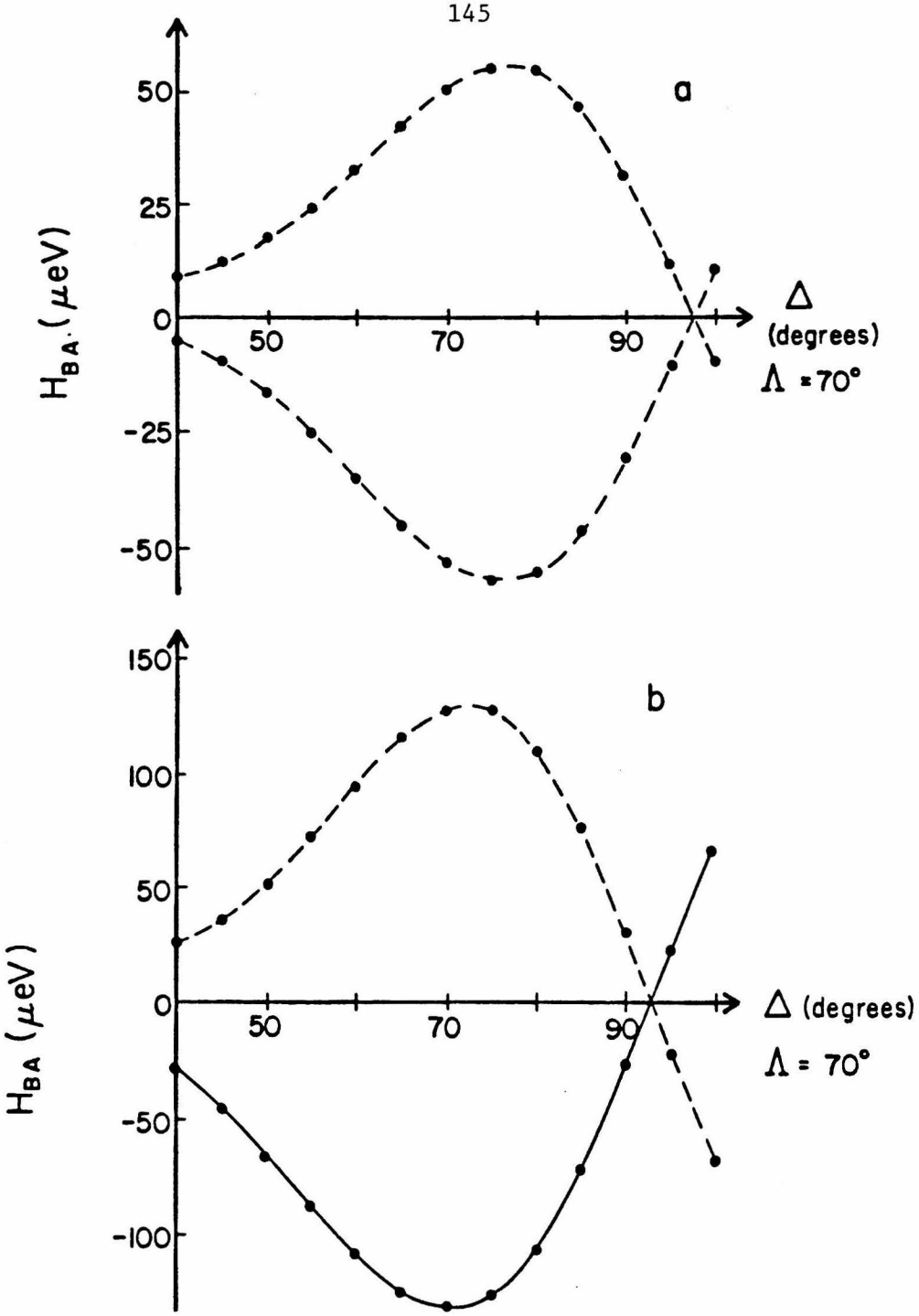

Fig. 13. Matrix element H_{BA} as a function of Λ for Δ = 70° where Δ and Λ are defined in Fig. 5e at a center-to-center separation R of 13 Å. Both wells have a = 5 Å, b = 2 Å. The states and conventions used are those of Fig. 12. (a) $(5,\pi) \rightarrow (5,\pi)$ transfer. (b) $(5,\pi) \rightarrow (4,\pi)$ transfer.

presented there.

In Figures 6 and 7 it is seen that the results are generally similar at the two interplane separations. For the $(5,\pi) \rightarrow (5,\pi)$ transfer in Figure 6 the maximum in $|H_{BA}|$ occurs at $\delta = 0$ Å with secondary maxima near $\delta = 2$ Å and 4 Å. The $(5,\pi) \rightarrow (4,\pi)$ results in Figure 7 show a zero for $|H_{BA}|$ at $\delta = 0$ Å and local maxima near $\delta = 1$ Å and 3.5 Å. The difference between forward and back transfer near $\delta = 0$ Å is purely an orbital shape effect, due to orthogonality of the $\Phi_m(\varphi)$ functions for $m = 4$ and $m = 5$ in the face-to-face configuration. When the z axes of each well lie along a common line, the product $\Phi_4(\varphi_A)\Phi_5(\varphi_B)$ vanishes by symmetry when integrated over φ_A. (Note, the integration is over well A in this case since back transfer occurs from B to A.) This large difference in forward and reverse matrix elements is very orientation-dependent: Comparing Figures 6 and 7 it is seen the forward and back transfer H_{BA}'s become of comparable magnitude for δ>3Å.

Experimental work on such face-to-face porphyrins appears to indicate[8-10] fast, light-driven forward electron transfer (<6 ps) with slow back transfer to yield ground state products (~1 ns). It has been suggested that the back transfer is slow due to an avoided crossing of the electronic surfaces[10] or because of the large driving force and small activation energy of the process, i.e., the "inverted effect".[57] The results of Figures 6 and 7 indicate that an orbital orientation effect can also contribute to the difference in rates in this configuration.

In Figures 6 and 7 the x- and y-axes of the two wells are parallel. The orientations are inappropriate to discuss the results of Overfield *et. al.*[11,12] Instead, one should consider orientations with the wells in a face-to-face orientation with one of the wells rotated 180° about a line in

the xy-plane which bisects the angle between the $+x$ and $+y$ axes. Here, the z-axes of the wells are antiparallel, while the $x(y)$ axis of well A is parallel to the $y(x)$ axis of well B. With $\Phi_m(\varphi) = \cos m\varphi$ in each well, both the $(5,\pi) \rightarrow (5,\pi)$ and $(5,\pi) \rightarrow (4,\pi)$ cases would yield zeros for H_{BA} at $\delta = 0$ Å. (Calculations are not shown.) This feature is again an orbital shape effect peculiar to the $\delta = 0$ Å orientation and results from the orthogonality of the $\Phi_m(\varphi)$'s since in the rotated configuration for $\delta = 0$ Å $\varphi_B = \pi/2 - \varphi_A$, so that $\cos 5\varphi_B = \sin 5\varphi_A$, which is itself orthogonal to $\cos 5\varphi_A$.

In order for this result to be applicable to the results of Overfield *et al.*,[11,12] the actual excited donor orbital must be orthogonal to the acceptor orbital in this rotated configuration. If both the excited state of the donor and the acceptor state can be approximately described as the same single configuration states, a slow forward rate would be expected due to an electronic orientation effect. The high intensity of the Q bands in the spectra of Ref. 11 leads one to expect a largely single configuration excited state on the basis of the Four Orbital Model.[37]

The results given for the dependence of H_{BA} on the jawing angle α for face-to-face porphyrins (Figure 8) show a dramatic dependence on jawing angle. For the $(5,\pi) \rightarrow (5,\pi)$ and $(5,\pi) \rightarrow (4,\pi)$ transfers it is seen that only for values of α less than 20° are the forward and back transfer H_{BA} significantly different.

In the results of Figure 9, which considered an edge-to-edge orientation, it is seen that the shape of the H_{BA} vs Γ plot is relatively unaffected by an increase in separation distance although H_{BA} itself rapidly decreases.

In the calculations presented in Figures 10 and 11 H_{BA} is examined at fixed edge-to-edge separations as a function of the angle Θ. The plots for both the $(5,\pi) \rightarrow (5,\pi)$ and $(5,\pi) \rightarrow (4,\pi)$ transfers exhibit several zeros and maxima between $\Theta = 0°$ and $\Theta = 90°$. At $\Theta = 0°$ the forward transfer H_{BA} shows a relative maximum while the back transfer H_{BA} is zero, the explanation being that given for the $\delta = 0$ results of Figures 5 and 6. The orbital shape effect responsible for the difference in forward and back transfer H_{BA}'s for a face-to-face orientation ($\Theta = 0°$) is not operative in the edge-to-edge configuration ($\Theta = 90°$). The results illustrate the sensitivity of H_{BA} not only to the states involved in the transfer but also to the molecular orientation. The change in relative size of the several maxima in Figures 10 and 11 as a function of separation distance can be qualitatively understood on the basis of orbital shape arguments similar to those given earlier.[26]

The orientations examined in Figures 12 and 13 are of interest to discussions of forward and reverse electron transfer in bacterial photosystems. For the approximate experimental geometry[6] ($\Delta = \Lambda = 70°$) the back transfer matrix element, in fact, is somewhat larger than that for forward transfer. Figure 13 indicates that no appreciable lowering of H_{BA} for back transfer relative to that for forward transfer can be obtained by the rocking motion examined there. The present model therefore finds no indication of electronic effects which would control electron transfer between the initial donor and the nearest Bchl monomer *b* in bacterial photosynthesis.

Other factors may then be responsible for the control of the relative forward and reverse rates in this photosynthetic system as discussed earlier, for instance the inverted effect.[57] These back-electron transfers are

excellent candidates for such effects, due to the expected low reorganization energies[7-10] and the high driving forces. It is also possible that the initial acceptor is instead a Bph rather than the adjacent Bchl*b*, in which case the orientations of these compounds should be considered, possibly via a superexchange mechanism,[19,20,58-60] with the intermediate Bchl*b*.

In general, the present results exhibit several maxima and zeros in H_{BA} as a function of the variation of a given orientational parameter. To the extent that the π-orbitals of the actual systems have shapes similar to the model wavefunctions used here, and to the extent that many-electron effects can be neglected, qualitative agreement with the present results can be expected. However, deviations of the actual positions of the maxima would not be unexpected.

We have noted that the present one-electron model predicts a large difference in forward and back transfer H_{BA}'s in the face-to-face configuration. It is useful to inquire how model-dependent this is. In D_{4h} porphyrins the HOMO and LUMO are predicted to belong to different irreducible representation of the molecular point group[36,40-41] and thus will be orthogonal in the face-to-face configuration not only for the present wavefunctions but also for more detailed ones. If the actual many-electron potential can be approximated as reasonably smooth one would expect that back transfer would be predicted to be slow using these more detailed wavefunctions. Deviations from D_{4h} symmetry do not appear to affect the general shape of the HOMO or LUMO orbitals in *ab initio* calculations,[39-41] so it is reasonable to expect that this particular prediction for the face-to-face configuration is not highly model-dependent.

The medium between two reactants is sometimes ordered and

sometimes disordered. What has not been investigated in the present paper is the detailed effect of such environments on modifying, in a superexchange mechanism, the broad picture of the relative orientation effects described in this paper. The general effects are expected to continue, nevertheless. Clearly, experimental results when they become available will be particularly helpful in defining the practical utility of the present model and its predictions.

Acknowledgments

It is a pleasure to acknowledge support of this research by the Office of Naval Research, and by the Office of Basic Energy Sciences of the U. S. Department of Energy. The calculations reported in this paper made use of the the computational facilities of the Notre Dame Radiation Laboratory and, at Caltech, of the Dreyfus-NSF theoretical chemistry computer which was funded through grants from the Camille and Henry Dreyfus Foundation, the National Science Foundation, and the Sloan Fund of the California Institute of Technology.

Appendix A: Evaluation of H_{BA} as a Surface Integral.

A simplified method for evaluating H_{BA} is presented here, based on a method introduced by Bardeen.[61] The method is applicable to all geometries of non-overlapping wells.

In the present model the main contribution to the thermal matrix element for electron transfer, H_{BA}, may be written as a volume integral over well B. That is,

$$H_{BA} = -V_0^B \int_{well B} \Psi_A \, \Psi_B^* \, d\tau \tag{A1}$$

where $d\tau$ signifies a three-dimensional integral. In well B, $-V_0^B \, \Psi_B^*$ equals $(E - T) \, \Psi_B^*$ where T is the one-electron kinetic energy operator. (We write E rather than E_B, since we consider $E_A = E_B$, as noted in the text. The method described in this Appendix is inapplicable unless the orbital energies E_A and E_B are equal.) Then eq (A1) becomes

$$H_{BA} = \int_{well B} \Psi_A \, (E - T) \, \Psi_B^* \, d\tau. \tag{A2}$$

Since

$$\Psi_B^* \, (E - T) \, \Psi_A = 0 \tag{A3}$$

anywhere outside well A, the l.h.s. of Eq. A3 can be integrated over well B and subtracted from the integral of Eq. A2 without changing the value of H_{BA}. We thus obtain

$$H_{BA} = - \int_{well B} (\Psi_B^* \, T \, \Psi_A - \Psi_A \, T \, \Psi_B^*) d\tau \ . \tag{A4}$$

The latter can be rewritten as eq A5,

$$H_{BA} = - \int_{well B} \nabla \cdot (\Psi_B^* \, \nabla \, \Psi_A - \Psi_A \, \nabla \, \Psi_B^*) d\tau \ . \tag{A5}$$

Application of the divergence theorem[62] transforms this volume integral to a surface integral which may be evaluated on any surface that does not enclose well A. For analytical results, the choice of a plane between the centers of the wells proved particularly convenient.[26] For numerical calculations, we have found it convenient to choose the surface as the boundary of well B. With this choice, H_{BA} becomes

$$H_{BA} = - \int_{surface\ of\ well\ B} \mathbf{n} \cdot (\Psi_B^* \nabla \Psi_A - \Psi_A \nabla \Psi_B^*) d\tau \ , \qquad \text{(A6)}$$

where $\mathbf{n}$ is a unit vector normal to the surface of well B. Thus, the only part of $(\Psi_B^* \nabla \Psi_A - \Psi_A \nabla \Psi_B^*)$ which needs to be calculated is the derivative normal to the surface; i.e.,

$$\mathbf{n} \cdot (\Psi_B^* \nabla \Psi_A - \Psi_A \nabla \Psi_B^*) = \Psi_B^* (\partial \Psi_A / \partial \xi_B) - \Psi_A (\partial \Psi_B^* / \partial \xi_B) \qquad \text{(A7)}$$

In Eq. A7, ξ_B denotes the coordinate ξ of the oblate spheroidal coordinate system (ξ,η,φ) which has its origin at the center of well B. The normal derivative $\partial \Psi_B^* / \partial \xi_B$ can be calculated directly from the derivative with respect to ξ of individual oblate spheroidal radial functions[34] $R_{mn}(\xi)$, centered at well B. (Ψ_B^* is an η-dependent sum of such functions.) The derivative $\partial \Psi_A / \partial \xi_B$ was calculated using a two-point central difference approximation to the derivative. In the several cases tested, it was found that $\Delta\xi = 0.001$ yielded at least three-place agreement with the three-dimensional integration for H_{BA}. The computation time for the two-dimensional integral (Eq. A6) was a factor of six to ten times less than that for the three-dimensional one.

Appendix B: Application to Multiconfiguration Excited States

We here assume that in electron transfers involving porphyrin excited states the first excited singlet state is adequately described by the Four Orbital Model.[37] For concreteness the x-polarized transitions are considered. In representing the present wavefunctions all doubly occupied molecular orbitals are neglected and assumed to be unaffected by the presence or absence of the transferable electron. Furthermore, the ξ and η dependant parts of the wavefunctions will not be considered explicitly. The functions corresponding to primitive single excitations polarized in the x direction are

$$\Psi_1 = \cos 4\varphi_A \cos 5\varphi_A \ , \quad \Psi_2 = \sin 4\varphi_A \sin 5\varphi_A \ . \tag{B1}$$

In general the two electron wavefunction should be antisymmetric under particle exhange. However, antisymmetrization will be neglected in what follows for notational simplicity, the results are not affected by this. Each of the above functions neglect two-electron interaction terms. One can include such terms approximately by allowing for configuration interaction. Within the Four Orbital Model[37] it is assumed that only the above two primitive excitations contribute significantly to the lowest excited singlet state. The secular equation which then determines the multi-configuration excited state is

$$\begin{bmatrix} E_1 & H_{12} \\ H_{21} & E_2 \end{bmatrix} \begin{bmatrix} C_1 \\ C_2 \end{bmatrix} = E \begin{bmatrix} C_1 \\ C_2 \end{bmatrix}. \tag{B2}$$

E_1 and E_2 are the energies of the primitive excitation functions of Eq. B1. H_{12} ($= H_{21}$) is a two-electron interaction term. The solutions of this equation are linear combinations of ψ_1 and ψ_2 which are then taken to model the x-polarized Q and B bands of the porphyrin. In the present

model $E_1 = E_2$ so the states obtained lead to $C_1 = \pm C_2$ but in examining asymmetric systems the spectra indicate that $E_1 \neq E_2$ in general.[46] The mixing coefficients could be taken from semiempirical[46] or *ab initio*[42] calculations while still using ψ_1 and ψ_2 to model the electronic wavefunctions. In what follows it is assumed for simplicity that $C_1 = -C_2$ but this is not necessary.

The thermal matrix element, H_{BA} is

$$H_{BA} = < \Psi_{donor} \mid V_{acceptor} \mid \Psi_{acceptor} >. \tag{B3}$$

It is assumed that Ψ_{donor} is the wavefunction corresponding to the Q branch; i.e.,

$$\Psi_{donor} = \frac{1}{\sqrt{2}}(\cos 4\varphi_A \cos 5\varphi_A - \sin 4\varphi_A \sin 5\varphi_A). \tag{B4}$$

Substituting into eq B3 H_{BA} becomes

$$H_{BA} = \frac{1}{\sqrt{2}} <\cos 4\varphi_A \cos 5\varphi_A - \sin 4\varphi_A \sin 5\varphi_A \mid V_{acceptor} \mid \Psi_{acceptor} >. \tag{B5}$$

Since the wavefunctions here are two-electron wavefunctions $V_{acceptor}$ is of the form $V_B(1) + V_B(2)$. It will be shown below, however, that only the one-electron functions computed in the text are required. In choosing $\Psi_{acceptor}$ it is assumed that the electronic state on the acceptor can be represented by a single configuration, say $\cos 4\varphi_B$. Then the possible $\Psi_{acceptor}$ states are (again neglecting all doubly occupied orbitals)

$$\Psi_{acceptor} = \begin{cases} \cos 4\varphi_A \cos 5\varphi_B \\ \sin 4\varphi_A \cos 5\varphi_b \end{cases}. \tag{B6}$$

When $< \sin 5\varphi_A \mid \cos 5\varphi_B > = 0$, as is the case for all orientations in the present article, H_{BA} becomes

$$H_{BA} = \frac{1}{\sqrt{2}} < \cos 4\varphi_A \cos 5\varphi_A \mid V_{acceptor} \mid \cos 4\varphi_A \cos 5\varphi_B >. \tag{B7}$$

This reduces to $1/\sqrt{2}$ times the individual one-electron elements calculated in the text, upon neglect of terms of order S^2.

References

1. Boxer, S.G. *Biochim. Biophys. Acta* **1983,** *726*, 265-292.

2. Dickerson, R.E. and Timkovich, R. In "The Enzymes," Boyer, P. D. Ed.; Academic Press: New York, 1975; pp. 397-547.

3 Marcus, R. A. and Sutin, N. *Biochim. Biophys. Acta*, in press.

4 McGourty, J.L.; Blough, N.V.; and Hoffman, B.M. *J. Am. Chem. Soc.* **1983,** *105*, 4470-4472.

5. Makinen, M. W.; Schichman, S. A.; Hill, S. C.; and Gray, H.B. *Science* **1983,** *222*, 929-931.

6. Deisenhofer, J.; Epp, O.; Miki, K.; Huber, R.; and Michel, H. *J. Mol. Biol.*, **1984,** *180*, 385-398.

7 Chang, C. K.; *J. Heterocycl. Chem.* **1977,** *14*, 1285-1288.

8. Netzel, T. L.; Kroger, P.; Chang, C.-K.; Fujita, I.; and Fajer, J. *Chem. Phys. Lett.* **1979,** *67*, 223-228.

9. Fujita, I.; Fajer, J.; Chang, C.-K.; Wang, C.-B.; Bergkamp, M.A.; Netzel, T.L. *J. Phys. Chem.* **1982,** *86*, 3754-3759.

10. Netzel, T.L.; Bergkamp, M. A.; Chang, C.-K. *J. Am. Chem. Soc.* **1982,** *104*, 1952-1957.

11. Overfield, R.E.; Scherz, A.; Kaufmann, K. J.; Wasielewski, M.R. *J. Am. Chem. Soc.* **1983,** *105*, 4256-4260.

12. Overfield, R.E.; Scherz, A.; Kaufmann, K. J.; Wasielewski, M.R. *J. Am. Chem. Soc.* **1983,** *105*, 5747-5752.

13. Wasielewski M. R.; Niemczyk, M. P. *J. Am. Chem. Soc.* **1984,** *106*, 5043-5045.

14. Dodelet, J.-P.; Lawrence, M. F.; Ringuet, M.; Leblanc, R. M. *Photochem. Photobiol.* **1981,** *33*, 713-720.

15. Ratner M. A.; Madhukar, A. *Chem. Phys.* **1978,** *30*, 201-215.

16. Rice S. A.; Pilling, M. J. *Progr. React. Kinet.* **1978,** *9*, 93-194.

17. Brocklehurst, B. *J. Phys. Chem.* **1979,** *83*, 536-543.

18. Doktorov, A. B.; Khairutdinov, R. F.; Zamaraev, K. I. *Chem. Phys.* **1981,** *61*, 351-364.

19. Larsson, S. *J. Am. Chem. Soc.* **1981,** *103*, 4034-4040.

20. Larsson, S. *J. Phys. Chem* **1984,** *88*, 1321-1323

21. Newton, M. D. *Int. J. Quantum Chem.: Quantum Chem. Symp.* **1980,** *14*, 363-391.

22. Hay, P. J.; Thibeault, J. C.; Hoffman, R. *J. Am. Chem. Soc.* **1975,** *97*, 4884-4899.

23. Hodgson, D.J. In "Extended Interactions Between Metal Ions," L. V. Interrante, Ed., ACS Symposium Series, 5, 1974; pp. 94-107.

24. Hatfield, W. E. *ibid*., pp. 108-141.

25. Hopfield, J. J., In "Phenomenes electrique au niveau des membrane biologique. Proc. 29th Int. Congr. Societe Chimie Physique," E. Roux, Ed., Elsevier: Amsterdam, 1977; pp. 471-492.

26. Siders, P.; Cave, R.J.; Marcus, R.A. *J. Chem. Phys.* **1984,** *81*, 5613-5624.

27. Levich, V. G.; Dogonadze, R. R. *Collec. Czech. Chem. Commun.* **1963,** *26*, 193-214. Translator, O. Boshko, University of Ottawa, Ontario, Canada.

28. Kestner, N. R.; Logan, J.; Jortner, J. *J. Phys. Chem.* **1974,** *78*, 2148-2166.

29. Ulstrup, J. "Lecture Notes in Chemistry, No. 10," Springer: New York, 1979.

30. Buhks, E.; Bixon, M.; Jortner, J.; Navon, G. *Inorg. Chem.* **1979,** *18*, 2014-2018.

31. Siders, P.; Marcus, R.A. *J. Am. Chem. Soc.* **1981,** *103*, 741-747.

32. Siders, P.; Marcus, R. A. *J. Am. Chem. Soc.* **1981,** *103*, 748-752.

33. Brunschwig, B. S.; Logan, J.; Newton, M. D.; Sutin, N. *J. Am. Chem. Soc.* **1982,** *102*, 5798-5809.

34. Flammer, C. "Spheroidal Wave Functions," Stanford University Press: Stanford, California, 1957.

35. Gouterman, M. In "The Porphyrins," Vol. III, D. Dolphin, Ed., Academic Press: New York, 1978, Chap. 1.

36. Simpson, W. T. *J. Chem. Phys.* **1949,** *17*, 1218-1221.

37. Gouterman, M. *J. Molec. Spectrosc.* **1961,** *6*, 138-163.

38. Longuet-Higgins, H. C.; Rector, C. W.; Platt, J. R. *J. Chem. Phys.* **1950,** *18*, 1174-1181.

39. Spangler, D.; Maggiora, G. M.; Shipman, L. L.; Christoffersen, R. E. *J. Am. Chem. Soc.* **1977,** *99*, 7470-7477.

40. Spangler, D.; Maggiora, G. M.; Shipman, L. L.; Christoffersen, R. E. *J. Am. Chem. Soc.* **1977,** *99*, 7478-7489.

41. Christoffersen, R. E. *Int. J. Quantum Chem.* **1979,** *16*, 573-604.

42. Petke, J.D.; Maggiora, G.M.; Shipman, L. L.; Christoffersen, R.E.; *Photochem. Photobio.* **1979,** *30*, 203-223.

43. Malley, M.; Feher, G.; Mauzerall, D. *J. Molec. Spectrosc.* **1968,** *26*, 320-324.

44. Barth, G.; Linder, R. E.; Bunnenberg, E.; Djerassi, C.; Seamans, L.; Moscowitz, A. *J. Chem. Soc. Perkin Trans.* **1974,** *2*, 1706-1711.

45. Canters, G. W.; van der Waals, J. H. In "The Porphyrins," Vol. III, D. Dolphin, Ed.; Academic Press: New York, 1978; Chapter 12.

46. Gouterman, M. In "The Porphyrins," Vol. III, D. Dolphin, Ed.; Academic Press: New York, 1978; Chapter 1.

47. Fajer, J.; Davis, M.S.; In"The Porphyrins," Vol. IV, D. Dolphin, Ed.; Academic Press: New York, 1979, Chapter 4.

48. Petke, J.D.; Maggiora, G.M.; Shipman, L. L.; Christoffersen, R.E.; *Photochem. Photobio.* **1980,** *302*, 399-414; *ibid.* **1981** *33* 663-671.

49. Webb, L. E.; Fleischer, E. B. *J. Am. Chem. Soc.* **1965,** *87*, 667-669.

50. Collman, J. P.; Chang, A. O.; Jameson, G. B.; Oakley, R. T.; Rose, E.; Schmittou, E. R.; Ibers, J. A. *J. Am. Chem. Soc.* **1981,** *103*, 516-533.

51. Hiom, J.; Paine III, J. B.; Zapf, U.; Dolphin, D. *Can. J. Chem.* **1983,** *61*, 2220-2223.

52. Alexandrov, I.V.; Khairutdinov, R.F.; Zamaraev, K.I. *Chem. Phys.* **1978,** *32*, 123-141.

53. Beitz, J.V.; Miller, J.R. *J. Chem. Phys.* **1979,** *71*, 4579-4595.

54. Miller, J.R., Beitz, J.V. *J. Chem. Phys.* **1981,** *74*, 6746-6756.

55. Strauch, S.; McLendon, G.; McGuire, M.; Guarr, T.; *J. Phys. Chem.* **1983,** *87*, 3579-3581

56. Miller, J. R.; Hartman, K. W.; Abrash, S. *J. Am. Chem. Soc.* **1982,** *104*, 4296-4298.

57. Marcus, R.A. *J. Chem. Phys.* **1965,** *43*, 679-701.

58. Halpern, J.; Orgel, L. E. *Discuss. Faraday Soc.* **1960,** *29*, 32-41.

59. McConnell, H. M. *J. Chem. Phys.* **1961,** *35*, 508-515.

60. Beratan, D. N.; Hopfield, J. J. *J. Am. Chem. Soc.* **1984,** *106*, 1584-1594.

61. Bardeen, J. R. *Phys. Rev. Lett.* **1961,** *6*, 57-59.

62. Reitz, J. R.; Milford, F. J. "Foundations of Electromagnetic Theory," 2nd ed.; Addison-Wesley: Reading, 1967; p. 13.

Chapter 5

Orientation Effects on Electron Transfer Rates: A Semiclassical Approximation for Spherical States

I. Introduction

The effect of separation distance on the rate of thermal electron transfer has been of recent interest, particularly for reactants which are held in fixed positions,[1,2] as, for instance, in some biological electron transfers.[3] Orientation effects are also expected to be of importance.[4] We have recently described a simple model for estimating orientation effects:[5] Each reactant was treated as a spheroidal or spherical well of constant (negative) depth with a zero potential outside each well. The electronic matrix element for electron transfer was calculated using the one-electron wavefunctions located at each site. The depth of the wells was chosen to yield a distance dependence of the matrix element similar to experimental estimates.[6-8] (Current experimental evidence is indirect but indicates an exponential decay of rate with distance.)

Comparison of the spherical and spheroidal results in Ref. 5 revealed two contributions to the orientation effects, namely, an orbital effect and a geometrical shape effect. The first occurs in both the spherical and spheroidal results, while the second, of course, contributes only in the spheroidal case.

In the present chapter *WKB* and uniform semiclassical approximations to the radial wavefunctions for the spherical well states are used and the results are compared with exact results for eigenvalues, wavefunction dependence on distance, and electron transfer matrix elements. The usefulness of the semiclassical methods are several: 1) their ability to treat problems having potentials which do not admit solutions in closed form, 2) the shorter computational time required, and 3) the greater transparency of the results.

Also, in the present chapter a faster method for calculation of H_{BA} is

tested which evaluates the matrix element as a two-dimensional integral using a steepest descents method. The overall savings in computational time is about a factor of sixty over the previously used method.

II. Theory

a) T_{BA} and Exact Wavefunctions

Within nonadiabatic theories of electron transfer[9,10] the rate of transfer of an electron from site A to site B is proportional to the square of the absolute value of the electron transfer matrix element, T_{BA},[9,10]

$$T_{BA} = (H_{BA} - S_{AB}H_{AA})/(1 - |S_{AB}|^2) \ , \tag{1}$$

where for eigenfunctions of the individual single-site Hamiltonians

$$H_{BA} = \int d\tau \, \Psi_B^* V_B \Psi_A \ , \quad H_{AA} = \int d\tau \, \Psi_A^* V_B \Psi_A \ ,$$
$$S_{AB} = \int d\tau \, \Psi_A^* \Psi_B \ . \tag{2}$$

Ψ_A is the wavefunction for an electron localized at site A in the absence of site B, Ψ_B is defined analogously, and V_B is the potential associated with site B (defined below). The integrals are over all space. In all cases in which T_{BA} and H_{BA} were calculated[5] it was found that

$$T_{BA} \cong H_{BA} \tag{3}$$

within an accuracy of better than 10%. Consequently, only H_{BA} is computed here.

The single-site wavefunctions satisfy a single-particle Schrödinger equation

$$(-\frac{\hbar^2}{2m}\nabla^2 + V)\Psi = E\Psi \tag{4}$$

where m is the electronic mass and

$$V = \begin{cases} -V_0, & r \le r_0 \\ 0, & r > r_0 \end{cases} . \qquad (5)$$

r_0 is the well boundary for the relevant site; i.e., r_0 equals r_0^A for site A. A standard solution of Eqs. (4)-(5) is given in Ref. 11 and yields wavefunctions of the form

$$\Psi(r,\theta,\varphi) = A\, j_l(\beta r)\, P_l^m(\theta)\Phi_m(\varphi), \quad r \le r_0, \quad \beta = [2(E-V)]^{1/2} \qquad (6a)$$

$$\Psi(r,\theta,\varphi) = B\, k_l(\alpha r) P_l^m(\theta)\Phi_m(\varphi), \quad r \ge r_0, \quad \alpha = [-2E]^{1/2} , \qquad (6b)$$

where energies and lengths are in atomic units (i.e., $\hbar$ = m = 1). These units will be used throughout. l and m are the total angular momentum of the electron and the z component of the angular momentum, respectively; $P_l^m(\theta)$, $j_l(\beta r)$, and $k_l(\alpha r)$ are an associated Legendre polynomial, a spherical Bessel function of the first kind, and a modified spherical Bessel function of the second kind,[12] respectively. Φ_m is any linear combination of $\sin m\psi$ and $\cos m\psi$. These wavefunctions can be used in Eq. (2) to calculate H_{BA}. Note, the integration over all space reduces to an integral over well B due to the form of the potential (cf. Eq. (5)).

The functions $j_l(\beta r)$ and $k_l(\alpha r)$, while readily computed, are multiterm sums for $l>0$. They are not easily visualized and complicate any approximate analytical expression due to the contribution of several terms in the sums. This led us to explore the use of *WKB*, uniform semiclassical, and asymptotic expressions for the radial portion of $\Psi(r,\theta,\varphi)$

b) *WKB* Eigenvalues and Normalization

The potential for radial motion for a typical set of l, m, E, and V values is shown in Fig. 1. Due to the form of V this potential is discontinuous at $r = r_0$, the outer turning point for classical radial motion. The

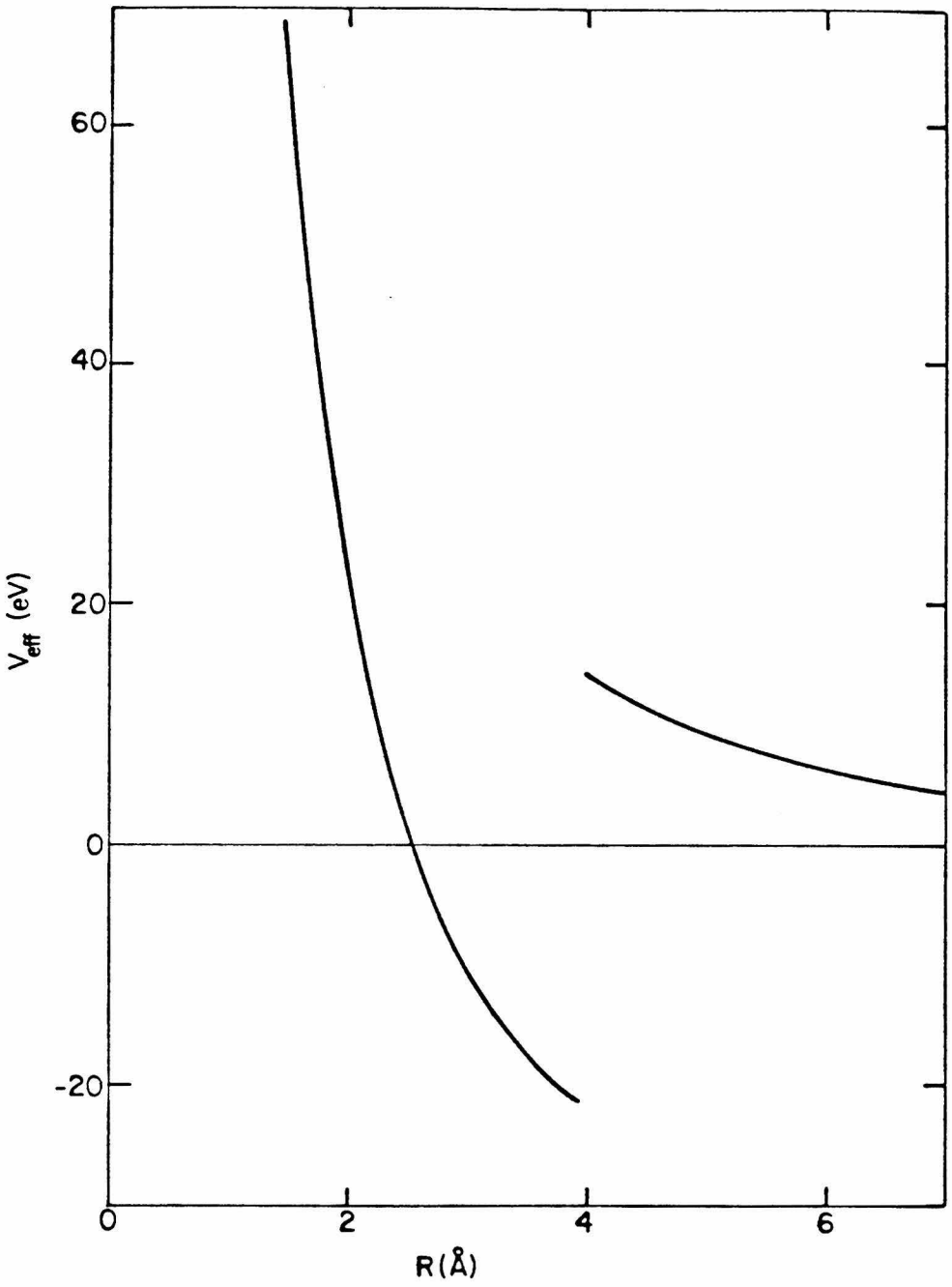

Fig. 1. Radial potential energy as a function of r. The potential parameters were l=5, V_0=18.0313 eV, and r_0= 3.91448 Å. The discontinuity at r_0 is due to the square-well potential used.

WKB approximation[13] to the inner radial function ($r \leq r_0$) is first considered.

The region $r \leq r_0$ is subdivided into two regions, $0 \leq r \leq r_<$ and $r_< \leq r \leq r_0$, where $r_<$ is the inner classical turning point for radial motion. The *WKB* expressions for $\psi_{r,i}$ (i.e., the inner radial wavefunction) that exist in each region are given by Eqs. (7) and (8), with p_r^i defined by Eq. (9).

$$\psi_{r,i}^{WKB} = \frac{B_l}{2}\exp\left(-\int_r^{r_<} |p_r^i|\,dr\right) / \left(r\sqrt{|p_r^i|}\right) \quad (0 \leq r < r_<) \ . \tag{7}$$

$$\psi_{r,i}^{WKB} = B_l \sin\left(\int_{r_<}^{r} p_r^i\,dr + \frac{\pi}{4}\right) / \left(r\sqrt{p_r^i}\right) \quad (r_< < r \leq r_0) \ . \tag{8}$$

where

$$p_r^i = \left[2\,(E + V_0) - (l + \tfrac{1}{2})^2 / r^2\right]^{\frac{1}{2}} \ . \tag{9}$$

The replacement of $l(l+1)$ in the standard radial equation by $(l + \frac{1}{2})^2$ is the usual Langer modification.[14] The outer *WKB* wave function ($r > r_0$) is similarly obtained and is given by Eq. (10) with p_r^o defined by Eq. (11).

$$\psi_{r,o}^{WKB} = C_l \exp\left(-\int_{r_0}^{r} p_r^o\,dr\right) / \left(r\sqrt{p_r^o}\right) \quad (r > r_0) \ . \tag{10}$$

$$p_r^o = \left[-2E + (l + \tfrac{1}{2})^2 / r^2\right]^{\frac{1}{2}} \quad (r > r_0) \ . \tag{11}$$

Quantization is accomplished by matching the inner and outer logarithmic derivatives of the wavefunction at r_0, as in the case of the exact wavefunction. The results using inner and outer *WKB* wavefunctions for various l, m, and V are given in Table I together with results from exact calculations. The results are generally good, the largest error being 11% for the $l = 5$ eigenvalue of the smallest well size examined.

In the present article we are primarily concerned with obtaining estimates of H_{BA}. If one is only interested in relative values of H_{BA} at various distances or orientations for a given pair of states it is not necessary to calculate the normalization constant, it being only a multiplicative factor. However, for comparison of values of H_{BA} for different pairs of states, the normalization constant is required. Therefore, an expression for it is presented below. It is assumed that the angular part of the wavefunction $(P_l^m(\theta)\Phi_m(\psi))$ is normalized to unity and the normalization constant for the radial portion of the wavefunction is obtained.

The ratio of C_l / B_l (cf. Eqs. (8), (10)) is fixed by the requirement of continuity of the wavefunction at the well boundary. B is obtained by setting $\int_0^\infty r^2 \mid \psi_r^{WKB} \mid^2 dr$ equal to unity, thereby yielding Eq. (12).

$$1 = \frac{B^2}{2}\int_{r_<}^{r_0}\frac{dr}{p_r^i} - \frac{B^2}{4(p_r^i(r_0))^2}\cos\left[2\int_{r_<}^{r_0} p_r^i\, dr\right] \qquad (12)$$

$$- \frac{C^2}{4E_0 r_0}\left[\frac{l + \tfrac{1}{2} + \sqrt{(-2E)r_0^2 + (l + \tfrac{1}{2})^2}}{r_0(-2E)^{\frac{1}{2}}}\right]^{2l+1} \exp[-2(-2Er_0^2 + (l + \tfrac{1}{2})^2)^{\frac{1}{2}}] \,.$$

The B^2 terms arise from a standard approximate evaluation of the integral for $r < r_0$.[15,16] The C^2 term is a steepest descents value of the integral from r_0 to ∞, where the exponent of the exponential part was approximated using the first two terms of its Taylor's expansion about r_0. The outer portion of Eq. (12) (the C^2 term) was tested using numerical quadrature to evaluate the radial integral outside the well. For high l states the expression for the outer portion of the normalization integral was reasonably accurate (< 10% error) but for low l states the errors increased. Nevertheless, since the outer contribution to the total

normalization constant is small, the errors in normalization constant were < 10% for a variety of states using the above analytic expression. For the comparisons of wavefunction decay and H_{BA} given below, however, the normalization constant was obtained using numerical quadrature for the outer portion of the normalization integral.

At $r_<$, the primitive semiclassical wavefunction is undefined, since $p_r^i = 0$. Near $r_<$ there will be errors in the semiclassical wavefunction due to this singularity. To improve the accuracy of the semiclassical eigenvalues, a more accurate representation for the inner wavefunction is required.

c) Uniform Semiclassical Approximation to the Inner Radial Function

To avoid the singularities inherent at the classical turning points a uniform semiclassical wavefunction was introduced. Standard methods were followed.[15,17,18] This being a one turning point problem, the Airy function, Ai, was used as a comparison function. Within this approximation one obtains

$$\psi_{r,i}^{USC} = \left[\frac{3}{2}\int_r^{r_<} |\, p_r^i\,|\, dr\right]^{\frac{1}{6}} Ai\left[\frac{3}{2}\int_r^{r_<} |\, p_r^i\,|\, dr\right]^{\frac{2}{3}} / (r\sqrt{|p_r^i|}) \qquad (0 \le r < r_<)$$

$$\psi_{r,i}^{USC} = \left[\frac{3}{2}\int_{r_<}^{r} p_r^i\, dr\right]^{\frac{1}{6}} Ai - \left[\frac{3}{2}\int_{r_<}^{r} p_r^i\, dr\right]^{\frac{2}{3}} / (r\sqrt{p_r^i}) \qquad (r_< < r \le r_0). \tag{13}$$

Since for $r > r_0$ there are no classical turning points for the outer radial motion the outer radial function can again be approximated using Eqs. (10) and (11). Quantization proceeds as before. Energy eigenvalues calculated using the uniform semiclassical inner radial function are com-

pared with the exact values in Table I. The agreement is excellent, generally being less than 1% error.

One could normalize the radial wavefunction numerically, or using an approximate analytical scheme such as steepest descents, but we have used another method which makes use of the accuracy of the semiclassical wavefunctions and the analytic normalization integrals for the exact radial wavefunctions.

For large r, the uniform semiclassical radial wavefunction can be written (using the first term in the asymptotic expansion for the Airy function[19]) as

$$\psi_{r,i}^{USC} \sim \frac{1}{\pi^{1/2} r (E + V_0)^{1/4}} \sin\left[(E + V_0)^{1/2} r - \frac{l\pi}{2} - \frac{\pi}{4}\right] . \tag{14}$$

The asymptotic form of $j_l(\beta r)$ when $\beta = (E + V_0)^{1/2}$ is[15]

$$j_l(\beta r) \sim \frac{1}{r(E + V_0)^{1/2}} \sin\left[(E + V_0)^{1/2} r - \frac{l\pi}{2} - \frac{\pi}{4}\right] . \tag{15}$$

Therefore, at large r the relation between $\psi_{r,i}^{USC}$ and j_l is

$$\psi_{r,i}^{USC} = \frac{(E + V_0)^{1/4}}{\pi^{1/2}} j_l(\beta r) . \tag{16}$$

Since the uniform approximation to j_l is a good one at all r the factor in Eq. (16) then relates $\psi_{r,i}^{USC}$ in Eq. (13) to j_l at all r. Similarly, one finds that the *WKB* expression for the outer function is related to the exact function by

$$\psi_{r,i}^{USC} = (-E)^{1/4} k_l(\alpha r) . \tag{17}$$

Introducing these two relations into $\int_0^\infty |\psi_r^{USC}|^2 r^2 dr = 1$ one obtains

$$1 = \frac{B^2 (E + V_0)^{1/2}}{\pi} \int_0^{r_0} j_l^2(\beta r) r^2 dr + (-E)^{1/2} C^2 \int_{r_0}^\infty k_l^2(\alpha r) r^2 dr \tag{18}$$

TABLE I: Energies[a] for Various States

V_0(eV), r_o(Å)	l	Exact[a]	WKB[a]	USC[a]	IWKB[a]
40, 3.91448	5	-21.46	-21.61	-21.47	-21.46
	3	-29.62	-29.73	-29.63	-29.62
	1	-35.70	-35.77	-35.71	-35.70
20, 3.91448	5	-2.85	-3.01	-2.86	-2.85
	3	-10.32	-10.42	-10.33	-10.32
	1	-15.96	-16.03	-15.97	-15.96
40, 3.0	5	-10.15	-10.42	-10.17	-10.15
	3	-23.20	-23.38	-23.22	-23.20
	1	-33.01	-33.12	-33.03	-33.01
70, 2.0	5	-5.20	-5.82	-5.25	-5.22
	3	-33.33	-33.73	-33.37	-33.33
	1	-54.69	-54.94	-54.74	-54.69

a) All energies in eV's.

where

$$\frac{C}{B} = \psi_{r,i}^{USC}(r_0) / \psi_{r,o}^{WKB}(r_0) \quad . \tag{19}$$

If one assumes

$$\psi_{r,i}^{USC}(r_0) / \psi_{r,o}^{WKB}(r_0) = (E + V_0)^{1/4} j_l(\beta r_0) / (\pi^{1/2}(-E)^{1/4} k_l(\alpha r_0)), \tag{20}$$

then Eq. (18) reduces to

$$1 = B^2 \frac{r_0^3 (E + V_0)^{1/2}}{2\pi^{1/2}} \left[\frac{j_l^2(\beta r_0)}{k_l^2(\alpha r_0)} k_{l-1}(\alpha r_0) k_{l+1}(\alpha r_0) - j_{l-1}(\beta r_0) j_{l+1}(\beta r_0) \right] \tag{21}$$

thus normalizing the radial function. (Eq. (21) was obtained using the exact expressions for the radial normalization integrals for spherical Bessel functions and modified spherical Bessel functions.[20]) The above (Eq.(21)) assumes the proportionality of the semiclassical and exact functions over the entire range of r. While this is not exact it is an excellent approximation due to the accuracy of the uniform semiclassical inner radial function and the *WKB* outer function.

To illustrate the accuracy of these calculations, the exact and approximate outer radial wavefunctions are compared in Table II as functions of distance for a state having l=5. For applications to molecules of biological interest the states of most interest have (l,m) = (5,4) and (6,5): These states are π-like and approximate, within the present spherical model, the HOMO and LUMO of the porphine-type molecules, as determined in *ab initio* electronic structure calculations.[5,21] Even though both the *USC* and the *WKB* results use primitive semiclassical outer wavefunctions, we compare both to the exact results to illustrate the effects of error in quantization and normalization. For the *USC* results it is apparent that the outer semiclassical function reproduces the exact one quite accurately. The normalization employed for the *USC*

wavefunctions is also quite accurate. The principal error in the *WKB* result is caused by an error in quantization. The incorrect energy eigenvalue in the *WKB* case leads to a faster decay rate than the exact results. Still, the agreement is quite reasonable over several orders of magnitude and the functions are certainly accurate enough for many applications (see below).

For comparison, the asymptotic expansion for $k_l(\alpha r)$ using the first two terms is also included in Table II. The value of the function was normalized by equating it to the exact function at the boundary. At large distances it will decay at the same rate as the exact function, but at the distances of interest here it is clearly inaccurate.

d) Improved *WKB* Wavefunction (*IWKB*)

Rather than using a uniform semiclassical approximation to the inner radial function, one could instead use the exact inner function and retain the outer *WKB* function due to its great accuracy. It will be shown below that one only need know the outer radial wavefunction of either site to obtain H_{BA} in most cases of interest and one would therefore need only the exact inner function for quantization.

Quantization proceeds as before; the inner and outer logarithmic derivatives are matched at the well boundary to obtain the spherical eigenvalues. These values are given in Table I and are the same as the exact values to four places.

To normalize the IWKB wavefunction one again sets $\int_0^\infty r^2 |\psi_r|^2 dr$ equal to unity, where now $\psi_{r,i} = B_l j_l(\beta r)$. C_l / B_l is obtained from continuity of the wavefunction at r_0. The inner portion of the integral can be

TABLE II. Exact and Approximate Outer Radial Functions[a] for $l = 5$

r	Exact[b]	WKB[c]	USC[d]	k_5^{asy} [e]
5	1.2(-2)[f]	1.2(-2)	1.2(-2)	2.2(-2)
7	1.2(-3)	1.1(-3)	1.1(-3)	3.9(-3)
9	1.6(-4)	1.5(-4)	1.6(-4)	8.3(-4)
11	3.0(-5)	2.5(-5)	3.0(-5)	2.0(-4)
13	6.2(-6)	5.0(-6)	6.1(-6)	4.9(-5)
15	1.4(-6)	1.1(-6)	1.4(-6)	1.3(-5)

a) $V_0 = 18.0313\text{eV}$ $r_0 = 3.91448\text{Å}$, r is the radial distance from the well center. The value of the outer wavefunction in each case is the radial function multipled by the appropriate normalization constant.

b) $E_{Exact} = -1.1525\text{eV}$

c) $E_{WKB} = -1.3142\text{eV}$

d) $E_{USC} = -1.1642\text{eV}$

e) k_5^{asy} is the first two terms in the asymptotic series for $k_5(\alpha r)$. The value was set by equating k_5^{asy} and the exact function at r_o.

f) The numbers in parentheses are the powers of ten by which each entry should be multiplied.

done analytically.[20] The outer portion can be evaluated analytically by taking advantage of the accuracy of the outer *WKB* wavefunction as was done in the previous section.

III. Calculation of H_{BA}

Use of the inner and outer semiclassical wavefunction results in a conceptually simpler radial wavefunction. A further simplification can be made in the evaluation of H_{BA} using an approach due to Bardeen.[22]

The volume integral for H_{BA} is converted to a surface integral over the surface of well B by application of the divergence theorem. Further, since the potential is zero outside each well, this surface can be extended to include any region enclosing well B which does not also enclose well A, as long as the energies of the quantum states in each well are equal (cf. Refs. 5,22). These energies are equal at the intersection of the pair of nuclear potential energy curves for reactants and products appearing in theories of electron transfer reactions.[23]

The surface chosen for the surface integral evaluation is a closed hemispherical surface which encloses well B. The radius of the hemisphere is allowed to approach infinity. The planar portion of the hemisphere is chosen perpendicular to the line connecting the centers of wells B and A. For equal well sizes and the same state in each well it is convenient to have the plane bisect the line of centers, but this is not necessary. When the states in the two wells are different, this surface may still be used but is no more convenient than any other due to the lack of symmetry. When the radius of the hemisphere approaches infinity only the planar portion of the surface integral contributes to H_{BA} and one obtains[5]

$$H_{BA} = \frac{-\hbar^2}{2m} \int_0^{\infty} b\,db \int_0^{2\pi} d\alpha \left[\Psi_A \frac{\partial \Psi_B^*}{\partial z} - \Psi_B^* \frac{\partial \Psi_A}{\partial z} \right] , \qquad (22)$$

where (b, α, z) denote cylindrical coordinates, z being the coordinate normal to the planar portion of the hemisphere.

Up to this point the procedure has been exact. Therefore, one could evaluate Eq.(22) numerically and obtain the same value as the 3D volume integral, i.e., Eq. (2) for H_{BA}. There would be a considerable savings in doing this. As a rule of thumb one expects 10-15 integration points per dimension for integrations of this type. However, in Eq. (22) there are four function evaluations per point, as opposed to two per point in Eq. (2), yielding a savings of a factor of between five and eight. However, we have also explored the use of approximate integration techniques to obtain simpler, more compact, expressions for H_{BA}. These turn out to be significantly faster than direct numerical evaluation.

To evaluate the double integral in Eq. (22) it is convenient to use the method of steepest descents.[24] The integrand in Eq. (22), including the $(-\hbar^2 b / 2m)$ factor, is of the form $\varphi(b,\alpha) \exp[-\gamma(b,\alpha)]$, where the exponential parts of the various wavefunctions and of their z-derivatives have been written as $\exp(-\gamma)$ and where the pre-exponential part is denoted by φ. Eq. (22) can then be rewritten as

$$H_{BA} = \int_0^{\infty} \int_0^{2\pi} e^{-F(b,\alpha)}\, d\alpha db \qquad (23)$$

where

$$F(b,\alpha) = \gamma(b,\alpha) - \ln \varphi(b,\alpha) \quad . \qquad (24)$$

When $F(b,\alpha)$ is expanded quadratically about its minimum at (b_0,α_0) one obtains upon integration

$$H_{BA} = \frac{2\pi e^{-F(b_0,\alpha_0)}}{|F_{bb}F_{aa} - F_{ba}^2|^{1/2}} \tag{25}$$

where F_{bb} denotes the second derivative of F with respect to b evaluated at (b_0,α_0), etc. When there is more than one minimum in F in the plane one obtains

$$H_{BA} = \sum_{i=1}^{N} H_{BA}(b_0^i,\alpha_0^i) \ , \tag{26}$$

N being the number of minima of F in the plane and $H_{BA}(b_0^i,\alpha_0^i)$ being the contribution to H_{BA} from the i^{th} minimum. For a highly symmetric case such as the $\Theta = 90°$ orientation, there are four minima, all of which contribute equally, thus Eq. (26) becomes

$$H_{BA} = \frac{8\pi e^{-F(b_0,\alpha_0)}}{|F_{bb}F_{aa} - F_{ba}^2|^{1/2}} \tag{27}$$

where all quantities are evaluated at (b_0, α_0). These points, where F is a local minimum in the plane, are calculated as follows. The minimum in F as a function of b was calculated for several values of α in the region $(0,2\pi)$ using Newton's method.[25] The values were then fitted with a spline function and the minimum of this function with respect to α found. This point was identified with the minimum in F. The second derivatives at the minimum were calculated using a three-point finite difference scheme. In the case of $\Theta = 0$ (defined later), the α-integral in Eq. (22) can be evaluated analytically. One can then write Eq. (22) as

$$H_{BA} = \int_0^\infty e^{-G(b)}\, db \simeq (2\pi/|G_{bb}|)^{1/2} \exp[-G(b)] \quad (\Theta = 0^0) \tag{28}$$

where the steepest descents method was used to obtain the r.h.s. of Eq. (28).

IV. Results for H_{BA} and Discussion

In calculations of H_{BA} the coordinate system shown in Fig. 2 is used to specify the relative orientation of the two wells. For all calculations herein the z-axes and the xy-planes of the two wells are each parallel and the l's are equal for the states in each well, as are the m's. Results are given for the $\Theta = 0^0$ (face-to-face) and $\Theta = 90^0$ (edge-to-edge) orientations. The present approximate method of evaluation of H_{BA} is most easily applied for these orientations because of symmetry.

Results for H_{BA} for the $\Theta = 0^0$ orientation are presented in Table III and were obtained using a one-dimensional search for the minimum of G in Eq. (28). The exact and approximate results are seen to be in excellent agreement in the *IWKB* and *USC* cases. Similar accuracy is obtained for other values of l, r_0, and E. The *WKB* results show good agreement and are in error by at most 40% in absolute value over several orders of magnitude variation in H_{BA}.

Results for H_{BA} for the $\Theta = 90^0$ orientation are presented in Table IV. They were obtained using a two-dimensional search for the minimum in F, $F(b_0,\alpha_0)$. The agreement of the exact results for H_{BA} with the *IWKB* and *USC* results is excellent, typically better than 10% for a variety of values of l, E, and r_0. This error is most likely due to small errors in the steepest descents evaluation of the angular portion of the surface integral. Again, the *WKB* results show good distance dependence and acceptable agreement in absolute magnitude for the present application.

The errors in relative values of H_{BA} for two distances or orientations for a given pair of states using the *WKB* wavefunctions are due primarily to errors in the semiclassical eigenvalue. (The normalization constant

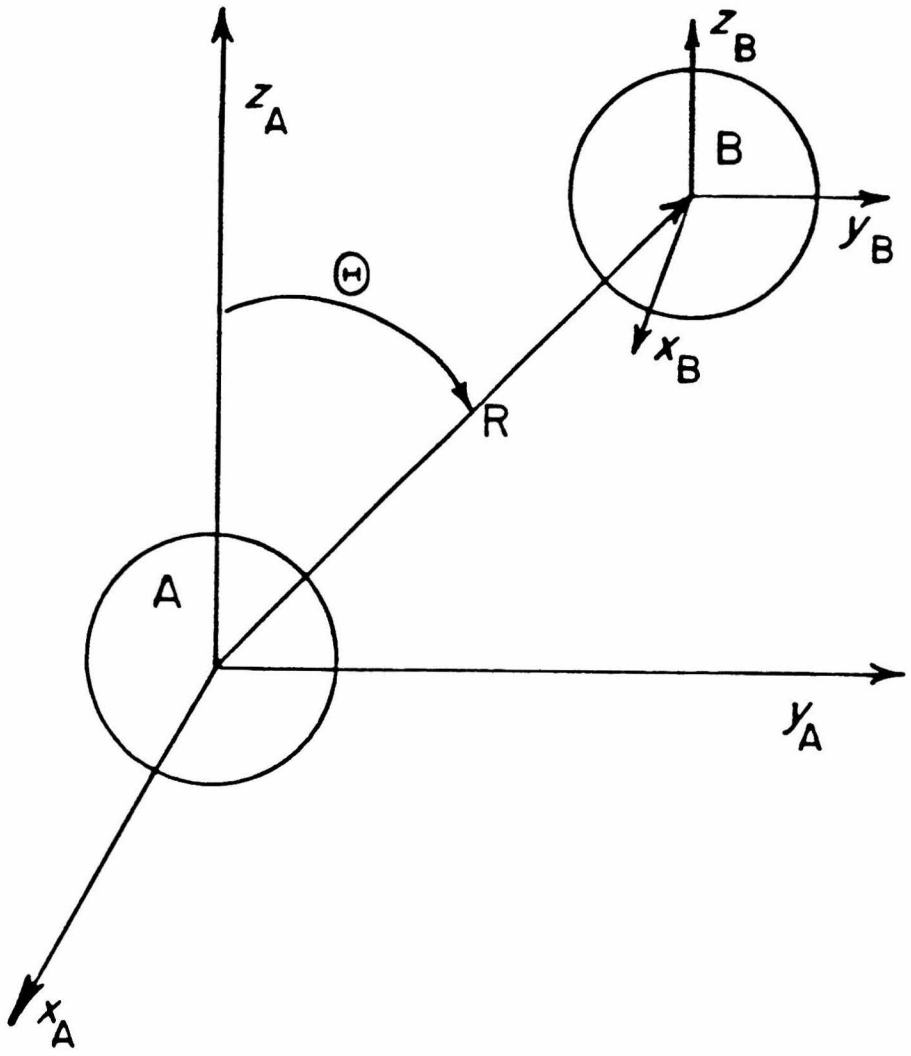

Fig. 2. Coordinate system used to specify the mutual orientation of wells A and B. The x axes of the wells are assumed parallel and lie in the plane of the figure. $\Theta = 0^{\circ}$ corresponds to the z axes of the wells lying along the same line.

will cancel when calculating relative values and the error from steepest descents integration is, at most, ~10%.) However, this is less than 20% over the entire range for the results of Tables (III) and (IV). (At 10 Å the exact H_{BA} ($\Theta = 90°$)/ H_{BA} ($\Theta = 0°$) is 14.3, the semiclassical value is 15.3. At 25 Å, the exact value is 41.1, the semiclassical value is 48.7.) Overall, the *WKB* results are quite accurate. Errors will be larger, however, for small r_0 (< 2.0 Å) or larger (l) values at fixed r_0. (We have examined up to $l = 6$ and found good agreement.) Neither case is of interest for biological systems. In general, calculations were performed by choosing a value of E which yields a given approximate decay for H_{BA} with distance. Therefore, the outer semiclassical wavefunction (*WKB*, *USC*, or *IWKB*) will have the same decay as the exact.

For fixed energy, distance, and l, it can be seen that the values of H_{BA} (and therefore T_{BA}) are quite different in the two orientations. The slopes of H_{BA} versus separation distance are also somewhat different. The difference in behavior of H_{BA} at the two orientations is due to the difference in the angular functions $P_l^m(\theta)$ in the region of greatest overlap of the two wavefunctions, and was discussed in Ref. 5. In general, one expects maxima and minima in $H_{BA}(\theta)$ to correlate with maxima and minima in $P_l^m(\theta_A)$ and $P_l^m(\theta_B)$.

Not only is the two-dimensional approximate evaluation of H_{BA} using *WKB* outer radial functions quite accurate, its evaluation is significantly faster than the three-dimensional exact calculation preformed previously. The exact calculations take from 10 to 12 CPU minutes per orientation on a VAX 11/780. The approximate results take ~15 CPU seconds. Possible approximate extensions of the present methods to the angular and radial oblate spheroidal wavefunctions appropriate to spheroidal

TABLE III. H_{BA} as a Function of Distance[a] for $\Theta=0^{\circ}$

R	Exact	WKB	USC	IWKB
10	7.0(-4)[b]	6.3(-4)	6.7(-4)	6.8(-4)
15	2.2(-6)	1.8(-6)	2.2(-6)	2.2(-6)
20	2.0(-8)	1.4(-8)	1.9(-8)	2.0(-8)
25	3.0(-10)	1.8(-10)	2.9(-10)	3.0(-10)

a) For each well the state considered has $l = 5$, $m = 4$, $r_o = 3.91448$Å, and $V_0 = 18.0313$eV.

b) The number in parentheses is the power of ten by which the entry should be multiplied.

TABLE IV. H_{BA} as a Function of Distance[a] for $\Theta = 90^{\circ}$

R	Exact	WKB	USC	IWKB
10	-9.9(-3)[b]	-9.6(-3)	-9.8(-3)	-9.9(-3)
15	-4.5(-5)	-4.0(-5)	-4.6(-5)	4.7(-5)
20	-5.8(-7)	-4.7(-7)	-6.0(-7)	6.1(-7)
25	-1.2(-8)	-8.7(-9)	-1.3(-8)	-1.3(-8)

a) For each well the state considered has $l = 5$, $m = 4$, $r_o = 3.91448$Å, and $V_0 = 18.0313$eV.

b) The number in parentheses is the power of ten by which each entry should be multiplied.

molecular shapes is being investigated.

V. Conclusions

A simple and relatively accurate approximate method is given for evaluating H_{BA} for states of spherical wells. The results agree with exact calculations for the $\Theta = 0°$ and $90°$ orientations over a wide range of distances. There is no significant loss of accuracy in using *WKB* outer radial wavefunctions. The inner function requires a uniform semiclassical approximation to be accurately represented inside the well. The two-dimensional integration yields a significant reduction in computation time which would be useful for cases where H_{BA} is needed for large numbers of orientations.

References

1. a) T.L. Netzel, P. Kroger, C.K. Chang, I. Fujita and J. Fajer, Chem. Phys. Letters **67,** 223 (1979); b) I. Fujita, J. Fajer, C.K. Chang, C.B. Wang, M.A. Bergkamp and T.L. Netzel, J. Phys. Chem. **86,** 3754 (1982); c) T.L. Netzel, M.A. Bergkamp and C.K. Chang, J. Am. Chem. Soc. **104,** 1952 (1982); d) C.K. Chang, J. Heterocyclic. Chem. **14,** 1285 (1977).

2. R.E. Overfield, A. Scherz, K.J. Kaufmann and M.R. Wasielewski, J. Am. Chem. Soc. **105,** 4256 (1983): *ibid.* **105,** 5747 (1983).

3. D. Devault, Q. Rev. Biophys. **13,** 387 (1980).

4. M.W. Makinen, S.A. Schichman, S.C. Hill and H.B. Gray, Science **222,** 929 (1983).

5. P.D. Siders, R.J. Cave and R.A. Marcus, J. Chem. Phys. **81,** 5613 (1985).

6. I.V. Alexandrov, R.F. Khairutdinov and K.I. Zamaraev, Chem. Phys. **32,** 123 (1978).

7. a)J.V. Beitz and J.R. Miller, J. Chem. Phys. **71,** 4579 (1979). b) J.R. Miller and J.V. Beitz, J. Chem. Phys. **74,** 6746 (1981).

8. S. Strauch, G. McLendon, M. McGuire and T. Guarr, J. Phys. Chem. **87,** 3571 (1983) .

9. V.G. Levich and R.R. Dogonadze, Collect. Czech. Chem. Comm. **26,** 193 (1961), Transl. O. Boshko, University of Ottawa, Ontario, Canada.

10. N.R. Kestner, J. Logan and J. Jortner, J. Phys. Chem. **78,** 2148 (1974).

11. L.I. Schiff, *Quantum Mechanics*, 3rd ed. (McGraw Hill, San Francisco, 1968), p. 83.

12. G. Arfken, *Mathematical Methods* for *Physicists*, 2nd ed. (Academic Press, San Francisco, 1970).

13. L.D. Landau and E.M. Lifshitz, *Quantum Mechanics (non-relativistic theory)* , 3rd ed. (Pergamon Press, New York, 1977), p. 164.

14. R.E. Langer, Phys. Rev. **51,** 669 (1937).

15. C.H. Bender and S.A. Orszag, *Advanced Mathematical Methods for Scientists and Engineers* (McGraw-Hill Co., San Francisco, 1978), p. 513.

16. The method used in Ref. (15) is an asymptotic method and its accuracy improves with increasing potential depth or decreasing l. It is sufficiently accurate to be employed here even though the strict conditions for accuracy in Ref. (15) are not met for the systems in this article.

17. S.C. Miller and R.H. Good, Phys. Rev. **91,** 174 (1953).

18. A. Erdelyi, J. Math. Phys. **1,** 16 (1960).

19. M. Abramowitz and I. A. Stegun, *Handbook of Mathematical Fuctions* (NBS, Washington, 1972).

20. I. S. Gradshteyn and I. M. Ryzhik, *Tables of Integrals, Series, and Products* (Academic Press, New York, 1980).

21. D. Spangler, G.M. Maggiora, L.L. Shipman and R.E. Christoffersen, J. Am. Chem. Soc. **99,** 7470, 7478 (1977).

22. J. Bardeen, Phys. Rev. Lett. **6,** 57 (1961).

23. R. A. Marcus, J. Chem. Phys. **43,** 679 (1965).

24. H. Margenau and G.M. Murphy, *The Mathematics of Physics and Chemistry* (D. Van Nostrand Company, Inc., New York, 1943), p. 443.

25. L. W. Johnson and R. D. Riess, *Numerical Analysis* (Addison Wesley, Reading, 1977), p. 129.

Chapter 6

A Semiclassical Model for Orientation Effects in Electron Transfer Using Oblate-Spheroidal Wells

I. Introduction

Increased understanding of biological redox systems has led to the need for detailed information regarding the effects of mutual orientation and separation distance on the rate of electron transfer. The nonspherical structure of many biological redox components, e.g., hemes, chlorophyll *a* and *b*, quinones, etc., leads one to expect that the mutual orientation of redox partners can significantly affect rates of electron transfer.

Examples include cytochrome *c* as well as various photosynthetic reaction centers. It will be recalled that cytochrome *c* is a complex in which a heme lies in a crevice created by a surrounding protein and is bonded to the protein by thioether bridges.[3] It is believed that electron transfers to and from the heme occur predominantly near the opening of the crevice to the solution.

Photosynthetic electron transport in plants and green algae is driven by light-activated electron transfer initiated at two photosystems (I and II).[4] The primary charge separation in photosystem II is believed to occur between an excited chlorophyll and a ground state pheophytin, perhaps mediated by another intervening chlorophyll.[5] Recent linear dichroism measurements[6] suggest that these components are held at fixed mutual orientations and separations, thus raising the question of whether these orientations and distances play a role in controlling relative rates of transfer.

The recent crystal structure determination of the reaction center in the bacterial photosystem *Rhodopseudomonas viridis*[7] reveals the relative orientations of a host of components involved in bacterial photosynthetic charge transport. The need to understand relative rates, both within the initial charge transfer step,[8] and between the various

cytochromes and the initial electron donor,[9] raises the question of the possible role played by the orientation of the components as a means of controlling rates.

Several previous studies have been aimed at qualitatively assessing orientational effects in certain simplified models.[10] Recently, Siders, *et al.*[1] have developed a one-electron model for examining orientation effects in large, delocalized aromatic systems, and have applied it to several systems of current experimental interest.[2] The basis of the model is the calculation of single-site, one-electron wavefunctions of oblate-spheroidal wells of constant potential. These wavefunctions are then used to calculate the electron-transfer matrix element, the predominant distance-dependent quantity in theories of nonadiabatic electron transfer.

In the present paper two simple approximations to this model are examined. The approximate model is both computationally much faster and conceptually simpler. It will be seen to yield accurate results for H_{BA}, within the original model. The paper is organized as follows. The exact model and the form of the electron transfer matrix element are outlined in Sec. II. The exact wavefunctions for the original model[1] are described in Sec. III and the two additional approximations introduced in this paper are discussed in Sec. IV. The results for the wavefunction and the electron transfer matrix element are compared and discussed in Sec. V, with concluding remarks made in Sec. VI.

II. The Theoretical Model

The present model[1] is intended to describe electron transfer between two fixed sites, A and B. In the zeroth-order problem A and B do not

interact and only the transferable electron is considered explicitly; i.e., each electronic wavefunction is a one-electron wavefunction. The state localized at site A is labeled Ψ^A; the state localized at site B is labeled Ψ^B. The model has been designed to assess orientational effects at various distances in electron transfer between large aromatic systems and it is assumed that the transferable electron is delocalized over the aromatic ring system.

Each isolated site is modeled as an oblate spheroid of constant negative potential inside the well and zero potential outside the well. Thus, in oblate spheroidal coordinates[11] (ξ,η,φ) the potential is given by Eq. (1) and is depicted in Fig. 1.

$$V \equiv \begin{cases} -V_0 \; ; & \xi \le \xi_0 \equiv 2b/d \\ 0 \; ; & \xi > \xi_0 \end{cases} \qquad (1)$$

The molecule is assumed to lie in the xy-plane of the potential. a (see Fig. 1) is chosen as an approximate in-plane radius of the molecule. b is chosen to yield a reasonable thickness for the electronic orbital of the molecule. The usual Cartesian coordinates are defined in terms of these coordinates by

$$x = \tfrac{1}{2} d\, [(1+\xi^2)(1-\eta^2)]^{\frac{1}{2}} \cos\varphi,\; y = \tfrac{1}{2} d\, [(1+\xi^2)(1-\eta^2)]^{\frac{1}{2}} \sin\varphi, \qquad (2)$$

$$z = \tfrac{1}{2} d\, \xi\eta \;,$$

where $d = 2\sqrt{a^2 - b^2}$, $0 \le \xi < \infty$, $-1 \le \eta \le 1$, $0 \le \theta \le 2\pi$.

The single-site one-electron Schrödinger equation may now be written as

$$(\nabla^2 + k^2)\, \Psi = 0 \qquad (3)$$

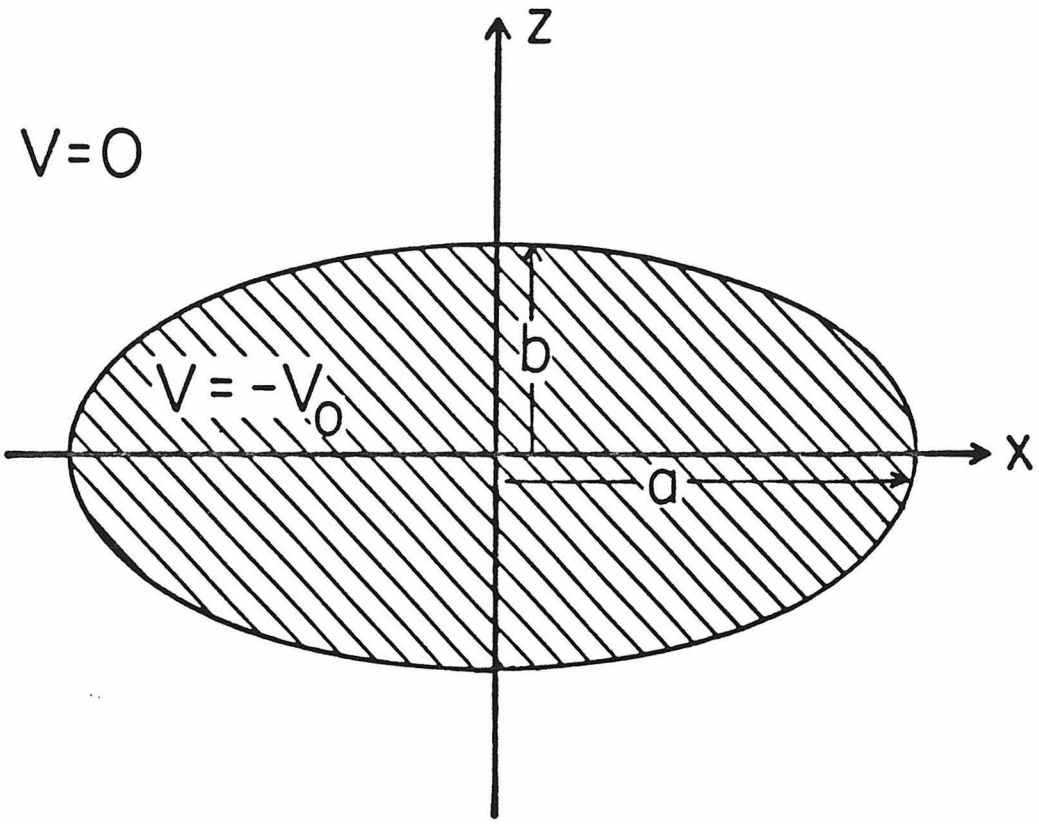

Fig. 1. Potential well for a single site. There is cylindrical symmetry about the z axis.

$$k^2 = \begin{cases} 2m(E + V_0)/\hbar^2 \equiv k_i^2 \; ; \; \xi \leq \xi_0 \\ 2m\, E/\hbar^2 \equiv k_0^2 \; ; \; \xi > \xi_0 \end{cases} . \tag{4a}$$

A choice of V_0 yields a specific value of the orbital energy E upon quantization. The value of E (and hence of V_0) is chosen so as to give a fall-off of the rate with distance which is consistent with presently available data.

The rate of nonadiabatic electron transfer between two such fixed states $A \rightarrow B$ may be written as[12-14]

$$k = \frac{2\pi}{\hbar} |T_{BA}|^2 \quad (F.C.) \; , \tag{5}$$

where (F.C.) is a Franck-Condon sum, discussed in detail elsewhere, e.g., Refs. 14-16. T_{BA} is the electronic matrix element which in the present model may be written as

$$T_{BA} = (H_{BA} - S_{AB} H_{AA})/(1 - |S_{AB}|^2) \; , \tag{6}$$

where

$$H_{BA} = \int \Psi^{B*} V^B \Psi^A \, d\tau \; , H_{AA} = \int \Psi^{A*} V^B \Psi^A \, d\tau \; , \tag{7}$$

$$S_{AB} = \int \Psi^{A*} \Psi^B \, d\tau \; .$$

V^B is the potential of the transferable electron for the isolated site B. T_{BA} is the primary distance and orientation dependent quantity in Eq. (5). In Ref. 1 it was found that T_{BA} and H_{BA} agree to within 10% at contact and the agreement increased with separation distance. Since T_{BA} requires considerably more computational time, only H_{BA} is calculated here.

The present semiclassical model was developed to obtain approximate expressions for Ψ^A and Ψ^B and thereby to significantly simplify the

evaluation of H_{BA}. To facilitate the description of the semiclassical method, the calculation of the exact wavefunction is outlined first.

III. The Exact Single-Well Eigenfunctions

In the oblate spheroidal coordinate system Eq. (3) is separable so that

$$\Psi_{mn}(\xi,\eta,\varphi) = R_{mn}(\xi)\, S_{mn}(\eta)\, \Phi_m(\varphi) \quad . \tag{8}$$

The resulting separated equations for $\xi \leq \xi_0$ (inside the well) are

$$\frac{d^2\Phi_m}{d\varphi^2} + m^2\Phi_m = 0 \tag{9a}$$

$$\frac{d}{d\eta}\left\{(1-\eta^2)\frac{dS^i_{mn}}{d\eta}\right\} + \left\{\frac{d^2}{4}\eta^2 k_i^2 - \frac{m^2}{1-\eta^2} + \lambda^i_{mn}\right\} S^i_{mn} = 0 \tag{9b}$$

$$\frac{d}{d\xi}\left\{(1+\xi^2)\,\frac{dR^i_{mn}}{d\xi}\right\} + \left\{\frac{d^2}{4}\xi^2 k_i^2 + \frac{m^2}{1+\xi^2} - \lambda^i_{mn}\right\} R^i_{mn} = 0 \quad . \tag{9c}$$

The superscript i indicates a function appropriate to the inner potential region; m and λ_{mn} are separation constants. $\Phi_m(\varphi)$ is equal to $A \sin m\varphi + B \cos m\varphi$ and since Φ_m must be single valued, m is an integer. The index n orders the eigenvalues λ_{mn} in order of increasing value and is chosen to have the possible values $n=m,\ m+1,\ m+2,\ldots$ This choice is convenient since in the spherical limit, where a tends to b, the eigenfunction given in Eq. (10) below is dominated by a single Ψ_{mn} term with $n - m = l$, l being the angular momentum quantum number of the particle for the spherical case.[11] For $\xi > \xi_0$ Eq. (3) can be separated in an identical manner, and all the i's are then replaced by o's to denote properties outside the well.

Since the method is primarily designed to assess orientation effects between delocalized π-systems, only states with no ξ-type nodes, and one η-type node will be considered. These states are odd with respect to reflection in the xy-plane and are labelled (m,π), i.e., a π-like state with azimuthal quantum number m. (A more complete description of the states is given in Refs. 1 and 2.)

The quantization condition (i.e., continuity of the wavefunction and its normal derivative at the well boundary) requires that the exact solution be written as a linear combination of the separated solutions,[1] that is,

$$\Psi_{m,\pi} = \begin{cases} \Psi^i_{m,\pi}(\xi,\eta,\varphi) = A_{m,\pi} \sum_{r=0}^{\infty} C^i_n \Psi^i_{mn}; & \xi \le \xi_0 \\ \Psi^o_{m,\pi}(\xi,\eta,\varphi) = A_{m,\pi} \sum_{r=0}^{\infty} C^o_n \Psi^o_{mn}; & \xi > \xi_0 \end{cases} \tag{10}$$

where $n = 2r + m + 1$ and $A_{m,\pi}$ is the normalization constant. Quantization is accomplished by iterating the energy E until $\Psi_{m,\pi}$ and its derivative are continuous at the boundary $\xi = \xi_0$.

IV. Approximate Single-Well Eigenfunctions

In obtaining approximate single-well functions for use in calculating H_{BA}, two approximations are made: 1) The sums in Eq. (10) are each truncated at a single term, one inside, one outside the well, and 2) Each R_{mn} and S_{mn} is evaluated semiclassically rather than as a sum of known special functions.[1,11,17] The first assumption was prompted by two observations: (a) In the spherical limit the inner and outer wavefunctions are each represented by a single mn term. (For the case of π-like states this single term has $n = m + 1$.) Since an oblate spheroid can be viewed as a

"flattened sphere" it is reasonable that the approximation of using one term in the sum will be adequate when the eccentricity is not too high. (b) Empirically, we noted in our numerical calculations that both inside and outside the potential well it is common for a single C_n^i and a single C_n^0 to dominate the other coefficients for the states considered.

In view of assumption (1) above, the total wavefunction may be written as

$$\Psi_{m,\pi} = \begin{cases} A_{m\pi} C^i_{m+1} \Psi^i_{m,m+1}(\xi,\eta,\varphi); & \xi \le \xi_0 \\ A_{m\pi} C^o_{m+1} \Psi^o_{m,m+1}(\xi,\eta,\varphi); & \xi > \xi_0 \,. \end{cases} \tag{11}$$

Because of this approximation the quantization conditions can only be approximately satisfied at the well boundary:

$$C^i_{m+1} \Psi^i_{m+1} \simeq C^o_{m+1} \Psi^o_{m+1} \tag{12a}$$

$$C^i_{m+1} \frac{\partial \Psi^i_{m,m+1}}{\partial \xi} \Big|_{\xi=\xi_0} \simeq C^o_{m+1} \frac{\partial \Psi^o_{m,m+1}}{\partial \xi} \Big|_{\xi=\xi_0} . \tag{12b}$$

To satisfy Eq. (12a) both sides were squared and then integrated over η at $\xi = \xi_0$, thereby averaging over the boundary. Taking the square root, and following the same procedure for Eq. (12b) yields

$$C^i_{m+1} R^i_{m,m+1}(\xi_0) = C^o_{m+1} R^0_{m,m+1}(\xi_0) \tag{13}$$

$$C^i_{m+1} \frac{d}{d\xi} R^i_{m,m+1}(\xi_0) = C^o_{m+1} \frac{d}{d\xi} R^0_{m,m+1}(\xi_0), \tag{14}$$

when S_{mn} and Φ_m are each normalized to unity. This procedure determines the approximate single site wavefunction to within a normalizaton constant, for any method of calculating the individual R_{mn} and S_{mn}'s.

A semiclassical approximation was used next to simplify the evaluation of the R_{mn} and S_{mn}. In previous applications,[1,2] the individual R_{mn}

and S_{mn} were evaluated through series expansions in spherical Bessel functions and associated Legendre polynomials,[11,17] a time-consuming method, particularly for high eccentricities. In the present study, uniform semiclassical approximations or primitive semiclassical approximations were obtained to the individual R_{mn}'s and S_{mn}'s and are seen to be quite accurate. Previous uniform semiclassical approximations to spheroidal wavefunctions have been described by Sink and Eu.[18]

It will be recalled that in a uniform semiclassical approximation a known function, the comparison function, is introduced together with a variable, the "mapping variable," related to the independent variable of the original differential equation. The approximate oblate-spheroidal functions will be considered in the following order: S^o_{mn}, S^i_{mn}, R^o_{mn}, R^i_{mn}. The $S^o_{mn}(\eta)$ of interest here can be approximated using a uniform approximation with the associated Legendre function as the comparison function (cf. Ref. 18 and Appendix A). For all $n,m > 0$ there will be two turning points for classical motion. The separation constant λ_{mn} is obtained using semiclassical quantization procedures.

The differential equation satisfied by $S^i_{mn}(\eta)$ is Eq. (9b), with $k_i^2 > 0$, since $(E-V) > 0$. Transforming the S^i_{mn} to remove first derivatives by introducing[18,19] $U_{mn}(\eta) = S^i_{mn}(\eta)\cdot(1-\eta^2)^{1/2}$ and using the Bethe modification, i.e., substituting m^2 for m^2-1 one obtains

$$\frac{d^2}{d\eta^2}U_{mn}(\eta) + \left[\frac{\lambda_{mn}+c_i^2\eta^2}{(1-\eta^2)} - \frac{m^2}{(1-\eta^2)^2}\right]U_{mn}(\eta) = 0 \ , \qquad (15)$$

where $c_i^2 \equiv \frac{d^2k_i^2}{4}$. When c_i^2 is zero, the numerator of the term in brackets placed over a common denominator $(1-\eta^2)^2$, is quadratic in η, with two zeros. For $c_i^2 \neq 0$, this numerator is quartic and for large enough c_i^2 has

four real zeros. This trend is seen by plotting the negative of the term enclosed in brackets in Eq. (15) as a function of η for various positive values of c^2. In Fig. 2 it is seen that as c^2 increases, the term in brackets changes from having two zeros to having four zeros. In the two-turning point case a treatment exactly analogous to that for $S^o_{mn}(\eta)$ yields accurate results.[18] (At a given c^2, as n increases, the four-turning point problem goes over to a two-turning point problem.) However, for the states of interest in the present paper the bracketed term in Eq. (15) typically has four turning points, and thus an alternative method for obtaining S^i_{mn} was needed.

In principle, a four-turning point problem can be treated with a comparison function which itself has four turning points, but such problems are typically as complicated as that for $S_{mn}(\eta)$ itself. Accordingly, results for two single-well problems were used. For a double-well problem, with the two wells separated by an infinite barrier, the eigenvalues occur in pairs and the eigenfunctions are symmetric and antisymmetric combinations of the one-well functions.[20] For the finite but large barriers examined here, a similar idea is exploited to obtain approximate S^i_{mn}'s. Single-well potentials were devised for the portion of the wavefunction localized to the left and the right of $\eta = 0$. Linear combinations of the two approximate single-well eigenfunctions were then taken to yield approximate $S^i_{mn}(\eta)$.

The effective single-well momentum for the portion of the wavefunction localized in $-1 \le \eta \le 0$ is chosen to be (Fig. 3)

$$P_I^2(\eta) = \left[\frac{m^2}{(1-\eta^2)^2} - \frac{\lambda_{mn} + c_i^2\eta^2}{(1-\eta^2)}\right], \quad -1 \le \eta \le 0 \tag{16a}$$

$$P_{II}^2(\eta) = [m^2 - \lambda_{mn}], \qquad 0 \le \eta \le \eta_i \tag{16b}$$

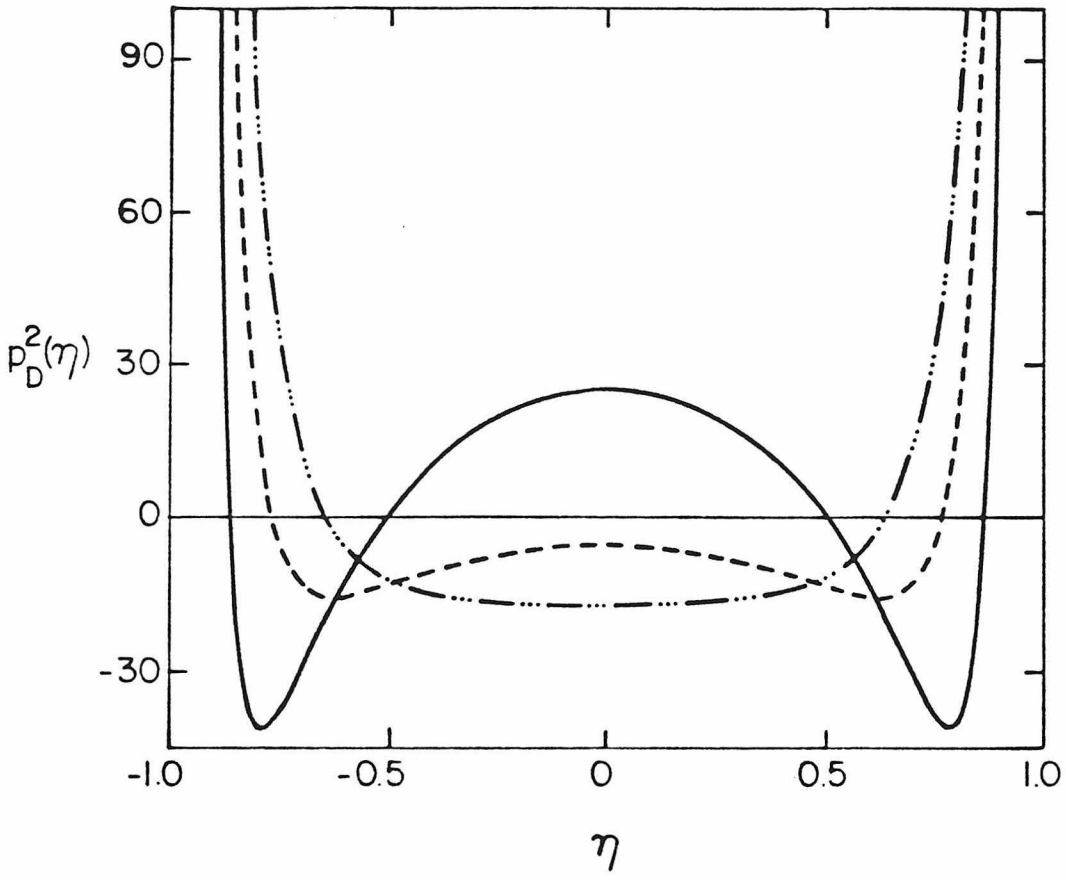

Fig. 2. The S^i_{mn} effective potential as a function of η for three different values of V_0. The other parameters used in all 3 plots are a = 5 Å, b = 2 Å, m = 5, n = 6 and E = -2.8 eV. ——— corresponds to V_0=26.3022 eV and λ^i_{56} = 0.3807. — — corresponds to V_0 = 12.00 eV and λ^i_{56} = 30.60. — ··· — corresponds to V_0 = 3.00 eV and λ^i_{56} = 42.02.

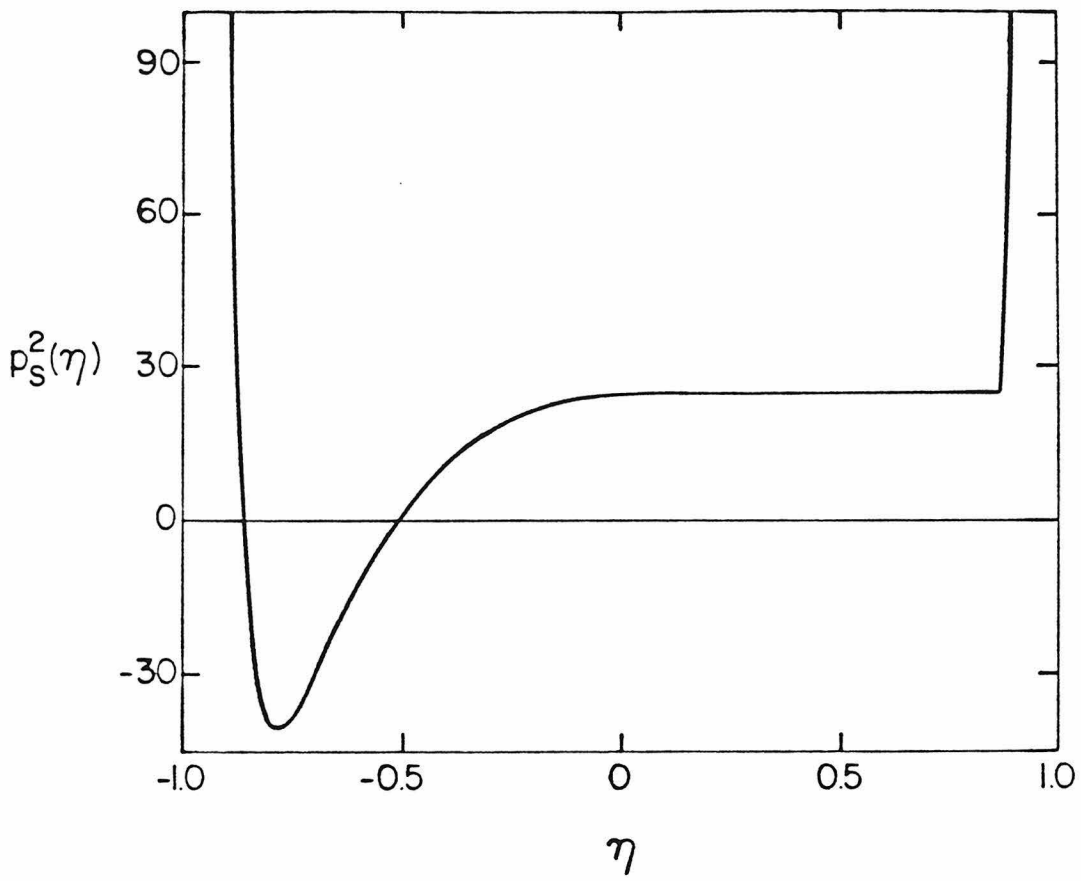

Fig. 3. The S^i_{mn} effective single well potential for the state localized between -1 ≤ η ≤ 0 as a function of η. The parameters used are a = 5 Å, b = m2 Å, m = 5, n = 6, E = -2.8 eV, and V_0 = 26.3022 eV.

$$P_{III}^2(\eta) = \left[\frac{m^2}{(1-\eta^2)^2} - \frac{\lambda_{mn}+c_i^2\eta^2}{(1-\eta^2)}\right], \quad \eta_i \le \eta \le 1\ , \tag{16c}$$

where η_i is the point in $(0 < \eta \le 1)$, where $P_{II}^2(\eta) = P_{III}^2(\eta)$. The single-well momentum for the portion of the wavefunction localized between $0 < \eta \le 1$ is simply the reflection of the potential depicted in Fig. 3 about $\eta = 0$. Each of these effective single-well momentums yields a two-turning point problem and may be solved using a uniform approximation with a two-turning point comparison equation. The harmonic oscillator equation is chosen as the latter[21] which involves mapping $-1 \le \eta \le 1$ onto $-\infty \le x \le \infty$. The mapping would yield poor results near $\eta = -1$, or 1, except that S_{mn}^i is rapidly approaching zero at those points for the states of interest in this article.

The single-well comparison function is the harmonic oscillator function which is the solution of

$$\left[\frac{d^2}{dx^2} + f^2(x)\right]\varphi_N(x) = 0\ , \tag{17}$$

where

$$f^2(x) = \frac{2m}{\hbar^2}(N + 1/2)\hbar\omega - \frac{m}{\hbar^2}x^2\ , \quad N = 0,1,\cdots \tag{18}$$

The choice of N is determined by the type of state to be modeled. The number of nodes for the function $S_{mn}(\eta)$ (excluding $\eta = \pm 1$) is $n-m$. Similarly, the number of nodes in the comparison function $\varphi_N(x)$ equals N. Since pairs of φ_N are combined, one member from each well, one can obtain $S_{m,m+1}$ states by taking the antisymmetric combination of two $N = 0$ functions, i.e., the antisymmetric combination of ground-state harmonic oscillator-like functions. $S_{m,m}$ states can be obtained by taking the symmetric combination of the $\varphi_0(x)$ solutions in each well. Similar

reasoning shows that for S_{mn} states for which $n > m+1$, where there are still four turning-points, linear combinations of φ_N with $N = 1,2$, etc. will be required.

Various authors have examined semiclassical approximations to spheroidal radial functions $R_{mn}(\xi)$.[18,19,22] The function $R^o_{mn}(\xi)$ outside the potential well satisfies the differential equation

$$\frac{d}{d\xi}\left\{(1+\xi^2)\frac{dR^o_{mn}}{d\xi}\right\} + \left\{\frac{d^2}{4}\xi^2 k_0^2 - \lambda^o_{mn} + \frac{m^2}{1+\xi^2}\right\} R^o_{mn}(\xi) = 0 \quad . \qquad (19)$$

The substitution $W_{mn}(\xi) = R_{mn}(\xi)(1+\xi^2)^{1/2}$ removes the first derivative and leads to an effective potential which, for $\xi > \xi_0$, has no zeros. A *WKB* approximation[23] is then used to obtain

$$R^o_{mn}(\xi) = \frac{\exp(-\int_{\xi^o}^{\xi} p_\xi d\xi)}{(\xi^2+1)^{1/2}(p_\xi^2)^{1/4}} \qquad (20)$$

where

$$p_\xi^2 = c_o^2 - \frac{\left[(c_o^2 + \lambda^o_{mn})(\xi^2+1) - (m^2-1)\right]}{(\xi^2+1)^2}$$

and

$$c_o^2 = \frac{d^2 k_o^2}{4} \quad .$$

The inner radial functions $R^o_{mn}(\xi)$ also satisfy Eq. (19), but with the substitution of i for o throughout. For choices of parameters appropriate to modeling large macrocyclic systems, it was found that there were no turning points for $\xi < \xi_0$. The tendency towards an absence of turning points increased with increasing d, increasing k_i^2, and with decreasing n.

When there are no turning points in the region of interest, as was

always the case for the states studied, a primitive semiclassical approximation can also be used with no divergences. One obtains for R^i_{mn}

$$R^i_{mn} = \frac{\sin(\int_0^\xi p_\xi d\xi + \beta)}{(\xi^2+1)^{1/4}(p^2)^{1/4}} \tag{21}$$

where $p^2(\xi) = c_i^2 - \frac{[(c_i^2 + \lambda^i_{mn})(\xi^2+1) - (m^2-1)]}{(\xi+1)^2}$ and β is a phase factor chosen to yield the correct phase for the semiclassical R^i_{mn}. To satisfy the π-like symmetry of the states studied here the radial wavefunction must vanish at $\xi = 0$, and so β must be equal to zero.

V. RESULTS AND DISCUSSION

In this section the exact and approximate results are compared and discussed for a number of states of interest. The physical significance of these (m,π) states was discussed earlier.[1,2] In particular, $(4,\pi)$ states are considered to model the HOMO of porphyrin derivatives and $(5,\pi)$ states are considered to model the LUMO in such molecules.

The present section contains a discussion of the single-term wavefunction; the quantities S^o_{mn}, λ^o_{mn}, S^i_{mn}, λ^i_{mn}, R^o_{mn}, R^i_{mn} calculated from the semiclassical approximations are then compared with those calculated from the exact series expansions in Tables I to V. The exact and approximate energy quantizations are next compared in Table VI, and the approximate and exact[1,2] electronic matrix element H_{BA} are compared in Table VII and Figs. 5, 6, and 8.

The largest difference between the exact and the present approximate wavefunctions occurs near the well boundary $\xi = \xi_0$. This is due to the inaccuracy of the single-term approximation to the exact wavefunc-

tion (Eq. 10). For ξ close to ξ_0 the magnitude of the R^o_{mn}'s increases rapidly with n. Also for η near ± 1 the $S^o_{mn}(\eta)$'s for $n > m + 1$ are larger than $S^o_{m,m+1}(\eta)$. Thus, even though C^o_{m+1} dominates the other expansion coefficients, the products $C^o_n R^o_{mn}(\xi) S^o_{mn}(\eta)$ (for $n > m + 1$) are of comparable magnitude to the product $C^o_{m+1} R^o_{m,m+1}(\xi) S^o_{m,m+1}(\eta)$, for ξ close to ξ_0 and η close to 1 or -1. These terms then contribute to the exact wavefunction and so the approximate wavefunction is inaccurate in these regions. However, as ξ increases all the $R^o_{mn}(\xi)$'s approach $R^o_{mm}(\xi)$ and the terms for $n > m + 1$ become unimportant for all η. The results for H_{BA} given below indicate that this occurs quickly enough for the single-term approximation to be useful.

A comparison of exact and approximate results for the S^o_{mn}'s and λ^o_{mn}'s for the two states used in the present H_{BA} calculations is given in Table I. The agreement for the S^o_{mn}'s is generally better than 1%.

In Table II, exact and approximate S^i_{mn}'s are compared for the above two states. The agreement is again good, the largest error being less than 1%. The approximate λ^i_{mn}'s are somewhat inaccurate. The λ^i_{mn}'s are determined from the semiclassical single-well quantization. At the lowest level of semiclassical approximation, λ^i_{mn} for $n = m$ and $n = m+1$ are equal. This is not true of the exact results since the barrier between the wells is finite. The splitting of the pairs of λ^i_{mn} can be obtained in several ways (including a standard semiclassical one). We have simply used the two single-well functions as basis functions and solved the two-by-two matrix equation obtained from Eq. (15). The λ's obtained in this way are shown in Table III. The calculated splitting is in good agreement with the splitting of the exact λ's. The absolute values of both of the approximate λ's are larger than the exact by essentially a constant amount. Neither

TABLE I. Outer $S_{mn}(\eta)$ for Various η

	$n = 6, m = 5$[a]		$n = 5, m = 4$[b]	
η	Semiclassical[c]	Exact	Semiclassical[c]	Exact
.9	9.83(1)[d]	9.83(1)	1.93(1)	1.92(1)
.8	4.71(2)	4.70(2)	6.81(1)	6.79(1)
.7	1.06(3)	1.06(3)	1.30(2)	1.30(2)
.6	1.71(3)	1.71(3)	1.89(2)	1.89(2)
.5	2.24(3)	2.24(3)	2.31(2)	2.31(2)
.4	2.48(3)	2.48(3)	2.44(2)	2.44(2)
.3	2.36(3)	2.36(3)	2.23(2)	2.23(2)
.2	1.84(3)	1.84(3)	1.70(2)	1.70(2)
.1	1.01(3)	1.01(3)	9.21(1)	9.21(1)

a) For both exact and semiclassical cases, E = -2.8 eV, V_0 = 26.3022eV, a = 5Å, b = 2Å, λ_{56}^{ex} = 44.95, λ_{56}^{sc} = 45.17.

b) For both exact and semiclassical cases, E = -2.8 eV, V_0 = 22.1985eV, a = 5Å, b = 2Å, λ_{45}^{ex} = 33.36, λ_{45}^{sc} = 33.67.

c) The semiclassical function was normalized to the exact function at η = 0.4. This was done for comparison purposes only and is not required for the calculations presented here.

d) The numbers in parentheses are the powers of ten by which each entry should be multiplied.

TABLE II. Inner $S_{mn}(\eta)$ for Various η

	$n = 6, m = 5$[a]		$n = 5, m = 4$[b]	
η	SC[c]	Exact	SC[c]	Exact
.9	8.03(3)[d]	8.03(3)	1.28(3)	1.28(3)
.8	1.78(4)	1.78(4)	2.15(3)	2.16(3)
.7	1.94(4)	1.94(4)	2.07(3)	2.07(3)
.6	1.60(4)	1.60(4)	1.58(3)	1.59(3)
.5	1.13(4)	1.14(4)	1.08(3)	1.08(3)
.4	7.35(3)	7.36(3)	6.81(2)	6.84(2)
.3	4.44(3)	4.45(3)	4.06(2)	4.08(3)
.2	2.45(3)	2.46(3)	2.23(2)	2.25(2)
.1	1.08(3)	1.09(3)	9.79(1)	9.88(1)

a) For both exact and semiclassical cases, E = -2.8eV, V_0 = 26.3022eV, a = 5Å, b = 2Å, $\lambda_{56}^{ex} = -.1111$, $\lambda_{56}^{sc} = .4718$.

b) For both exact and semiclassical cases, E = -2.8eV, V_0 = 22.1985eV, a = 5Å, b = 2Å, $\lambda_{45}^{ex} = -9.371$, $\lambda_{45}^{sc} = -8.790$.

c) The semiclassical functions were normalized to the exact functions at $\eta = 0.60$. This was done for comparison purposes only and is not required for the calculations presented here.

d) The numbers in parentheses are the powers of ten by which each entry should be multiplied.

TABLE III. Improved λ^{sc}

	$m = 5^a$			$m = 4^b$	
λ_{ij}	Exact	Semiclassical	λ_{ij}	Exact	Semiclassical
λ_{55}	-.293	.381	λ_{44}	-9.49	-8.85
λ_{56}	-.111	.562	λ_{45}	-9.37	-8.73

a) E, V_0, a, and b are as for the m=5, n=6 state of Table II.
b) E, V_0, and b are as for the m=4, n=5 state of Table II.

the semiclassical S_{mn} or R_{mn} are seriously affected by this error in λ^i_{mn}. For R^i_{mn} the appropriate λ^i_{mn} obtained from the splitting calculation is used.

The exact and semiclassical outer radial functions are compared in Table IV for sample values of k_o^2, m, and d of interest here. For comparison purposes, the functions are equated at the smallest ξ . The agreement is excellent over the entire region of interest. Similar accuracy is obtained for other states. The respective λ^o_{mn} values used in the calculations of R^o_{mn}'s for Table IV were from exact and semiclassical methods, respectively.

The exact and semiclassical R^i_{mn}'s for the case of no inner turning point are compared in Table V. The agreement is again quite good and similar accuracy can be expected for other states.

Using the above semiclassical approximations to the individual R_{mn} and S_{mn}, together with the single term approximation, the energy values can be calculated using Eq. (12)-(14) for given values of the potential and for various states. The exact and approximate quantization results are compared in Table VI. There is a fairly large error in the calculated orbital energy which could be anticipated from the observed contribution of several terms to the total wavefunctions near the well boundary. Accurate quantization for a given value of the potential is not necessary but is examined for completeness: the general procedure for calculations of H_{BA} (both approximate and exact) is to choose a value for E which yields the desired decay of H_{BA} with distance by adjusting V. Also shown in Table VI are the values of V_0 appropriate to equal energies for the exact and approximate methods. It should be stressed that the error in the semiclassical energy quantization is not due to the use of semiclassical

TABLE IV. Outer $R_{mn}(\xi)$ for Various ξ

	$n = 6, m = 5$[a]		$n = 5, m = 4$[b]	
ξ	Semiclassical[c]	Exact	Semiclassical[c]	Exact
1.0	3.47(-2)[d]	3.47(-2)	1.44(-2)	1.44(-2)
2.0	2.03(-4)	2.05(-4)	1.12(-4)	1.13(-4)
3.0	1.86(-6)	1.88(-6)	1.20(-6)	1.21(-6)
4.0	2.19(-8)	2.21(-8)	1.55(-8)	1.57(-8)
5.0	2.97(-10)	3.00(-10)	2.23(-10)	2.27(-10)
6.0	4.38(-12)	4.43(-12)	3.44(-12)	3.50(-12)
7.0	6.83(-14)	6.90(-14)	5.53(-14)	5.63(-14)
8.0	1.11(-16)	1.12(-16)	9.18(-16)	9.35(-16)

a) For both the exact and semiclassical cases, E = -2.8eV, V_0 = 26.3022eV, a = 5Å, b = 2Å, $\lambda_{56}^{ex} = 44.95$, $\lambda_{56}^{sc} = 45.17$.

b) For both the exact and semiclassical cases, E = -2.8eV, V_0 = 22.1985eV, a = 5Å, b = 2Å, $\lambda_{45}^{ex} = 33.36$, $\lambda_{45}^{sc} = 33.67$.

c) The semiclassical function was normalized to the exact function at $\xi = 1.0$. This was done for comparison purposes only and is not required for the calculations presented here.

d) The numbers in parentheses are the powers of ten by which each entry should be multiplied.

TABLE V. Inner $R_{mn}(\xi)$ for Various ξ

	$n = 6, m = 5$[a]		$n = 5, m = 4$[b]	
ξ	Semiclassical[c]	Exact	Semiclassical[c]	Exact
.05	3.24(-2)[d]	3.18(-2)	3.38(-2)	3.35(-2)
.10	6.25(-2)	6.14(-2)	6.51(-2)	6.48(-2)
.15	8.80(-2)	8.68(-2)	9.19(-2)	9.16(-2)
.20	1.07(-1)	1.06(-1)	1.12(-1)	1.12(-1)
.25	1.18(-1)	1.18(-1)	1.24(-1)	1.24(-1)
.30	1.20(-1)	1.20(-1)	1.27(-1)	1.27(-1)
.35	1.13(-1)	1.13(-1)	1.20(-1)	1.20(-1)
.40	9.59(-2)	9.73(-2)	1.04(-1)	1.04(-1)
.45	7.13(-2)	7.31(-2)	8.02(-2)	7.99(-2)
.50	4.08(-2)	4.29(-2)	5.00(-2)	4.93(-2)

a) For both the exact and semiclassical cases, E = -2.8 eV, V_0 = 26.3022eV, a = 5Å, b = 2Å, $\lambda_{56}^{ex} = -.111$, $\lambda_{56}^{sc} = .562$.

b) For both the exact and semiclassical cases, E = -2.8eV, V_0 = 22.1985eV, a = 5Å, b = 2Å, $\lambda_{45}^{ex} = -9.37$, $\lambda_{45}^{sc} = -8.73$.

c) The semiclassical function was normalized to the exact function at $\xi = .30$. This was done for purposes of comparison only and is not required for the present claculations.

d) The number in parenthesis is the power of ten by which the entry should be multiplied.

TABLE VI. Comparison of Exact and Semiclassical Energies

	$n = 6, m = 5^a$			$n = 5, m = 5^a$		
	Exact	SC(E)[b]	SC(V)[c]	Exact	SC(E)[b]	SC(V)[c]
V_0	26.3022[d]	25.5316	26.3022	22.1985	21.4993	22.1985
E	-2.8	-2.8	-3.4647	-2.8	-2.8	-3.3934

a) For both the exact and semiclassical cases a = 5Å, b = 2Å.
b) SC(E) denotes a semiclassical state with the energy equal to that of the given state of interest.
c) SC(V) denotes a semiclassical state with potential equal to that of the given exact state of interest
d) All energies are in eV.

R_{mn} and S_{mn} but is due to the single-term expansion of the wavefunction. It will be shown below, however, that these single-term functions are still accurate enough to yield reasonable results for H_{BA}.

To describe the orientation of the two wells the coordinate system shown in Fig. 4 is used. Unless otherwise specified, the xy planes of both wells are chosen to be parallel and the centers of each well are held at a given separation distance R. $\Theta = 0^o$ (see Fig. 4) corresponds to a "face-to-face" configuration and $\Theta = 90^o$ to an "edge-to-edge" one.

The exact and approximate H_{BA} is presented as a function of distance for transfer between two $(4,\pi)$ states, for the $\Theta = 0^o$ and $\Theta = 90^o$ orientations in Table VII. The agreement is seen to be quite good. The deviation at small R, especially in the $\Theta = 0^o$ orientation is due to the contribution of other states in the exact state sum over $R_{mn}\,S_{mn}$ as noted previously (cf. Eq. (10)). It is clear that this contribution from other n-states is only serious at very small R. For comparison, results using spherical wells of similar volume and energy are also given in Table VII. They are seen to be significantly less accurate than the present approximation to the spheroidal problem, particularly at $\Theta = 0^0$.

In Fig. 5 exact and approximate results for $(5,\pi)$ states are compared at constant edge-to-edge distance for various Θ's. It is seen that as the edge-to-edge distance increases from 0Å to 4Å, the accuracy of the present approximate calculation increases. The agreement is quite good for an edge-to-edge distance of 4Å, and for larger separation the agreement remains good.

In Fig. 6 H_{BA}'s for the same set of orientations for transfer between $(5,\pi)$ and $(4,\pi)$ states are given. Calculations similar to those in Figs. 5 and 6 have been used previously to model electron transfer orientation

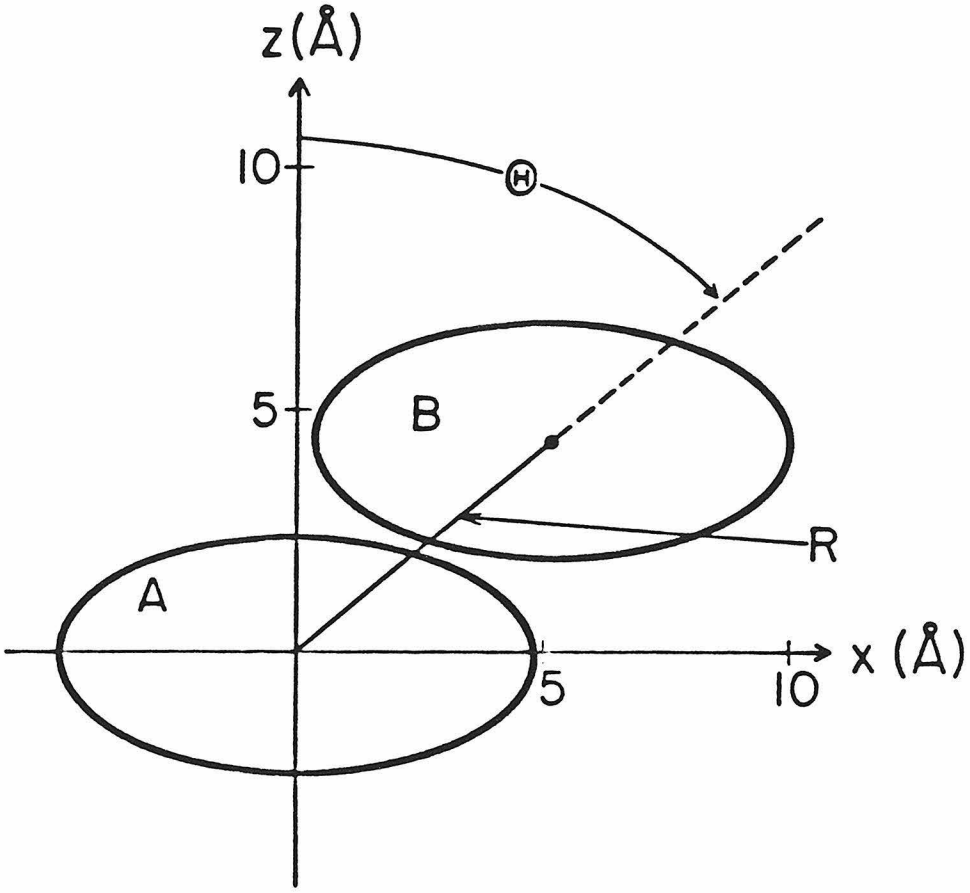

Fig. 4. Coordinate system used to specify the mutual orientation of well *A* and well *B*. The x axes of the wells are parallel and lie in the plane of the figure in all geometries. $\Theta = 0°$ corresponds to the z axes of the wells being superimposed.

TABLE VII. Exact and Approximate H_{BA} for a pair of $(4,\pi)$ States as a function of distance at $\Theta = 0°$ and $\Theta = 90°$.

Θ (degrees)	R(Å)	H_{BA}^{ez} [a]	H_{BA}^{sc} [b]	H_{BA}^{sphere} [c]
0°	10	3.8 (-4)[d]	3.0(-4)	7.0(-4)
	15	2.0(-6)	1.8(-6)	2.2(-6)
	20	2.2(-8)	2.1(-8)	2.0(-8)
	25	3.8(-10)	3.7(-10)	3.0(-10)
90°	10	-4.1(-2)	-5.8(-2)	-9.9(-3)
	15	-1.3(-4)	-1.5(-4)	-4.5(-5)
	20	-1.5(-6)	-1.7(-6)	-5.8(-7)
	25	-3.0(-8)	-3.4(-8)	-1.2(-8)

a) For each $(4,\pi)$ state $E = -1.1525$eV, $V_0 = 17.35297$eV, $a = 4.85$Å, $b = 2.55$Å.

b) For each $(4,\pi)$ state $E = -1.1525$eV, $V_0 = 17.54121$eV, $a = 4.85$Å, $b = 2.55$Å.

c) For each $(4,\pi)$ spherical state $E = -1.1525$eV, $V_0 = 18.0313$eV, $r = 3.915$Å.

d) The number on parentheses to the power of ten by which each entry should be multiplied.

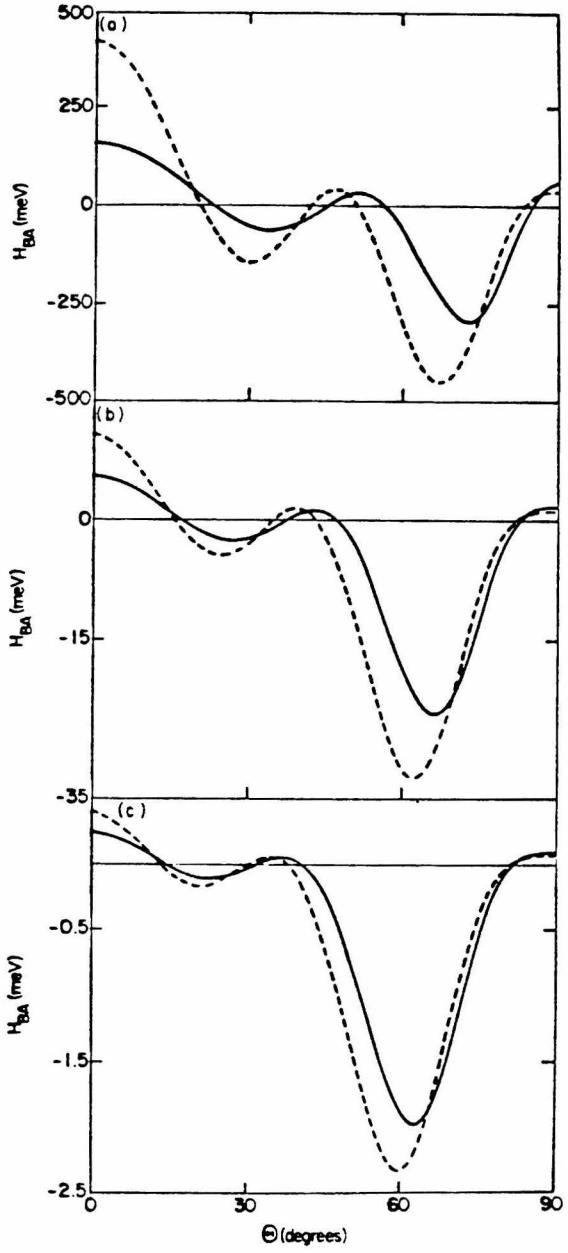

Fig. 5. The matrix element H_{BA} as a function of Θ at several fixed edge-to-edge separations for $(5,\pi) \Rightarrow (5,\pi)$ transfer. For the donor and acceptor states a = 5 Å, b = 2 Å, E = -2.8 eV. — — corresponds to the exact calculations where V_0 = 26.302 eV. ——— corresponds to the semiclassical calculations where V_0 = 25.532 eV. (a) Edge-to-edge separation of 0 Å. (b) Edge-to-edge separation of 2 Å. (c) Edge-to-edge separation of 4 Å.

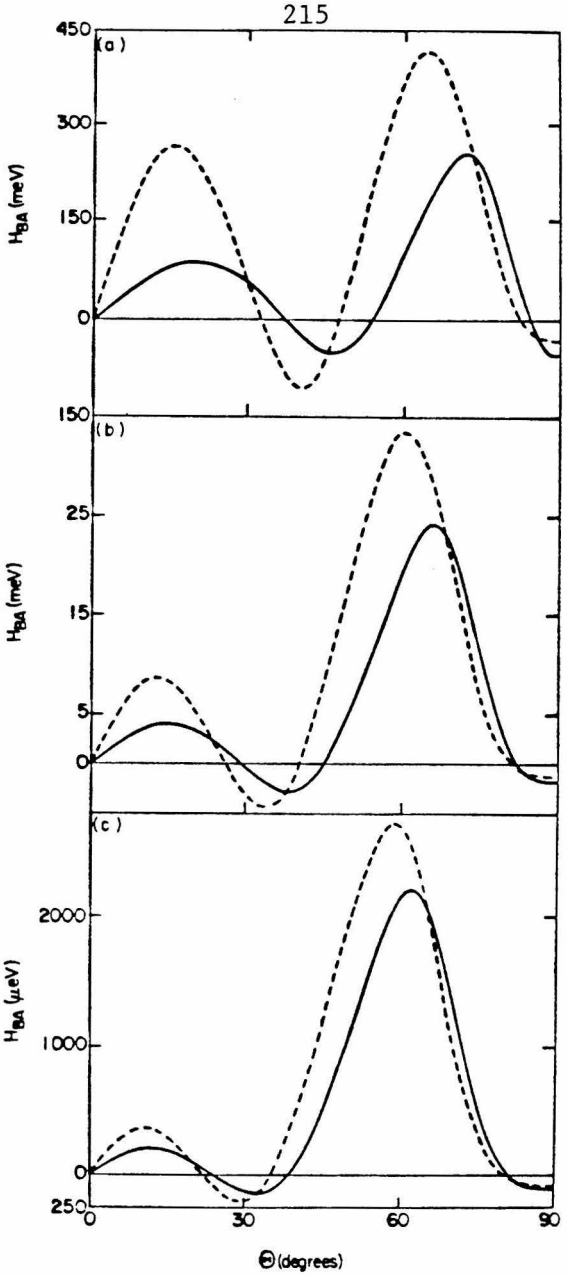

Fig. 6. The matrix element H_{BA} as a function of Θ at several fixed edge-to-edge separations for $(5,\pi) => (4,\pi)$ transfer. For the donor and acceptor states a = 5 Å, b = 2 Å, E = - 2.8 eV. For the exact calculations (— —) the donor V_0 is 26.302 eV and the acceptor V_0 is 22.199 eV. For the semiclassical calculations (———) the donor V_0 is 25.532 eV and the acceptor V_0 is 21.499 eV. (a) Edge-to-edge separation of 0 Å. (b) Edge-to-edge separation of 2 Å. (c) Edge-to-edge separation of 4 Å.

dependence between two porphyrins. Again, at all distances the approximate results for the H_{BA}'s show similar behavior to the exact ones and by 4 Å edge-to-edge separation the agreement has become excellent.

Results for a different class of orientations (cf. Fig. 7) are given in Fig. 8. For these results, the wells are held at a given R, in the edge-to-edge ($\Theta = 90°$) orientation, but the xy-planes are twisted about the line of centers through an angle γ relative to each other. Again, the agreement is quite good at all distances.

There are several advantages of the present approximation over the exact method developed in Ref. 1: 1) The present method is significantly easier to implement. In the exact method the individual R_{mn}'s and S_{mn}'s were constructed as sums of known special functions. Each sum was then checked for convergence at every value of the argument for which the function was evaluated. Moreover, the total wavefunction was itself (in principle) an infinite sum which must be checked for convergence at each evaluation. In the present method each R_{mn} and S_{mn} is evaluated as single term, with convergence needed only for the respective integrals involved in the semiclassical expressions. The problem of convergence of a sum thus disappears. 2) The current method is substantially faster computationally. For each geometry in Figs. 5-7, the current method treating H_{BA} as a three-dimensional volume integral required ~ 10 min CPU time (VAX 11-780) while the exact method required ~ 50 times longer. (A method of reducing computation time for the exact method is given in Ref. 2. It could be applied under further approximations to the present wavefunctions. Its accuracy has not been examined). 3) The accuracy of the present method supports the simple conceptual model previously introduced[1,2] to understand the orientation dependence of

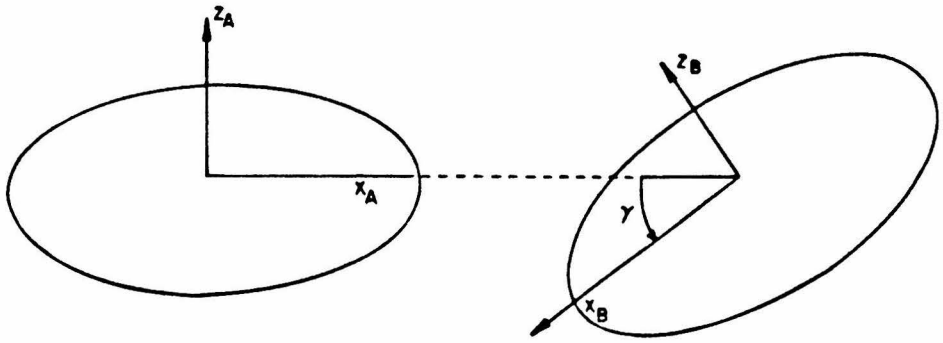

Fig. 7. Coordinate system used to specify the mutual orientation of the wells for the calculations presented in Fig. 8. The x-axes of the wells lie in the plane of the figure and for $\gamma = 0°$ the x-axes are antiparallel and lie along the same line.

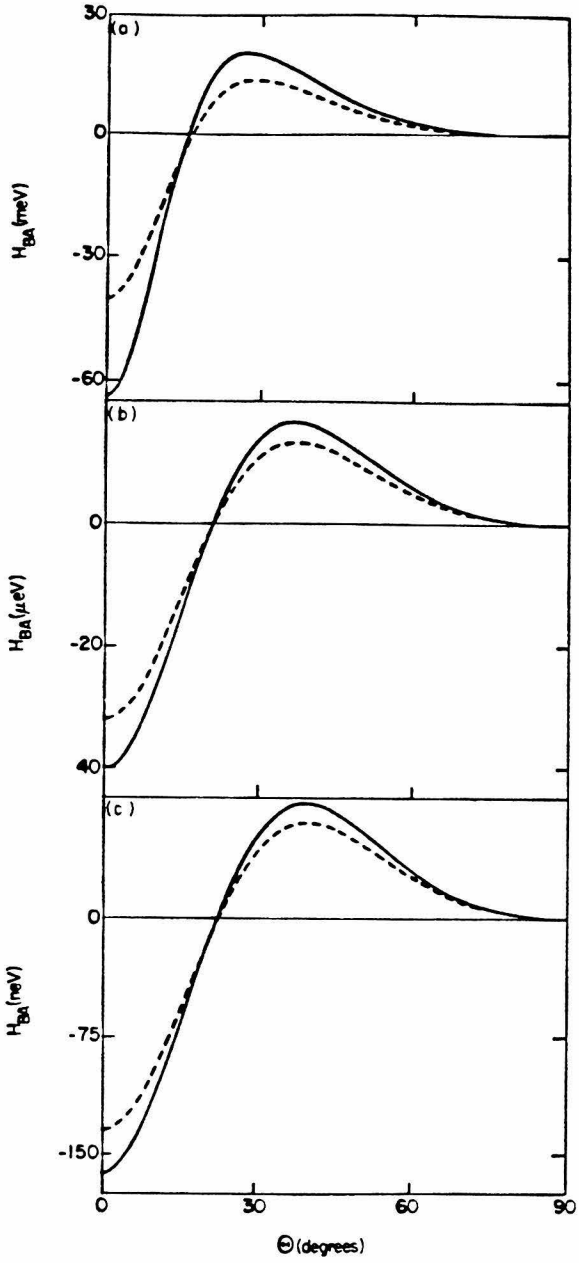

Fig. 8. The matrix element H_{BA} as a function of Γ at several fixed edge-to-edge separations for $(5,\pi) \Rightarrow (5,\pi)$ transfer. For the donor and acceptor states a = 5 Å, b = 2 Å, E = - 1.867 eV. For the exact calculations (— —) the donor and acceptor V_0 is 25.191 eV. For the semiclassical calculations (———) the donor and acceptor V_0 is 24.438 eV. (a) Edge-to-edge separation of 0 Å. (b) Edge-to-edge separation of 5 Å. (c) Edge-to-edge separation of 10 Å.

H_{BA}. Previously, this simple conceptual model has been understood by analogy with results from the use of spherical wells, where the inner and outer wavefunctions are each single terms. The spheroidal functions were envisioned to be continuously distorted spherical functions. Here, the assumption is explicitly made in treating the inner and outer Ψ's as single-term functions. The accuracy of these results therefore supports this model.

VI. CONCLUSION

A semiclassical method of calculating the electron transfer matrix element H_{BA} has been formulated. It was shown to yield good agreement with results in which the exact solution of the Schrödinger equation for the same model potential was used. This semiclassical method also has much greater computational efficiency. In any future applications of the model of Ref. 1 to the calculation of mutual orientation and separation distance effects, use of the semiclassical method should be appropriate.

Acknowledgement:

It is a pleasure to acknowledge support of this research by the Office of Naval Research. SJK gratefully acknowledges the support of a Natural Sciences and Engineering Research Council of Canada postgraduate scholarship, 1984-1985. The calculations reported in this paper made use of the Dreyfus-NSF theoretical chemistry computer which was funded through grants from the Camille and Henry Dreyfus Foundation, the National Science Foundation, and the Sloan Fund of the California Institute of Technology.

Appendix A: Uniform Semiclassical Analysis

The general method for obtaining uniform semiclassical approximations to the solutions of homogeneous second-order differential equations is discussed by a number of authors.[25,26] The present treatment follows the method of Miller and Good[25] and is similar to the treatment presented earlier by Sink and Eu[18] with certain modifications. The outer S_{mn} are examined for illustrative purposes and similar considerations yield the other semiclassical functions used.

The differential equation satisfied by $S^o_{mn}(\eta)$ is Eq. (9b) with the replacement of k_i^2 by k_o^2 ($k_o^2 < 0$). It is convenient to convert this equation to a purely second-order differential equation by the substitution $S^0_{mn} = U^0_{mn}/(1-\eta^2)^{1/2}$, yielding

$$\left[\frac{d^2}{d\eta^2} + p_\eta^2\right] U^0_{mn} \tag{A1}$$

where

$$p_\eta^2 \equiv \frac{\lambda^o_{mn} + \eta^2 d^2 k_o^2/4}{(1-\eta^2)} - \frac{(m^2-1)}{(1-\eta^2)^2} \,. \tag{A2}$$

For states with $m > 1$, p_η^2 will have two zeros for η in the interval (-1,1). Since a primitive semiclassical approximation for U^0_{mn} will fail at and near these zeros, a uniform approximation is required there.

In the limit $d \to 0$ the $S^0_{mn}(\eta)$ reduce to associated Legendre functions P_l^m, with $l = n - m$, thus P_l^m will be used as a comparison function when $d \neq 0$.[18] A new independent variable ν is used, and setting $P_l^m(\nu) = V_{ml}/(1-\nu^2)^{1/2}$ the associated Legendre equation becomes

$$\left[\frac{d^2}{d\nu^2} + p_\nu^2\right] V_{ml}(\nu) = 0 \tag{A3}$$

where

$$p_\nu^2 \equiv \frac{l(l+1)}{1-\nu^2} - \frac{(m^2-1)}{(1-\nu^2)^2}, \tag{A4}$$

which serves as the "comparison equation" for Eq. (A2).

Following standard procedures,[25] one then writes

$$U_{mn}(\nu) = T(\eta) V_{ml}(\nu(\eta)) \ , \tag{A5}$$

with $T(\eta) \equiv (d\nu/d\eta)^{-1/2}$.

Equation (A5) is then substituted into Eq. (A2) to obtain

$$-p_\nu^2 \left(\frac{d\nu}{d\eta}\right)^2 + p_\eta^2 + T''/T = 0 \ , \tag{A6}$$

where the primes denote derivatives. Under the assumption that T''/T can be neglected, the positive square root in Eq. (A6) yields

$$d\nu\, p(\nu) = d\eta\, p_\eta \ . \tag{A7}$$

This equation defines ν, the new variable, in terms of η. To ensure that the approximation to U_{mn} given by Eq. (A5) has no artificial zeros or singularities it is required that the zeros of p_ν and p_η in the regions of interest be mapped onto one another; that is, it is demanded that

$$\int_{-\eta_{TP}}^{+\eta_{TP}} p_\eta d\eta = \int_{-\nu_{TP}}^{\nu_{TP}} p(\nu) d\nu \ , \tag{A8}$$

where $\pm\eta_{TP}$ are the zeros of p_η and $\pm\nu_{TP}$ are those of p_ν. In general, Eq. (A8) will only be satisfied for a single value of λ_{mn}. Thus Eq. (A8) determines λ_{mn}. With Eq. (A8) satisfied $T(\eta)$ is finite over the entire range of interest, since the order of the zeros of p_η and p_ν is the same and the order of singularities of p_η and p_ν is also the same.

Once λ_{mn} is obtained, the mapping variable $\nu(\eta)$ can be obtained for any η by solving for $\nu(\eta)$ in

$$\int_{\eta_{TP}^{i}}^{\eta} p_{\eta} d\eta = \int_{\nu_{TP}^{i}}^{\nu(\eta)} p_{\nu} d\nu \tag{A9}$$

where η_{TP}^{i} is the zero of p_{η} closest to η and ν_{TP}^{i}, is the zero of p_{ν} associated with η_{TP}^{i} via Eq. (A8). Thus, S_{mn}^{0} is determined. There are two differences between the present treatment and that of Sink and Eu.[18] 1) Sink and Eu[18] make the Langer modification,[27,28] in Eq. (A4); i.e., they set $l(l+1) \rightarrow (l+\frac{1}{2})^2$. 2) In both Eqs. (A2) and (A4) they make a modified Bethe modification,[18,19] $(m^2-1) \rightarrow (m+d)^2$. Their interest was in constructing a single uniform approximation, valid in form for all mn pairs. If the Bethe modification was not modified, the method would not yield a single valued mapping function for the case of $l = m = 0$. The above modified Bethe substitution corrected for this shortcoming and was employed by Sink and Eu[18] for all m and n.

In the present case, however, high n and m states are considered. Thus the question of single valuedness for the mapping variable does not arise. If the Langer modification is not made the S_{mn}^{0} reduce asymptotically to the corresponding P_{l}^{m}, as $n \rightarrow \infty$. However, the difference between using and not using the Langer modification was quite small ($< 0.1\%$) for the states examined here. The motivation for the standard Bethe modification is not present here since the mapping function is defined on a finite interval and has singularities of the same order as the differential equation for the S_{mn}. Thus, neither the Bethe or Langer modifications are made in the present semiclassical approximation to the outer function S_{mn}^{0}.

Entirely analogous methods were used in obtaining the semiclassical expressions for the other oblate spheroidal functions used in the present article. The differences between the functions is merely in the comparison function used to represent a given function and, of course, the form of the effective potential.

REFERENCES

1. P. Siders, R.J. Cave, and R.A. Marcus, J. Chem. Phys. **81,** 5613 (1984).

2. R.J. Cave, P. Siders, and R.A. Marcus, J. Am. Chem. Soc., in preparation.

3. R.A. Marcus and N. Sutin, Biochim. Biophys. Acta, in press.

4. Cf. *Encyclopedia of Plant Physiology, 5, Photosynthesis I,* eds. A. Trebst, M. Avron (Springer-Verlag, New York, 1977).

5. R.J. Cogdell, Ann. Rev. Plant Physiology **34,** 21 (1983).

6. I.B. Ganago, V.V. Klimov, A.O. Ganago, V.A. Shuvalov, and Y.E. Erokhir, FEBS Lett. **140,** 127 (1982).

7. J. Deisenhofer, O. Epp, K. Miki, R. Huber, and H. Michel, J. Mol. Biol. **180,** 385 (1984).

8. Cf. W.W. Parson, Ann. Rev. Biophys. Bioeng. **11,** 57 (1982).

9. Cf. P.L. Dutton and R.C. Prince in *The Photosynthetic Bacteria,* eds. R.K. Clayton and W.R. Sistrom (Plenum, New York, 1978), 525 ff.

10. a) S.A. Rice and M.J. Pilling, Progr. React. Kinetics **9,** 93 (1978); b) B. Brocklehurst, J. Phys. Chem. **83,** 536 (1979), c) A.B. Doktorov, R.F. Khairutdinov, and K.I. Zamaraev, Chem. Phys. **61,** 351 (1981).

11. C. Flammer *Spheroidal Wavefunctions* (Stanford University Press. Stanford. CA, 1957).

12. V.G. Levich and R.R. Dogonadze, Collect. Czech. Chem. Commun. **26,** 193 (1961); Translator, O. Boshko, University of Ottawa, Ontario, Canada.

13. R.R. Dogonadze, A.M. Kuznetsov, and M.A. Vorotyntsev, Phys. Status Soildi B. (Ger.) **54,** 125, 425 (1972).

14. N.R. Kestner, J. Logan, and J. Jortner, J. Phys. Chem. **78,** 2148 (1974).

15. B.S. Brunschwig, J. Logan, M.D. Newton, and N. Sutin, J. Am. Chem. Soc. **102,** 5798 (1980).

16. P. Siders and R.A. Marcus, J. Am. Chem. Soc. **103,** 741 (1981).

17. D.B. Hodge, J. Math. Phys. **11,** 2308 (1970).

18. M.L. Sink and B.C. Eu, J. Chem. Phys. **78,** 4887 (1983).

19. S.S. Gershtein, L.I. Ponomarev, and T.P. Puzyninca, Sov. Phys. JETP **20,** 418 (1965).

20. M.A. Morrison, T.L. Estle, and N.F. Lane, *Quantum States of Atoms, Molecules, and Solids* (Prentice-Hall, New Jersey, 1976), p. 276.

21. Unlike the case of S^{o}_{mn}, the associated Legendre equation was not used. Since the single-well solutions are quite different from Legendre polynomials, the use of the latter as a comparison function presents no advantage. Further, when using the Legendre equation as a comparison equation the mapping function must be inverted numerically to obtain the mapping variable. This is not the case

when an $N = 0$ harmonic oscillator function is used as a comparison function.

22. W. Pauli, Ann. Physik **68,** 177 (1922).

23. L.D. Landau and E.M. Lifshitz, *Quantum Mechanics* (Pergammon Press, Oxford, 1977) 3rd ed. Chap. VII, p. 164.

24. The matrix equation obtained from Eq. (15) results in a corrected λ^i_{mn} but does not give a corrected S^i_{mn}. The form of the semiclassical S^i_{mn} precludes inclusion of the the corrected λ^i_{mn} in the S^i_{mn} calculation.

25. S.C. Miller, Jr. and R.H. Good, Jr., Phys. Rev. **91,** 1741 (1953).

26. A. Erdelyi, J. Math. Phys. **1,** 16 (1960).

27. R.E. Langer, Phys. Rev. **51,** 669 (1937).

28. M.S. Child, *Molecular Collision Theory* (Academic Press, New York, 1974) App. C, p. 249.